UNIVERSITY OF LIVERPOOL

FACULTY OF SCIENCE AND ENGINEERING

Computational modelling of the condensation process of the fast pyrolysis vapours in liquid collection systems

Kiran Kumar Palla Venkata Satya

This thesis is submitted for the degree of

Doctor of Philosophy

October 2015

Abstract

The aim of the present thesis is to model the conversion process of the fast pyrolysis vapours into liquid bio-oil in liquid collection systems. The study focuses on the two major types of condensation systems namely the indirect contact condensers and the direct contact condensers (quenching columns).

In the first part of the research, the hydrodynamic and heat transfer characteristics of a bench scale quenching column are presented by conducting numerical simulations based on the immiscible Eulerian-Eulerian model. The simulations are compared with experimental observations on flooding phenomena and various design variants are proposed for their elimination.

In the second part, a multiphase multi-component model, with the condensable vapours and non-condensable gases as the gaseous phase and the condensed bio-oil as the liquid phase, has been developed. Species transport modelling has been used to capture the detailed physical phenomena of 11 major compounds present in the pyrolysis vapours. The development of the condensation model relies on the saturation pressures of the individual compounds computed based on the corresponding state correlations.

In the final part, detailed information is provided on the vapour phase change dynamics implemented on a disc and donut quenching column design obtained from the first part. The study investigates the effect of the different numbers of disc and donut pairs on the condensation performance of the column. The numerical simulations showed that different number of stages can significantly affect the final bio-oil composition. It is shown that heavy molecular weight compounds, condense rapidly even with a low number of stages, whereas an increased number of stages is needed to completely capture the heavier acidic fractions. The modelling results are in good agreement with data published in the existing literature.

Declaration

I, Kiran Kumar Palla Venkata Satya, hereby declare that the thesis and the work presented in it except where specific reference is made to the work of others, are original and have not been submitted in whole or in part for consideration for any other degree or qualification in this, or any other University. This Thesis is the result of my own work and includes nothing which is the outcome of work done in collaboration, except where specifically indicated in the text. Parts of this work have been published as given in the list of publications.

Kiran Kumar Palla Venkata Satya

2015

Acknowledgements

I would like to take this opportunity to express my heart felt gratitude to my advisor and supervisor Dr Konstantinos Papadikis. Still I remember when I first met him four years ago. The meeting laid the foundation for this work. With his great patience and enthusiasm, he has taught me the skills of systematic scientific research. I thoroughly admire him as a human being with great traits and remarkable teacher.

I would also want to thank Professor Sai Gu who provided immense support on the project and more importantly for giving me an opportunity to be with the wonderful research community in China as well as in UK. I express my sincere thanks to Dr Spyros Kamnis, Haji, Ebi and Zhang Duo for their valuable comments and encouragement during my tenure as a PhD student.

I would like also to take this opportunity to acknowledge the examiners, Dr Tjalfe Poulsen and Dr Zheng-Tong Xie and my UoL supervisor Dr Xiaoxiang Zhang for their incredibly valuable comments and feedback which incented me to widen my research from various perspectives.

I also express my thanks to Professor R. H Liu, Yuan Fei Mei from SJTU, China and Professor Tony Bridgwater and Dr Scott Banks from EBRI, Aston University, UK for allowing me to visit their laboratories. These visits provided me good insights into their experiments.

I would also like to extend my acknowledgement to my friends in Suzhou for their support throughout my PhD student life.

Last but not least, a special note of thanks to my parents, and to my wonderful wife Shirisha and little naughty Pranav for their understanding and patience and moreover their unconditional love and support.

I would like to dedicate this thesis to

my parents and teachers.

Contents

List of Figures

List of Tables

Nomenclature

Latin symbols

A_c	Curtain area, m^2
A_w	Window area, m^2
C_D	Drag coefficient
C_{p_m}	Mixture heat capacity J/kg K
d	Droplet/ bubble diameter, m
f	Drag function
f_0, f_1	Functions in the three parameter corresponding state equation
f_l^i	Liquid fugacity, Pa
f_v^i	Vapour fugacity, Pa
F_σ	Surface tension force, N/m^3
g	Gravitational acceleration, m/s^2
G	Superficial gas flow rate, kg/m^2-s
h	Specific enthalpy of the phase, J/kg
H_p^i	Enthalpy of the species
$H_{s,p}$	Latent heat source, W/m^3

H_v^i Heat of vaporisation or latent heat, J /kg

k_m Mixture thermal conductivity W/ m K

K_{pq} Interphase momentum exchange coefficient, kg/m^{3}s

k_p Curvature

L Superficial liquid flow rate, kg/m^2-s

M^i Mole fraction, g/mol

M_m Mixture molecular weight, g/mol

$\bar{M}_{s,p}$ Momentum source vector, N/m^3

$\dot{m}_c^i$ Mass condensed, kg/m^{3}s

$\dot{m}_{qp}$ Mass transfer rate between phase q to phase p, kg/m^{3}s

n Unit normal

p Pressure, Pa

P Pressure, Pa

P^i Partial pressure, Pa

P_c^i Critical pressure, bar

P_{cm} Mixture critical pressure, Pa

P_r^i Reduced saturation pressure

q Heat flux, W/m^2

Q Volumetric rate of energy transfer, W/m^3

$\dot{Q}$ Volumetric flow rate, m^3/s

R Universal gas constant, J/ mol K , atm cm^3/ mol-K in Eq. (10)

Re Reynolds number

$\bar{R}$ Interaction force vector, N/m^3

S^i Species source, mol/ m^3

T Temperature, K

T_b^i Boiling temperature, K

T_c^i Critical temperature, K

T_r^i Reduced temperature

T_{rm} Mixture reduced temperature

t Time, s

U_f^n Volume flux, m^3/s

Vc Curtain velocity, m/*s*

Vw Window velocity, m/s

V_c^i Critical volume, cm^3/mol

x^i Mole fraction

y^i Mass fraction

Z_c^i Critical compressibility factor

Greek symbols

α Volume fraction

γ Universal coefficients used in f_0, f_1 functions

λ The dimensionless parameter used in bakers chars.

μ Dynamic viscosity, Pa – s

μ_m Mixture viscosity, Micro Poise (μP)

v Velocity vector, m/s

ξ_m Inverse viscosity, μP^{-1}

ρ Density, kg/m^3

ρ_{rp} Volume averaged density, kg/ m^3

σ Surface tension, N/m

τ Particulate relaxation time, s

τ^i Inverse of the reduced temperature

$\bar{\bar{\tau}}$ Stress tensor, N/m^2

ϕ^i Fugacity coefficient

ϕ^i_{sat} Fugacity coefficient at saturation condition

ψ The dimensionless parameter used in bakers chars.

ω^i Acentric factor

Subscripts

A Air

b Properties at boiling point

c Critical properties

f face index

p, q Phase index

pq Volume averaged properties

l	Liquid
g	Gas
m	Vapour mixture
max	Maximum value
W	Water

Superscripts

i	i^{th} specie

Chapter 1 Introduction

1.1 Overview

The aim of this project is to develop a modelling strategy for multiphase-multicomponent flow within liquid collection systems used in pyrolysis processes. This approach will be used as a tool to aid the design and development of efficient liquid collection systems for bio oil production. The computational dynamics (CFD) software ANSYS FLUENT has been used as the computational platform in this project with in-house code which enhances the current capability of the commercial software. The supporting computational work conducted at XJTLU, whilst experimental works at the Bio Energy Research Group (BERG) of Aston University was leveraged for validation of the computational models.

1.2 Background

The demand for fossil fuels such as natural gas, petroleum, as well as coal-based fuels has been increased over past few decades due to the rapid growth in terms of global industrialization and development. Moreover, the depletion of fossil fuel reserves coupled with the increasing energy consumption and greenhouse gas emissions poses new challenges. These factors put thrust on the development of a range of novel technologies for the utilisation of renewable energy resources, such as biomass, solar and wind energy. In addition, many countries pledged to reduce the greenhouse gases, which have further intensified the need for renewable energy sources [1].

The use of renewables, in particular biomass as a source for energy, in industrial and non-industrial sectors, is one of the alternatives that can contribute to decreasing the share of fossil fuels [2]. Moreover, this will also lead to the reduction of greenhouse gas emissions [3]. Carbon balances of energy from different fuels can be seen in the Figure 1.1. This clearly highlights the key benefit of using biomass as an alternative for the fossil fuel. When compared with other renewable energy sources used for the production of heat and power, biomass stands as the only source for solid, liquid and gaseous fuels [4].

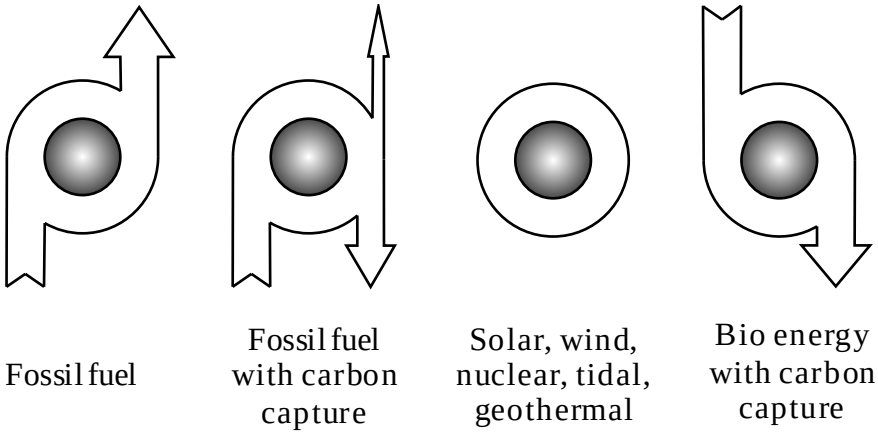

Figure 1.1– Carbon balance of energy from different sources.

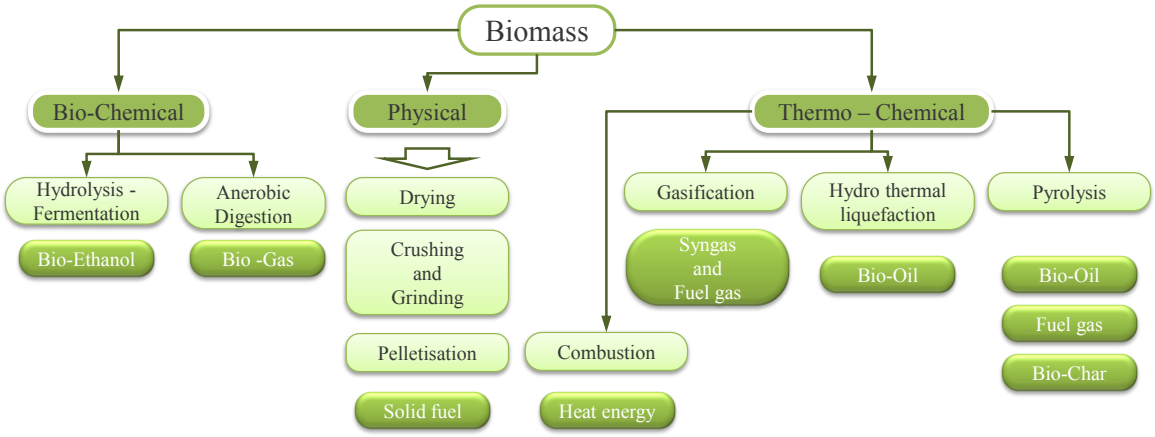

Figure 1.2– Biomass conversion paths for energy generation.

Figure 1.2 shows various ways of converting biomass into useful forms of energy. Among all the conversion techniques available, the fast pyrolysis process presents certain advantages for the generation of liquid fuels [4]. The biomass fast pyrolysis process can provide a liquid fuel that has the potential to be a substitute for fossil fuel oil in any static heating or electricity generation application [4-6].

Pyrolysis is a process where the organic matter undergoes thermal degradation in the absence of oxygen to produce condensable vapours, non-condensable gases and char. In the present work, the condensable vapours are also denoted as liquids. Slow pyrolysis has been used from ancient times to produce charcoal, whilst more recently the fast pyrolysis process gained popularity for its capability to produce higher yields of liquids. In the fast pyrolysis process, the thermal decomposition of biomass occurs at moderate temperatures (around $500^{O}C$) and very short reaction times (around 2 s) with higher rates of heat transfer in the reaction zone. The process results in high yields of liquids (bio-oil) of up to 75 wt. % which can be used directly in a variety of applications or used as an efficient energy carrier in the upgraded form [7, 8].

In the fast pyrolysis process, the liquid bio-oil is produced by the rapid condensation of pyrolysis vapours within the heat exchangers called liquid collection systems (LCS). Several types of heat exchangers are available for this purpose, ranging from simple indirect contact heat exchangers to more complicated and sophisticated quenching columns and spray columns. Inert gas like nitrogen is used to transport the pyrolysis vapours from the reactor to the heat exchanger with the aim of minimising the residence time to avoid secondary reactions. This is unavoidable as the higher residence time results in secondary reactions which will eventually reduce the liquid yields and convert vapour into permanent non-condensable gases [9, 10]. The presence of these transport gases in the system, pose significant resistance to the heat and mass transfer, and thereby forcing the conventional indirect contact heat exchangers to larger sizes. Indirect contact heat exchangers can also cause preferential deposition of lignin-derived components, leading to liquid fractionation

and eventually blockage of the pipelines and consequently the heat exchanger itself [4]. Hence the direct contact heat exchangers are more preferable in pyrolysis processes over indirect contact heat exchangers.

Several types of direct contact condensers are deployed in the fast pyrolysis liquid collection systems like spray columns and quenching columns. These direct contact heat exchangers, significantly minimise the previously stated limitations and provide greater surface area of contact between coolant and vapour which helps rapid cooling of the vapours as well as in capturing the condensed aerosols. The quenching column described in the current work uses either recirculated liquid bio-oil or an immiscible hydrocarbon solvent as a coolant medium. The advantages in using quenching columns for the condensation of pyrolysis vapours are the high heat transfer rates that can be obtained by the direct contact of the two working fluids, as well as the greater amount of gas scrubbing that can be achieved, something that could potentially lead to the complete removal of the electrostatic precipitator (ESP). This contributes in the reduction of the overall cost of the process, while making it more economically viable on a large scale.

Recently, the sequential condensation of the pyrolysis vapours is gaining significant popularity [11 - 13]. The advantage of sequential condensation is that different fractions of bio-oil can be produced with different compositions so that the partial upgrading process can be achieved within the pyrolysis process. This will also contribute to the overall thermal efficiency of the plant [14, 15]. For the previously stated reasons, it is essential to understand the physical behaviour of the flows within the liquid collection system so that efficient designs can be developed.

From the process point of view, rapid condensation of pyrolysis vapours is necessary to increase the final bio-oil yield. The design of efficiently operating quenching columns, using empirical relations, becomes extremely difficult, due to the high complexity of the physical phenomena involved in the process. The thermodynamics condenser model developed by Westerhof et al. [11], based on the well-known Rachford-Rice formulation [16], provided an

insight on how the water yield can be controlled during the pyrolysis vapour condensation process. However it only provides the mass balances, while it lacks the spatial and temporal hydrodynamic and thermodynamic details that are absolutely necessary for the development of efficient quenching column designs. The gas-liquid interactions, both in terms of mass, momentum and heat transport, result in complex flow regimes inside the quenching column, something that is difficult to predict by experimentation and physical models alone. Under these considerations, the employment of computational methods to provide an insight on the physical phenomena present in the process (i.e. hydrodynamics, heat transfer and phase change phenomena) becomes necessary.

1.3 Aims and objectives

The aim of the current work is to expand the capabilities of numerical modelling and build a strategy to simulate complex phase interactions such as mass, momentum, heat transport and phase transition phenomena among biomass pyrolysis vapours, liquid bio-oil and liquid coolant in direct contact heat exchangers. The model takes into account the gas-liquid interactions including the simultaneous condensation of pyrolysis vapours into liquid bio-oil.

Multiphase-multicomponent flows occur in the majority of processes like combustion, evaporation, pyrolysis, pneumatic transport, condensation etc. The understanding of the physical phenomena that govern such processes is extremely valuable as well as the incorporation of these physical laws into the mathematical models can be extremely useful in the efficient design and optimisation of the equipment used in the previously mentioned processes.

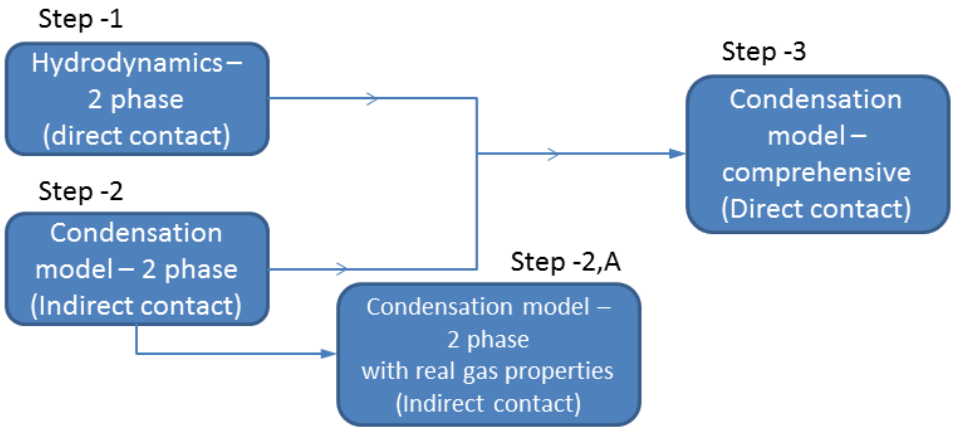

Figure 1.3– Steps followed for the development of the condensation model.

The scope of the present work is the numerical investigation of the liquid vapour interaction within the liquid collection system used in the pyrolysis process, where the condensation of the pyrolysis vapour leads to the formation of liquid bio-oil. In this study, a three-step approach has been implemented. In the first step, detailed hydrodynamics and heat transfer behaviour has been investigated within the quenching column which is a direct contact heat exchanger. In the second step, the condensation model has been implemented in an indirect contact water cooled condenser and validated against experimental data. Based on these two steps, a final comprehensive condensation model can be developed and applied in the quenching column. The steps followed in this work are better illustrated in Figure 1.3.

In the first step, the computational method developed to study hydrodynamics, was applied to a 5 kg/hr feed rate fast pyrolysis system. The quenching column used in the experimental setup at Aston University was chosen as the basis for the base line model. In the experimental investigation, it was mentioned that the quenching column suffered from flooding phenomena [17]. Hence, the investigation in the first step was focused on the mitigation and elimination of the flooding phenomena. Modified design variants of the quenching column were compared and the optimal design was proposed based on the numerical results.

In the second step, the condensation model was developed and implemented on a 100 g/hr bench scale reactor. The model geometry and operating conditions are similar to the experimental setup at Aston University. In this model the phase change phenomena between the condensable vapours and liquid bio-oil were studied and compared with the experimental data.

A comprehensive condensation model was implemented based on the two step studies and applied on the optimised design of the quenching column. This numerical model can be used for any type of condenser of this kind and is especially useful for optimisation studies. As an extension to the step 2, in the step 2A, the assumption of ideal gas has been assessed and compared with real gas models for future model developments.

The commercial code FLUENT which is based on the finite volume method has been used as the basic platform for the development of the comprehensive condensation model. This model uses extended subroutines in the form of user defined functions (UDF) to simulate the heat and mass transfer phenomena within the liquid collection systems in the pyrolysis process. This work is focused on the development of the code that extends the computational capabilities of FLUENT in order to model and analyse the following:

- Development of the baseline quenching column model based on the 5kg/hr experimental setup which uses octane as the coolant liquid entering the column at -5^{O}C.
- Column flooding phenomena and their relation with flow rates.
- Residence time of the vapours within the equipment.
- Temperature and pressure variations along the flow path of the vapours.
- Interphase heat exchange between liquid coolant and pyrolysis vapours.
- Impact of the disc and donut configuration on the temperature and pressure profiles.
- Evolution of the liquid bio-oil from the condensable pyrolysis vapours during the condensation process.

- Investigation of the condensation process to determine the influencing parameters like composition, temperature, pressure and design.

The physics involved in the simulation of the liquid collection system involves

- Multiphase-multicomponent flow of gas/liquid mixtures.
- Tracking of the miscible and immiscible interfaces between phases.
- Heat transfer between the coolant and the vapour.
- Mass transfer between vapour and liquid via phase change during the condensation.
- Momentum transfer due to phase change.

The computational model implemented for each one of the physical phenomenon according to the following procedure:

- Description of the computational models and methods used.
- Presentation of the physical principles that govern the process.
- Implementation of these principles in the computational model as an extension of the commercial code.

1.4 Elements of novelty

Numerous studies in the literature have been focused on simulating the hydrodynamics of fluidised beds or cyclones in the pyrolysis technology. As far as multiphase flow is concerned, most of the literature is focused on distillation column modelling without considering the heat transfer effects on it. Only few attempts to date have been identified on liquid collection system modelling using computational methods. None of these studies was focused on the quenching column which is a type of liquid collection system used in pyrolysis technology presented in the literature. As a matter of fact even the majority of the experiments related to the pyrolysis technology paid little attention to the liquid collection system design and its optimisation.

The novelty of the current work is the development of the comprehensive numerical condensation model for the quenching column used in the fast pyrolysis process and in the broader sense for any type of liquid collection system. This study investigates the detailed flow behaviour inside the liquid collection systems which includes hydrodynamics and phase change phenomena.

This numerical model provides the detailed selective condensation characteristics occurring within the condenser while pyrolysis vapours undergo phase change. This model also presents the way to represent the complex mixture of pyrolysis vapours in terms of simplified composition which eventually reduces the computational resource requirements. This work proposes an optimum quenching column design for better performance and better scalability.

This numerical model can be applied to different size physical models ranging from lab scale to industrial scale with suitable modifications to turbulence models according to the flow regimes. Different type of condensers either direct or indirect contact exchangers can be modelled using the developed numerical code. This general form of the computational code can be applied in different processes where multiphase flow involves condensation phenomena and where evaporation is neglected.

1.5 Progress of the research

The research started with the review of the literature on existing pyrolysis technologies and their liquid collection systems for the production of bio-oil. The operating principles of these technologies and their advantages and limitations were identified. A detailed review was also conducted to identify the appropriate numerical models. In order to cater to the aim of the project which is to develop a CFD methodology to design a liquid collection system for the bio oil production, a detailed three step strategy was formulated. Extensive focus was kept on understanding FLUENT's code structure to develop a customised code to enhance its

capabilities in phase change physics under multi-phase and multi-species regime which are essential for the development of the condensation model.

In order to understand the principles of the selective condensation, literature related to the fundamentals of physical chemistry and thermodynamic concepts were reviewed especially from the chemical engineer's perspective. With this understanding multiphase-multicomponent flow specific user defined functions (UDF's) were studied and practiced for the implementation of the condensation modelling. Different pyrolysis methods applied to bio-oil production were also reviewed.

Initially, 2D simulations of the multiphase flow in the quenching column were attempted. These studies showed that 2D models are not sufficient to capture transient and highly three dimensional features of the flows. For that reason, 3D models of the quenching column have been developed as a part of the step 1 program. In this step, several sensitivity studies were conducted on the gas and coolant flow rates to investigate the hydrodynamic and flooding phenomena. Based on the knowledge acquired from the CFD simulations on fluid flow behaviour, the quenching column design was suitably modified and simulated. From the CFD simulations it was observed that the modified models gave better performance in terms of heat transfer and flow rates. On the basis of these results a new set of disc and donut configurations were proposed.

With the help of the concepts gained while reviewing the physical chemistry and the previous work done on the condensation models, a new condensation model was developed as part of step 2. This model included detailed species transport which accounts for the condensation of individual components in the pyrolysis vapours. Thereby it allows us to study the selective condensation phenomena and be validated by the previous experiments highlighted in the literature. As an extension to step 2, a comparative study was conducted to investigate the effect of the real gas and ideal gas consideration. This study provides a clear understanding of the significance of an ideal gas assumption in contrast to the real gas behaviour.

The basic target of the project was achieved when the step 1 and step 2 methods were used and deployed in step 3. This is having three distinct multicomponent phases (vapours together with transport gases and non-condensable gas, as well as coolant and condensed bio-oil). This computation was done by coupling species transport modelling together with the hybrid Eulerian-Eulerian multiphase model. The source terms were calculated using user defined subroutines to account for heat and mass transfer together with momentum transfer.

During this period, parts of the research work were published in international journals and presented at three international conferences. The details of the research have been thoroughly analysed in the following chapters of the Thesis.

1.6 Report structure

This section outlines the report structure and gives a brief depiction of each chapter, starting from chapter two.

The second chapter introduces the liquid collection systems and explains their importance in pyrolysis technology. The scope of the subject is analysed and the different physical processes that occur within the liquid collection system are explained. It also details the existing literature on various experimental models as well as relevant numerical models.

The computational models and theory used in this work are detailed in the third chapter. Justification is also provided for the model selection for carrying out the simulations. The formulation described in chapter 3 has been used throughout this work unless otherwise stated.

The fourth chapter focuses on the formulations used for computing the fluid properties. The liquid-vapour equilibrium formulations which form the basis for the condensation model are also described in this section. The selection of each empirical relation for the computation of the mixture properties is mentioned in this chapter with justification and sample calculations.

The fifth chapter provides a brief outline about the existing quenching column design and its operating conditions which forms the platform for this work. This section is entirely dedicated to the results obtained from steps 1 to 3. The first part of the analysis presents the quenching column design optimisation on the basis of hydrodynamic modelling. In step 2, the model is tested for fractional condensation and validated with experimental results. In addition, a real gas model is also developed and compared against the results obtained from the ideal gas model. Finally in step 3, a combined model obtained from step 1 and 2 is applied in the quenching column with the detailed mass transfer mechanisms associated with three distinct multi-component phases. The impact of the number of disc and donut stages of the column in the overall conversion of the pyrolysis vapours into liquid bio-oil is also investigated and analysed.

The sixth chapter provides the summary of the main findings of the research and highlights the limitations of the developed model. Recommendations for future work are also listed at the end of this chapter.

Chapter 2 Literature review

This chapter introduces the liquid collection systems and explains their importance in the pyrolysis technology. The scope of the subject is analysed and the different physical processes that occur within the liquid collection system are explained. It also details the existing literature on various experimental models as well as relevant numerical models. The following section provides a brief outline about the existing quenching column design and its operating conditions which forms the platform for this work.

2.1 Fast pyrolysis

Pyrolysis is a thermochemical process where the biomass undergoes thermal decomposition in the absence of oxygen. It is typically classified into three categories slow, intermediate and fast pyrolysis respectively based on the heating rates. Fast pyrolysis produces three global products from biomass namely non-condensable gases, solid char and condensable organic vapours at various proportions depending on the conditions. The process can be seen in Figure 2.1. Compared to the other conversion processes such as gasification or carbonization, this process produces higher bio-oil yield [18]. Condensable vapours are converted into bio-oil in the liquid collection systems which can be used as fuel or a source for various chemicals. The typical vapour composition consists of condensable vapours of low molecular weight chemicals, water vapours and complex oxygenated compounds. Water vapour in bio oil is either produced during the pyrolysis process or due to the original feed moisture content.

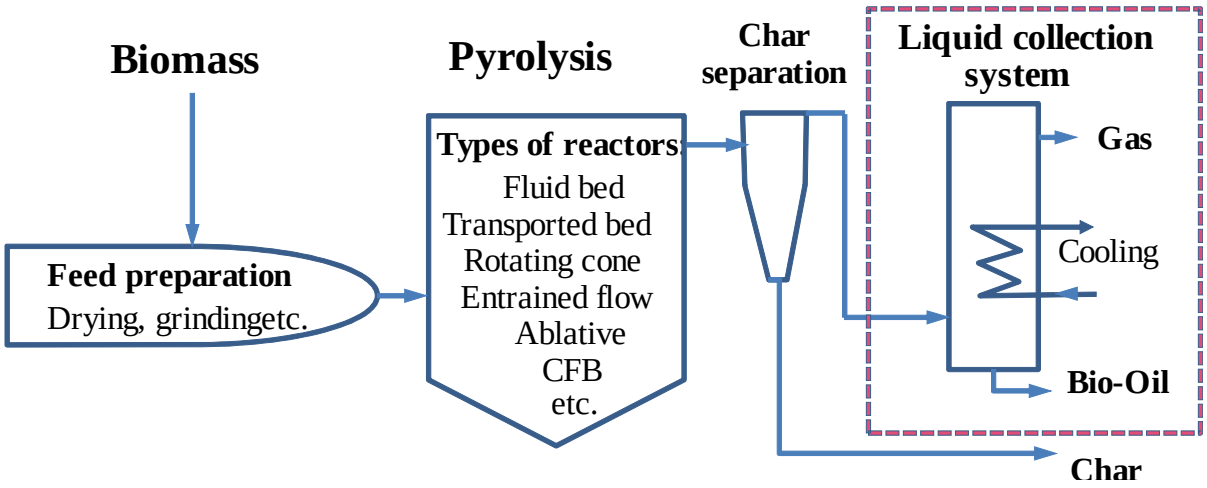

Figure 2.1– Fast pyrolysis process map.

In order to gain maximum yield of the bio-oils, the vapours must be transported from the pyrolysis reactor to the heat exchanger as quickly as possible (<0.5 s) mainly for two reasons. First, when the pyrolysis products are cooled below 400^{O}C, the hydrocarbons can combine to form visible aerosols which are tiny particles. These particles can readily stick to the surfaces which are less than 400^{O}C temperature thereby causing fouling problems. Secondly, if the vapour products are maintained above 450^{O}C for more than one second, secondary reactions will occur within vapour phase. To avoid these conditions, additional gas is supplied as a transport agent for the pyrolysis vapour. As the pyrolysis reaction needs to be carried out in an oxygen free environment, an inert gas such as nitrogen is used in varying proportions, depending on the reactor configuration. Some of the early types of pyrolysis reactors, as highlighted by Boukis et al. [19] are presented in Table 2.1.

Table 2-1 – Reactor types employed in pyrolysis process

Reactor type	**Organisation/country**	**Mode of heat transfer**
Up flow entrained flow bed	GTRI / USA [20]	5–10% Conduction 95–90% Convection
Down flow entrained flow bed	Egemin / Belgium [21]	5–10% Conduction 95–90% Convection
Fluidised bed	Univ. of Waterloo/Canada [22] Union Fenosa/Spain [23]	80–90% Conduction 20–10% Convection
Transport reactor	Occidental Research Corporation USA. [24] Ensyn, Inc./Canada [25]	30–40% Conduction 70–60% Convection 50–60% Conduction 50–40% Convection
Ablative pyrolysis systems	NREL/USA [26] Aston University/UK [27]	10% Convection 90% Conduction
Vacuum pyrolysis	University Laval/Canada [28]	

Before sending the pyrolysis products to the liquid collection system, char and suspended solid particles must be removed from it. This is mainly due to its catalytic nature which increases the vapour cracking and there by reduction in liquid yield. The conventional

technique for the removal of char and solids involves either cyclones or hot gas filtration. In the work of Diebold [29] it was shown that hot gas filtration is highly efficient. However, it is pointed out that the typical bag house residence time is approximately 6 seconds, which triggers secondary reactions within the vapours and eventually reducing the yield of liquids. For the above reasons cyclones are widely used to remove the solids. After the removal of suspended solids and char, it is necessary to condense and collect the liquid which is also referred as bio-oil.

2.2 Liquid collection system (LCS)

Understanding of the physics of the liquid collection has long been a major difficulty for the practicing engineer as well as for the researchers. Bridgwater [30] compared the pyrolysis products with the smoke emanating from cigarettes which has similar properties. According to this study, nearly all liquid collection devices used in the fast pyrolysis systems are inefficient in capturing condensable vapours.

As mentioned previously, the condensable vapours are present in large volumes of non-condensable gases at relatively low concentrations which present a significant heat and mass transfer resistance within the heat exchangers. The product vapours coming out from the pyrolysis reactor are in the form of mist or fumes which are not considered as true vapours. Moreover, the pyrolysis vapours characterised as a combination of micron sized droplets and polar molecules bonded with water molecules together with true vapours. This contributes to the collection problem as the requirement for the surface area is very high to capture the aerosols even after cooling below the dew point temperature [30]. This makes the usage of conventional heat exchangers inappropriate in this environment. In addition to this, pyrolysis liquids also cause significant fouling problems which make conventional heat exchangers inoperable.

ESP's are effective and many leading research laboratories (e.g. EBRI, SJTU) employ them at the end of liquid collection systems. However, they have inherent problems of blockages caused by the condensed heavy compounds. They are also more prone to get short out as the polar nature of the condensing products causes arcing while it flows. Currently the ESP's are the preferred method to capture aerosols at smaller scales up to pilot plants [4]. For large scale applications, they are considered expensive from the process economics point of view.

2.3 Experimental works

Although liquid collection systems are necessary and vital components in all pyrolysis processes, there is no significant amount of work done so far on their design. Extensive reviews have been conducted on the pyrolysis technology by Bridgwater and Peacocke [31]. From these reviews, one can see that the majority of the systems use direct contact heat exchangers for condensing the pyrolysis vapours. Many of the systems are multi-stage with multiple liquid collecting systems which aim at fractional condensation.

Fractional condensation is very important in the field of biomass pyrolysis. This is mainly due to the bio-oil properties which are highly dependent on chemical composition. The bio-oil properties can be significantly improved via catalytic reactions like cracking and hydro-treatment. However the main drawback is the economic viability as the liquid yield obtained from these methods is very low [32]. Bio-oil is a mixture of different compound groups which react under different conditions with different catalysts which makes it more difficult for the hydro-treatment [33]. For this reason, an efficient fractionation of bio-oil is necessary before upgrading it [34, 35]. Many experimentalists tried to achieve this by using different types of liquid collection systems.

In this report, the liquid collection systems are broadly classified into two types based on the method of cooling. The first one is the indirect contact condensers and second being direct

contact condensers. The condensers used in the pyrolysis process are briefly mentioned in the following paragraphs.

2.3.1 Indirect contact condensers

Due to their simplicity many of the experimental works use indirect contact condensers as their liquid collection systems. In indirect contact condensers, the vapours are passed through a liquid-gas heat exchanger. The cooling medium is thus separated from vapour stream. This has two main advantages; first one being the non-contamination of the cooling medium while the second one being that a separation stage is not needed to separate the bio-oil from the cooling medium. The details of the experimental setups which use indirect contact condensers as LCS in pyrolysis process are listed below.

A) BERG (Aston University):

The Bioenergy Research Group (BERG) at Aston University is a leading research group in fast pyrolysis with regular reviews on the process [36, 37]. The group's main focus is on applied research in all aspects of the fast pyrolysis process, starting with biomass preparation [38] and fast pyrolysis in fluid bed and ablative pyrolysis reactors from 100 g/h to 5 kg/h [39] with the backing of CFD modelling [40 - 46]. BERG has also been involved in the design and development of liquid collection and quenching systems.

With regards to liquid collection systems, indirect contact condensers are deployed for lab scale pyrolysis process with a feed rate of 150 g/hr. [47, 48]. Salter [48] employed two sets of liquid collection systems one with a three stage unit as shown in Figure 2.2 and another one with a two stage as shown in Figure 2.3. In the first unit, there is a provision for collecting three liquid bio-oil fractions, whereas in the second unit only one main liquid bio-oil collector and a small secondary bio-oil collector.

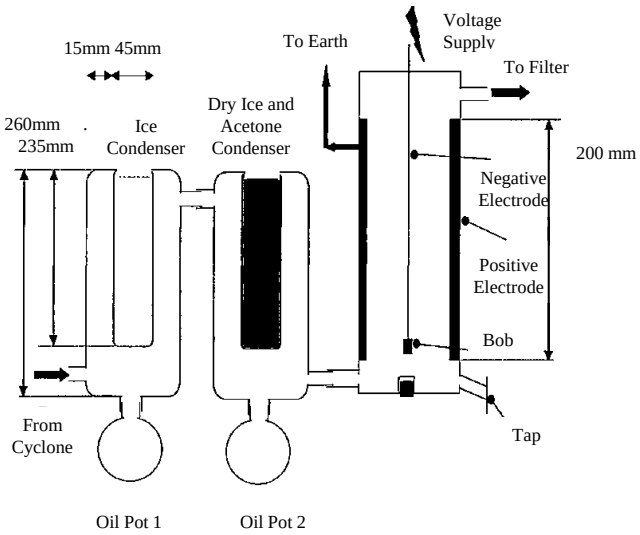

Figure 2.2– Three stage liquid collection system [48].

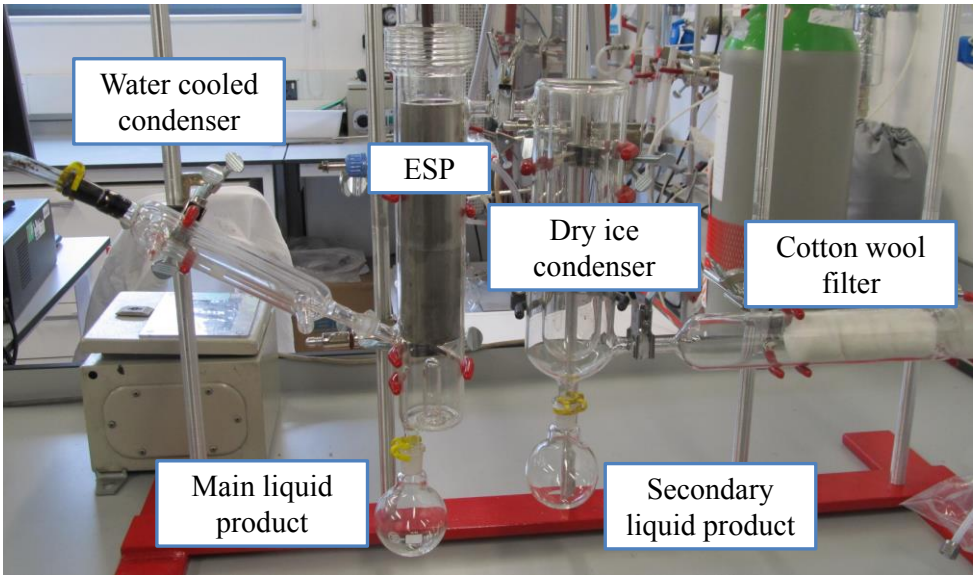

Figure 2.3– 150g/h single product water cooled condenser [47, 48].

In both liquid collection systems, the ESP was employed to collect the aerosols and particulates from the vapour. This was mainly to prevent the blockage of the cotton wool filter as the absence of ESP causes significant liquid collection in the filter. In the second type

of condenser, Salter used a Davies type double surface condenser to improve the contact area between the hot and the cold sides. Selecting the Davis type over the Liebig type in which the helical design gives much higher contact area is justified as the latter one is more prone to blockages and difficult to maintain.

According to the Salter's experimental work [48] a water flow of 1 to 2 l/ min at 15 ^{O}C achieved the required cooling of the vapours from 500^{O}C to 29^{O}C. Design of the condensers was carried out by computing the amount of heat transfer with standard LMTD equation.

B) BEERC (SJTU):

The Biomass Energy Engineering Research Centre at Shanghai Jiao Tong University (SJTU) is one of the leading laboratories in China in biomass pyrolysis. BEERC has conducted extensive research on bench scale fluidised bed reactors with biomass feed rate of 1-5 kg/hr capacity as shown in Figure 2.4. The research focus ranges from designing hot vapour filtration [50] to characterisation of bio-oils obtained from different sources of biomass [13, 51, and 52].

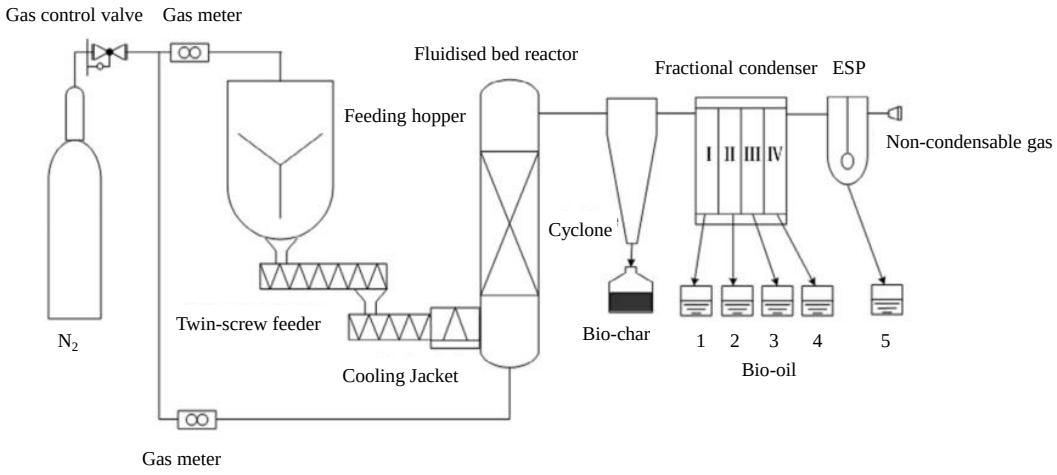

Figure 2.4– Schematic of fluidised bed reactor fast pyrolysis system at SJTU [13].

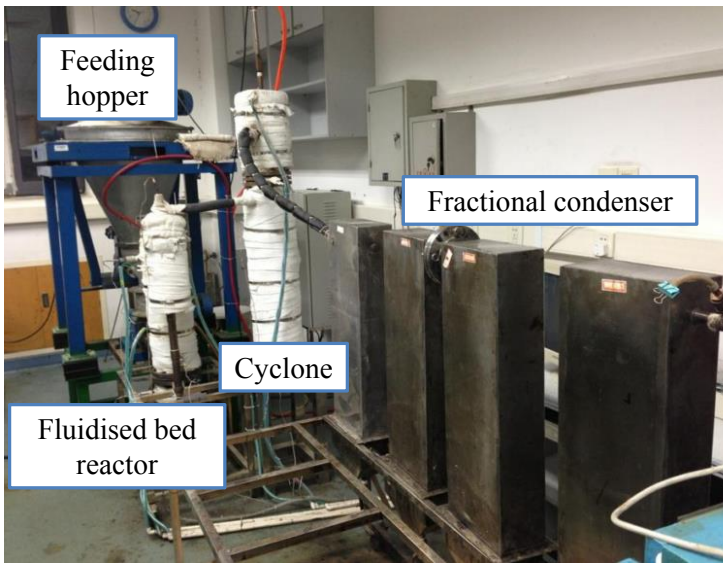

Figure 2.5– Fluidised bed reactor in lab scale at SJTU [49].

The bench scale experimental setup consists of four stainless steel condensers in series to collect the bio-oil fractions as shown in Figure 2.5. Water is used as the coolant medium and circulated through steel pipes within the condenser stages. The ESP was placed at the end of the condenser train to collect the escaping aerosols. The research in BEERC has shown that the fractional condensation is useful to separate water and chemical compounds from the final bio-oil. However most of the bio-oil is collected at the first stage of the condenser while the rest of the fractions are collected near the ESP [13]. Bio-oil yields of the condensers are 65.6, 6, 1, and 10.4% respectively followed by 17% in ESP. This is mainly due to the fact that the temperature of the vapour dropped in the first stage condenser from 500^{O}C to 37^{O}C whilst in the rest of the condensers the temperature of the vapours is 25, 23 and 22.5 ^{O}C respectively. The residence time in the each condenser has been reported to be 3.4 s. The overall bio-oil yield is reported as 43.5% which is well below the theoretical maximum potential bio-oil yield from the fast pyrolysis process. This can be attributed to larger residence times in the condenser coupled with slower cooling rates associated with indirect contact condensers.

C) ARS (USDA):

A bench scale fluidised bed fast pyrolysis reactor with a feed rate of 2.5kg/hr has been built at the Agriculture Research Service (ARS) of the U.S. Department of Agriculture (USDA) [53, 54]. This was constructed to convert energy crops such as switch grass into bio-oil through pyrolysis technology. The collection system comprises of an impinger (vapour jet impinges on free surface of the liquid pool) type condenser system with four canisters inserted in to a chilled water tank as shown in Figure 2.6. The final capture of the bio-oil is done by an ESP.

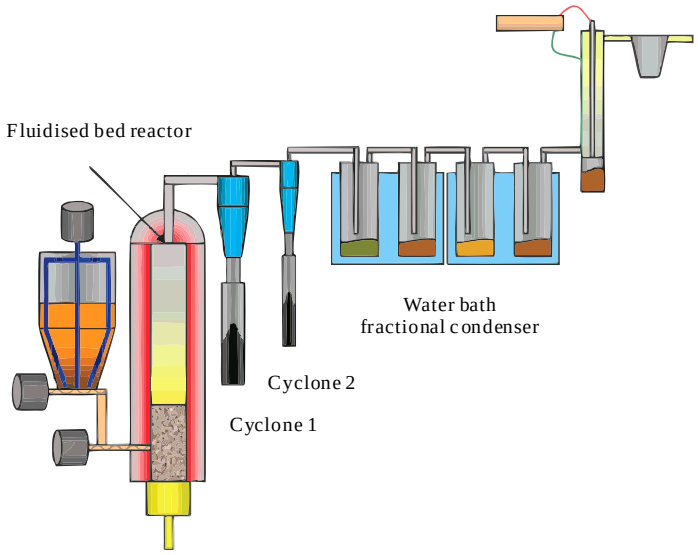

Figure 2.6– Fluidised bed reactor with fractional condensers at ARS [53].

The collected bio-oil at the each canister reported as 27.9, 17, 8.7 and 3.6 % respectively whilst the rest of the quantity, i.e. 42.7 %, was collected in the ESP. This accounts for 60.7% of the total biomass weight. It is worth to note from the finding that the residence time spent by vapours in the first canister is around 1.3 s after the reaction which yielded good condensation as compared to fourth canister where the residence time stretched to 5.7 s. Water content within the bio oil collected from the 2nd, 3rd and 4th canister were similar at about 30 wt.%. In the ESP it ranged from 6-8 wt.%. However the acid number of the

collected bio oil increased linearly from canister 1 to the ESP. This is due to the late condensation of acidic compounds like acetic acids.

D) BCRF (IASU):

Bio Century Research Farm (BCRF) at Iowa State University possesses an 8 kg/h feed rate pyrolysis development unit which has been used to study fractionation of the bio-oil within the liquid collection system [55, 56]. This unit consists of a five-stage liquid collection system comprising of three condensers and two ESPs arranged in alternating sequence as shown in Figure 2.7. The condensers used in this unit are shell and tube exchangers with the coolant being on the shell side while vapours pass through the tubes.

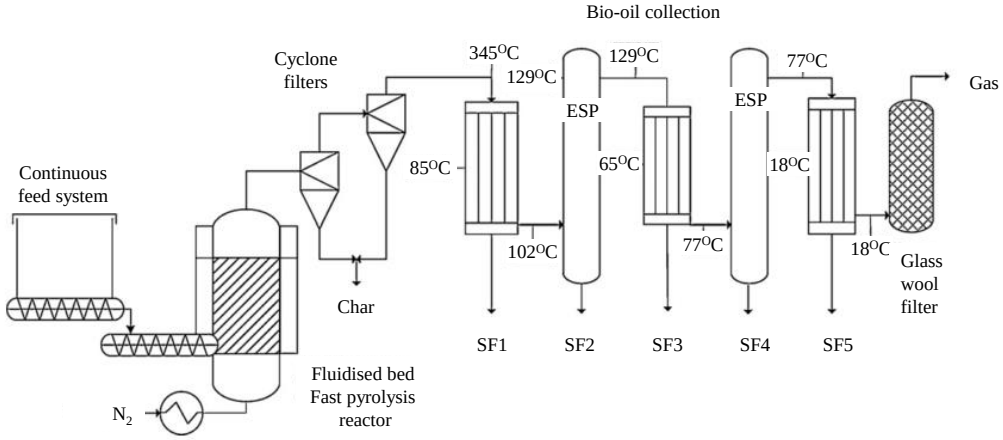

Figure 2.7– Pyrolysis process development unit at BCRF [55].

The coolant temperatures maintained at condensers from the first to the third are 85, 65 and 18^{O}C respectively. The condenser temperatures were designed to collect the fractions according to the dew point temperature. The placement of the ESP between the condensers is to capture the specific fractionate aerosols which are condensed in the preceding stage but escaped from it. From the results it is evident that the weight percentage of water increased from the first condenser to the last stage condenser significantly. Water content in the

collected bio-oil is 6.6, 8, 9, 14.8 and 63.3 on % wt. basis from condenser 1 to 5 respectively. The same trend was also observed for the acid number which is given in sequence from 1 to 5 as 34.9, 31, 79.1, 117.1 and 116.5. In the improved version, the results showed that the liquid collection system was able to recover distinct fractions which are robust in changes to the reactor temperatures and maximum bio-oil collection is around 67% on wt. basis [56].

E) University of Waterloo, Canada

The fluidised bed pyrolysis reactor developed by the University of Waterloo is the first of its kind in terms of selective fractionation by placing two condensers in series [57]. The condensers are simple indirect contact type heat exchangers maintained at 100 and $0^{O}C$ respectively. However the research focus was mainly on the role of the temperatures in the reactor itself, where the liquid yields were correlated with the pyrolysis temperature.

F) LSGC, Universite de Lorraine, France

Laboratoire des sciences du génie chimique (LSGC) ,Universite de Lorraine and Centre national de la recherche scientifique (CNRS) developed an 1 kg/h fast pyrolysis process using cyclone reactor [58 - 62]. For the collection of bio-oil, three water cooled heat exchangers in series is utilised as shown in Figure 2.8. The recovery of the heavy fractions of bio-oil is followed by a refrigerated coil heat exchanger, maintained at $-5^{O}C$, where light oil fraction is recovered. In order to capture the aerosols and recover the final fraction, electro-static and membrane filters are placed at the end of the liquid collection system.

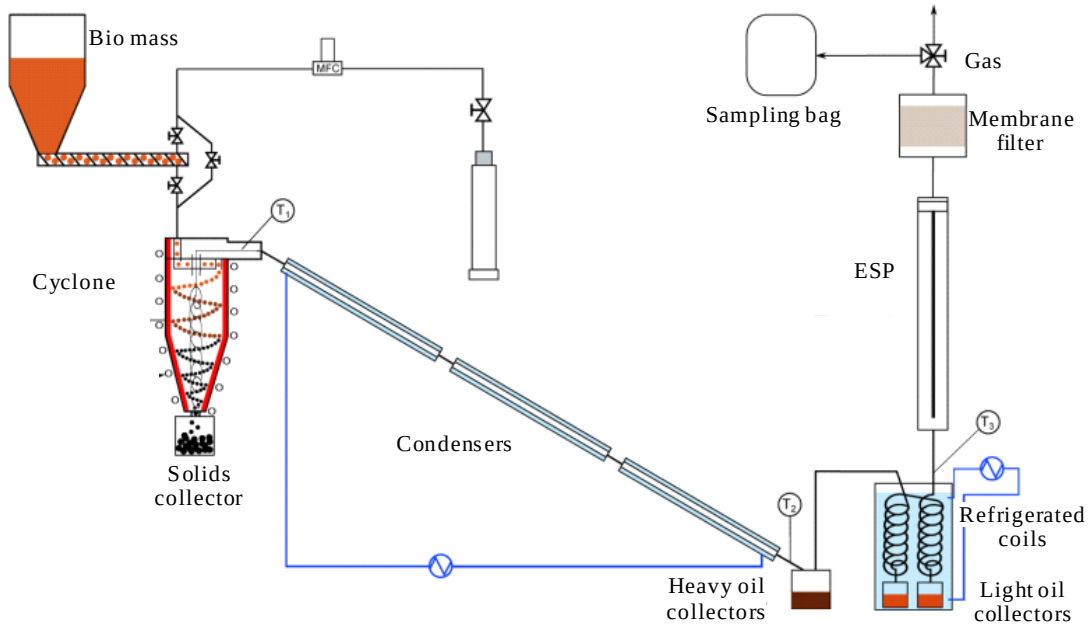

Figure 2.8– Cyclone reactor pyrolysis process unit at LSGC [60].

From the results, it has been observed that the total liquid yield is 62.6 wt. % followed by 25.7 and 11.7 for gas and solids respectively [60]. Heavy oils which contain water, have high viscosities and solid contents, while light oils would be more easily transportable but contain a much higher water content as of 45% [58].

G) Other labs

Williams et al. [63] from the University of Leeds constructed a pyrolysis reactor especially to pyrolyse tyre rubber and used a selective condensation system for the liquid collection. First three condensers are made up of stainless steel followed by a set of glass impingers (acetone and dry ice condensers) as seen in Figure 2.9.

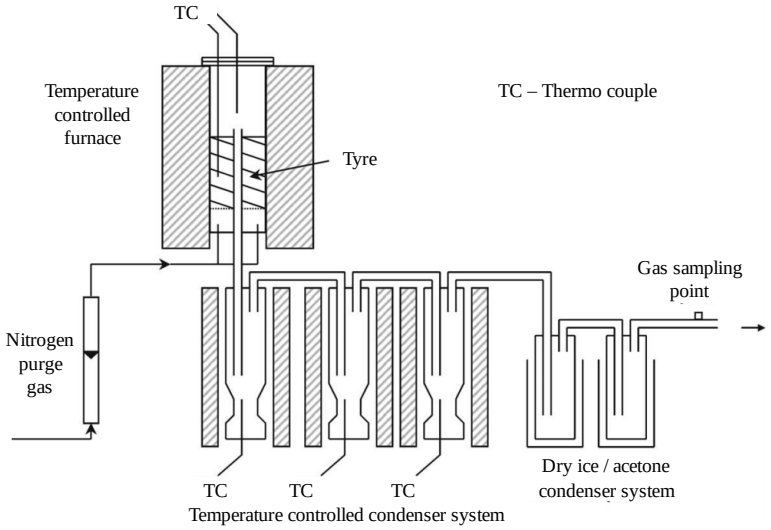

Figure 2.9– Tyre pyrolysis process unit at University of Leeds [63].

The liquid collection system has been tested for different temperatures of 100, 150, 200 and 250 ^{O}C and all steel condensers are maintained at the same temperature at a time. The glass impingers are maintained at -70^{O}C for all experiments. The influence of the temperature on the yield of each condenser can be seen in Figure 2.10 and the maximum yield is around 67% on wt basis.

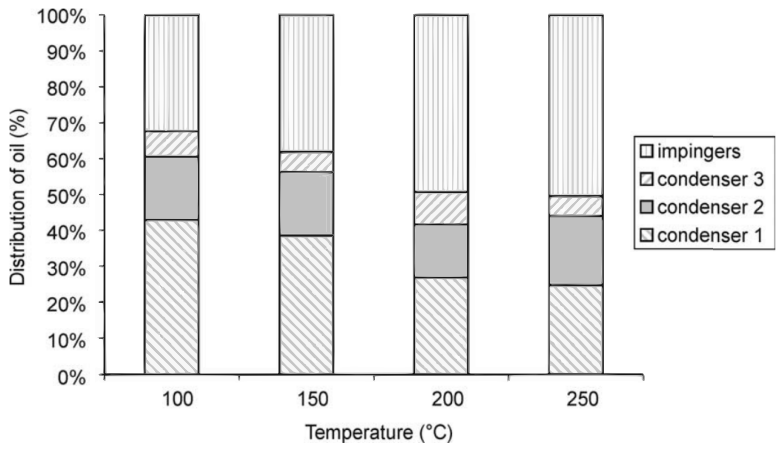

Figure 2.10– Temperature influence on yield of bio-oil at different stages of LCS [63].

2.3.2 Direct contact condensers

In these condensers, the coolant is brought into direct contact with the vapours that need to be condensed. Direct contact condensers (DCCs) possess many benefits as compared to indirect contact type condensers (e.g. shell and tube condenser). These benefits are the lower capital and maintenance costs, simplicity in its design, high heat transfer rates and transfer areas, as well as the elimination of problems with fouling and corrosion especially in the pyrolysis environment. Due to their improved thermal performance, up to 60% less cooling medium is often required than that needed in indirect contact condensers [64]. Moreover, the effective mixing of the two fluids in these type condensers makes it work efficiently under low temperature differences. In the pyrolysis process, two kinds of coolants either bio-oil or immiscible fluid are generally employed for the cooling purposes. There is no need of separation when bio-oil itself is used as the coolant whereas in the case of any immiscible fluid, it should be easily separable from bio-oil.

There are different types of direct contact condensers employed within the pyrolysis technology namely bubble, spray and film type condensers. Despite their popularity only few research groups have included direct contact condensers as their liquid collection system.

A) TCCB (University of Twente):

The Thermal Chemical Conversion of Biomass (TCCB) group at the University of Twente is actively working on converting biomass to biodiesel and bio-chemicals. They developed a one kg/hr, fluidised bed pyrolysis reactor as process development unit (PDU) to obtain proof of the principle data. Two counter current spray condensers are used as the main liquid collection system with a provision of collecting bio-oil fractions separately from them [11, 12, 65]. The arrangement of the condensers can be seen in the Figure 2.11. At the end of the LCS, an intensive cooler has been placed which operates on the knockout principle in which a quick change in gas direction takes place.

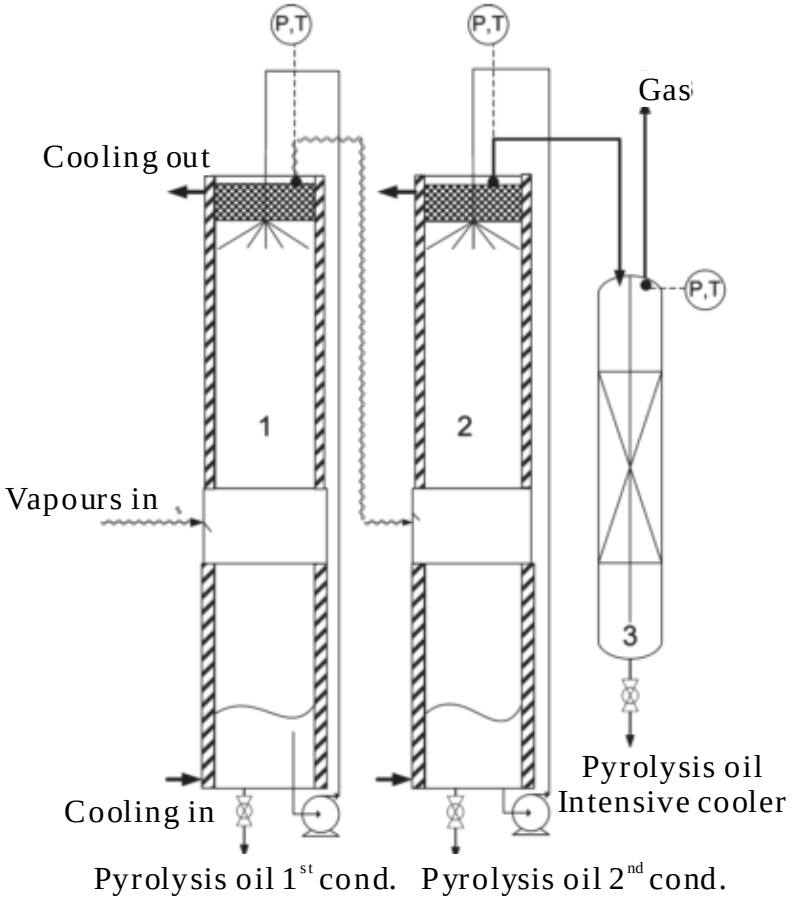

Figure 2.11– Counter current liquid spray column used in LCS [12].

In this system, Shell Ondina oil 917 was used as the coolant liquid. The vapour temperature at the entry of the first condenser is maintained at 400^{O}C while its exit temperature varies between 20 to 115^{O}C. The second condenser is kept at a constant temperature of 20^{O}C. The yields of bio-oil from the given biomass are given in the Figure 2.12.

From the results it was observed that up to 10% of acetic acid was captured in the second condenser when the first condenser operated at 70-90^{O}C. Under the same conditions, the bio-oil fraction collected from first condenser has less water (10-4 %) and less acetic acid (2-3%), which makes it more suitable for using as a fuel in transport sector.

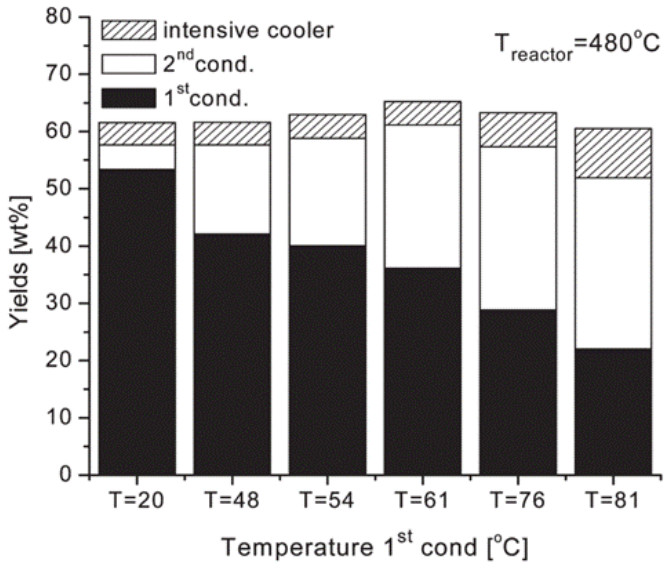

Figure 2.12– Bio-oil distribution at various stages condenser1 [12].

B) BERG (Aston University):

The Bioenergy Research Group (BERG) at Aston University has developed a novel ablative pyrolysis reactor [68, 69]. Even though the reactor is capable of handling up to 30 kg/hr, the actual pyrolysis of biomass that has been carried out in this unit is up to 3 kg/hr due to the feeder limitation. To collect the liquid bio-oil, a counter flow direct contact condenser also called quenching column was utilised as shown in the process flow diagram in Figure 2.13. At the end of the LCS, an ESP has been placed to capture the aerosols. Octane which is immiscible with the condensed bio-oil was utilised as a liquid coolant.

The pyrolysis reaction was carried out at 550^{O}C with a feed rate of approximately 1 kg/hr. The liquid coolant temperature was maintained at -5 ^{O}C. The liquid bio-oil yield obtained was up to 65 % including the water content. However, it was reported by Robinson [17] that the quenching column suffered from flooding during its operation. For that reason the flow rate of the coolant was reduced which significantly affected the final liquid bio-oil yield in later operations.

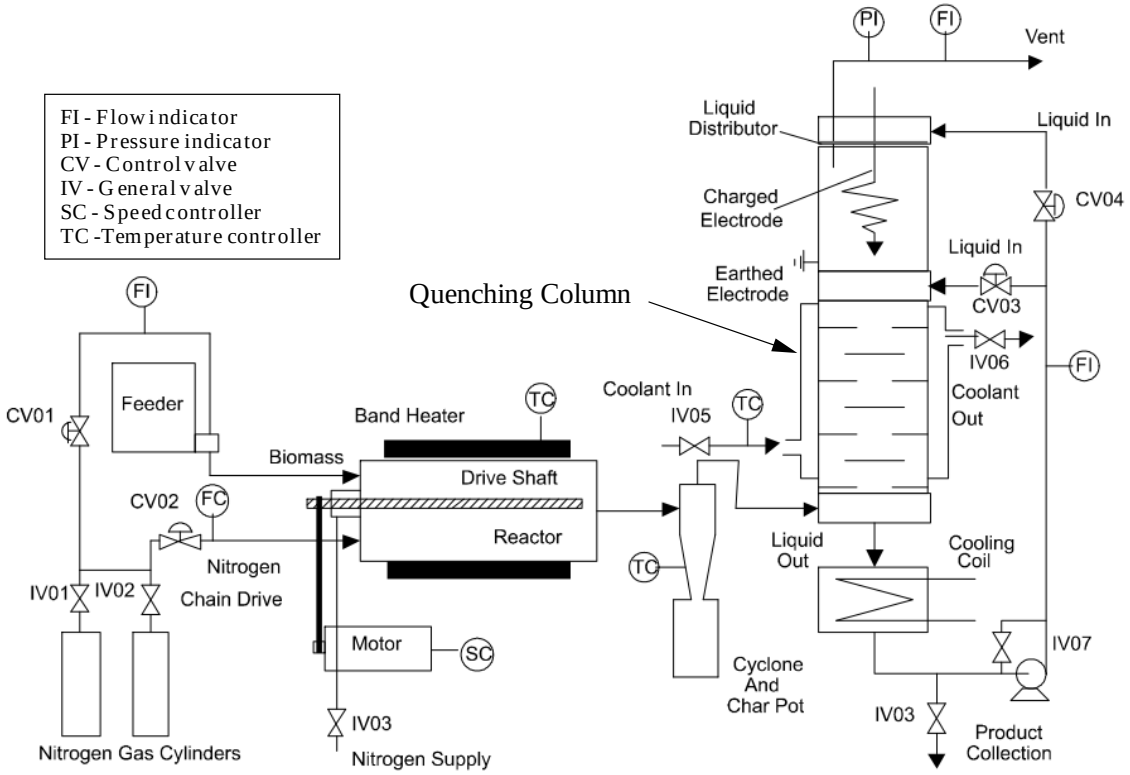

Figure 2.13– Ablative pyrolysis process flow diagram [17].

Due to the flooding issues faced earlier with the counter flow quenching column, the co-current configuration was developed for the 300 g/hr pyrolysis unit. This unit can be seen in Figure 2.14, where a dry ice condenser was placed after the ESP to collect the lighter fractions.

In their later works on the 1 kg/hr systems the co-current quenching column is utilised [72, 73]. Iso Par was used as the liquid coolant to quench the hot pyrolysis vapours. However from the observations, it was reported that the quenching column was frequently blocked due to the condensation of the heavy compounds forming on the plates within the quenching column [74].

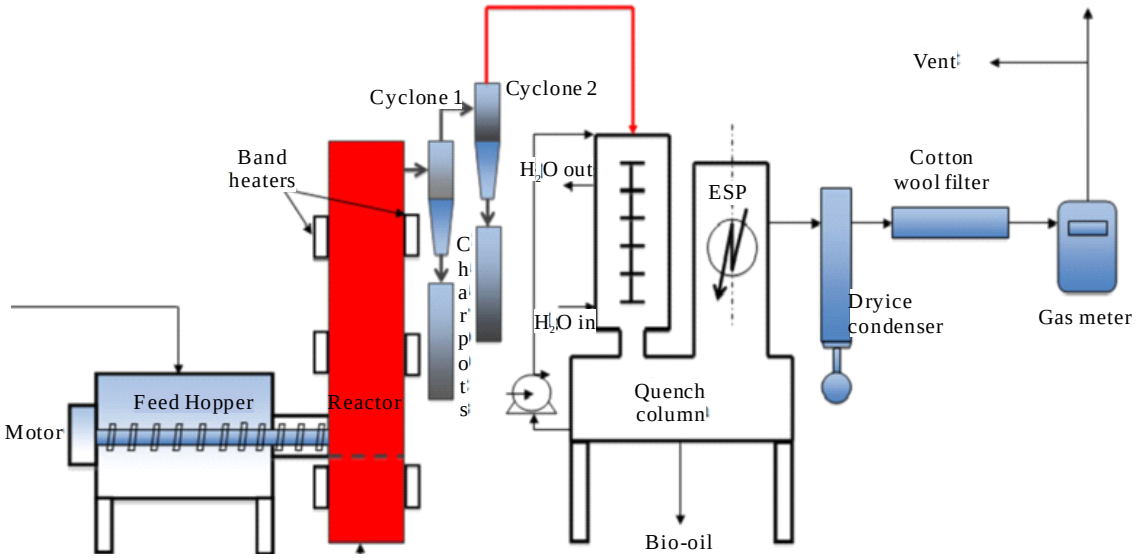

Figure 2.14– Process flow diagram for 300 g/hr unit [71].

2.4 Design of direct contact condensers used in pyrolysis.

The collection of liquids has been a major bottleneck in the operation of fast pyrolysis processes due to the nature of the condensable product which is mostly in the form of aerosols rather than true vapours [31]. Quenching, i.e. direct contact with the cooling medium is efficient but it needs careful design and control of temperature to avoid blockage and flooding. Many of the experimental systems mentioned previously have been focused either on reactor design or on the effects of the operating parameters or on the type of biomass feed. Almost none of them focused on the proper design of the liquid collection system. The design methods available for the liquid collection systems especially for quenching columns applied in pyrolysis technology are scarce. Few design methods are available for scrubbers but are not specific to this application.

The quenching of pyrolysis vapours may be considered to involve gas/vapour cooling with partial condensation. Typical equipment used for direct-contact heat transfer includes:

- Baffle-tray columns
- Spray columns
- Packed columns
- Cross-flow columns
- Pipeline contactors

The design methods for these kinds of equipment were summarised by Fair [75, 76]. The most commonly used industrial equipment is the baffle-tray column and the spray columns shown in Figure 2.15. Available data shows that they typically have a performance in which the number of transfer units (NTU) is only about one. Back-mixing, and in the case of baffle-trays the large gas-side pressure drop are the main issues for their reduced performance. As the pyrolysis process presents a significant fouling problem, baffle-tray columns are considered as a best choice for the liquid collection system.

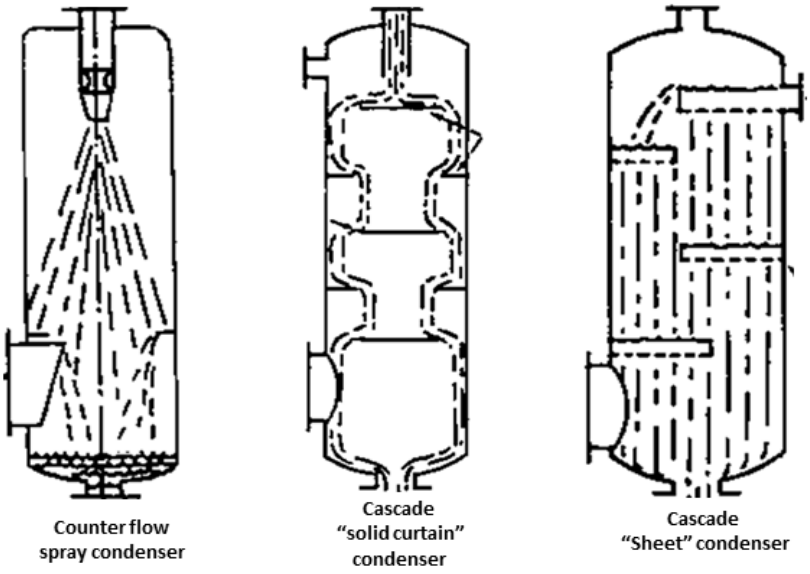

Figure 2.15– Direct contact condenser types [77].

One of the reasons direct-contact heat exchangers are not more prevalent in the industry is the lack of reliable design and performance prediction methods. This is because direct contact heat exchangers are difficult to analyse, particularly in the pyrolysis environment for the following reasons as listed by Robinson [17]:

- Vapour volumetric flow values and heat and mass transfer rates decrease continuously as phase change and temperature change occurs.
- The velocity of the vapour in a direct-contact device varies greatly with distance travelled due to the continuous condensation and cooling effects.
- Non-condensable gases are normally present and their effects on the mass transfer rate are difficult to predict under the varying flows experienced.
- In many situations transition from turbulent to laminar flow occurs.

Therefore, the widely used NTU design methods cannot be employed for designing these kinds of direct contact heat exchanger equipment [78]. This leaves only two options that may be employed for the design; either to use general design methods which utilises the specific design correlations or use of numerical methods.

2.4.1 General design methods

Heat exchangers involving the direct-contact between gas and liquid are designed along the same principles as gas absorbers and distillation columns. These principles are aimed to prevent excessive entrainment and flooding. In general, the liquid coolant will flow between trays through down comers in the case of distillation columns which utilise bubble trays. Whereas in the case of dual flow trays, the liquid coolant and vapour flow counter currently through the same openings over a plate or tray. These kinds of plates are useful especially when fouling is expected due to the condensation of heavy compounds with in a stage. However, they are not very popular due to their narrow operating range whilst they also lack design models which can be used for the prediction of their performance.

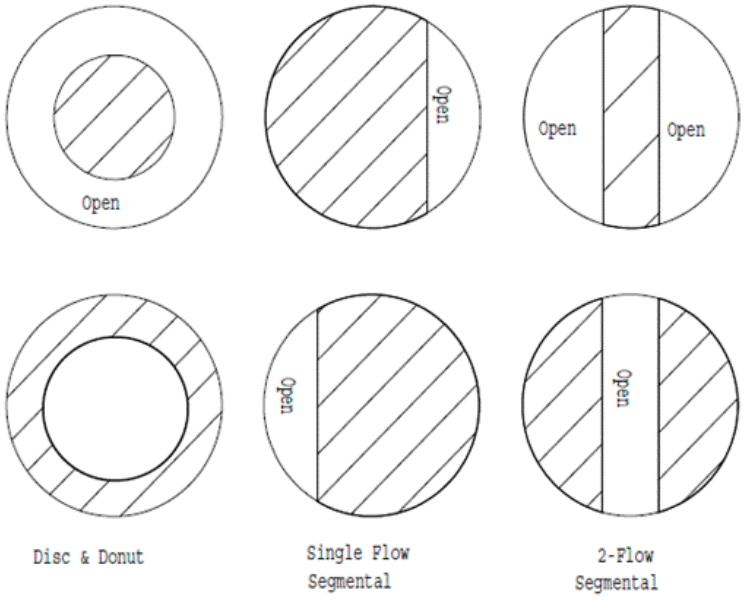

Figure 2.16– Baffle plate types [17].

Baffle trays shown in Figure 2.16, also called as dual flow trays, can be applied in many situations where a broad operating range is not necessary. Within the working range they provide high (Murphree efficiency is the measure of deviation of the actual concentration change in the phase to the change predicted by the equilibrium conditions) efficiency with low capital investment.. Moreover alternating liquid and vapour flow rates provide a self-cleaning action within the equipment. However, the fluctuations in vapour and liquid dominant flow areas on the baffle plates make it more instable [80]. In baffle-tray columns, gas-liquid contact occurs in the curtain of the liquid that cascades from plate to plate.

Very few results and design methods have been presented in the open literature as most of the design work has been done under proprietary works. Xu et al. [81] and Fair et al. [82, 83] have presented pioneering works on baffle trays where they especially attempted to generalise the calculations for tray efficiencies.

When the vapour velocity is high, more liquid entrainment will occur which eventually reduces the tray efficiency. In an extreme condition, with a higher vapour velocity, the down flow of liquid is prevented by the vapour flow, leading to flooding of the column [84]. For this reason, the accurate prediction of the hydraulic parameters is necessary. These parameters also help in the design of the equipment according to the requirement and capacity. The dimensions of the quenching column described in Robinson [17] works were chosen based on curtain and window velocities calculated near the bottom of the column where the maximum gas flow rate is expected. Note that the curtain and window velocities are computed based on flow rates and areas namely window area (minimum flow area on horizontal plane) and curtain area (surface area which can be identified with hypothetical surface formed by flow of liquid while falling vertically downwards). Correlations for these velocities are shown in Equations (2-1) and (2-2). The values 1.15 and 0.58 are the recommended Souders-Brown coefficients [85].

$$V_{c,\max} = 1.15\left[\frac{\rho_l - \rho_g}{\rho_g}\right]^{1/2} = \frac{\dot{Q}}{A_c} \tag{2-1}$$

$$V_{w,\max} = 0.58\left[\frac{\rho_l - \rho_g}{\rho_g}\right]^{1/2} = \frac{\dot{Q}}{A_w} \tag{2-2}$$

Calculations of the hydraulic parameters are based on the assumption that the properties of the mixture in the column are only function of the vertical distance as the mixture is nearly homogeneous in horizontal plane [86]. More recently an extensive review on the hydraulic correlations for baffle tray equipment was given by Mayer et al. [87]. This review states that many models ignored or did not disclose the hydraulic regime during operation which affected the application of these correlations under different operating conditions. Moreover most of the correlations were developed under inert environment and at room temperatures. It

also cautioned in evaluating the efficiencies because of the instabilities in the liquid vapour flow in the column.

2.4.2 Computational modelling of liquid collection system

Several process modelling software have been developed with the aim of simulating chemical processes. Aspen HYSYS [88] is one of these types of software that utilises various thermodynamic models to efficiently compute process parameters ranging from simple heat and mass balances to phase equilibrium behaviour and energy levels of both pure components and mixtures. In the works of Tumbalam Gooty et al. [89, 90], the results predicted by the models which are developed in HYSYS tool were utilised as guide to standardise the practical performance of the fractional condensation series.

The thermodynamics condenser model developed by Westerhof et al. [11, 12], based on the well-known Rachford-Rice formulation [16], provides an insight on how the water yield can be controlled during the condensation of pyrolysis vapours. However this model only provides the overall mass balances and lacks the spatiotemporal details of the parameters within the condenser which are necessary to develop efficient designs.

There is clear lack in the open literature in the area of CFD modelling of condensers and quenching columns used in the pyrolysis process. Most of the CFD work in the area of pyrolysis technology is focused on the pyrolysis reactor [92-99] or subsequent equipment like cyclone separators [100, 101] used for the separation of solid char particles and electrostatic precipitators [102, 103] used for aerosol capturing. One of the reasons for the lack of CFD models in this area is the scarcity of experimental data related to liquid collection systems. The experiments mentioned in the previous section gave a good insight on the inputs and outputs of the liquid collection system but failed to provide geometrical data onto the open literature. Another reason for the lack of condensation models for pyrolysis vapours is the complexity associated with the number and structure of the chemical compounds found in bio-oils. The determination of the thermodynamic properties, such as saturation vapour

pressures, of the highly complex compounds present in pyrolysis vapours as well as the appropriate group representation of certain compound families pose significant challenges in the correct and meaningful simulation of the condensation process.

Some CFD studies have been carried out on the sieve trays which are similar to baffle tray columns as mentioned section 2.3. Many mathematical models are available for predicting the liquid weeping [104 - 106], to understand the behaviour of the trays under different flow regimes; CFD was extensively used to investigate the hydrodynamics within the equipment. Gesit et al. [107] performed CFD studies to predict flow patterns and hydraulic behaviour on sieve trays. Further to it, Hirschberg et al. [108] conducted two phase CFD simulations and validated them with Fractionation Research Inc. (FRI) tests. More recently Rahimi et al. [109 -111] conducted several CFD models to obtain temperature and concentration data of liquid and vapour near the trays. Alizadehdakhel et al. [112] used the volume of fluid (VOF) model to simulate the performance of the valve tray column, while Yadav et al. [113] used Eulerian–Eulerian multiphase model to simulate a pulsed sieve plate column. However, all of these models were specifically focused on hydrodynamics while they did not take into account any phase change phenomena in their studies. Furthermore, the hydrodynamic modelling using multiphase models is not yet matured enough to capture heat and momentum transfer accurately and heavily rely on correlations developed under specific conditions.

The main challenge in the condensation or phase change modelling is the complexity of the composition of the pyrolysis vapours themselves. These vapours consist of more than hundred different compounds which are not in the form of true vapours which readily undergo phase change. As previously mentioned the pyrolysis vapours consist of a mix of aerosols, true vapours and non-condensable gases which also include the carrier gas. The presence of the inert carrier gas used in pyrolysis process attributes to the very low partial pressures of the condensable vapours which makes them more resistant to condensation.

Identifying the composition of the pyrolysis vapours is itself a challenge. In the open literature, several studies have been focused on the characterisation of the bio-oil product

under different reactor conditions and biomass feed types [114 - 117]. Very little research has been done on the determination and quantification of the representative compound groups because of the complexity of the bio-oil composition.

As far as phase change modelling is concerned, Hallett and Clark [118] worked on the evaporation of bio-oil droplets using continuous thermodynamics theory. This theory is based on the assumption that the mixture, in this case bio-oil, contains an infinite number of true components rather than a finite number of pseudo components [119]. The composition of such mixtures is best described via distribution functions with specific independent variables such as the boiling point or the molecular weight. The theory was first developed by Ratzsch et al. [120]. According to their work, this theory is best applied to petroleum fractions and coal derived liquids, tars and polymers which are distillable. The realistic mixture models are represented with probability distribution functions with two parameters, mean and standard deviation. These two parameters are computed based on the distillation curves [121]. However in most of the pyrolysis processes the final condensed bio-oil product is non-distillable. In spite of possessing certain advantages in terms of computational load reduction, when applied in certain processes such as combustion where detailed chemistry describing the multicomponent features, the applicability of the continuous thermodynamic models is limited [122]. It is inadequate when it is necessary to track the mass fraction of each component during the condensation process.

An alternative approach to simulate phase change in multicomponent fluids is the discrete component representation. The discrete multi-component (DMC) approach allows the tracking of the individual components within the vapour during the condensation and evaporation process. It allows coupling with the mass transfer mechanisms of the individual components. Brett et al. [123] used the DMC representation of bio-oil in their study, with the components and fractions chosen in such a way to discretely replicate the continuous representation of the bio-oil modelled by Hallett and Clark [118]. However, this approach is computationally expensive as additional transport equations need to be solved for each of the

phase components. However, this has become less of an issue in contemporary research as the computational capacity has been improved significantly and can be affordable.

Most of the phase change models developed within the domain of pyrolysis have been focused on the evaporation models, whereas condensation modelling in the open literature is very scarce. Papadikis et al. [124] first attempted to model the condensation phenomena occurring within a water cooled indirect contact condenser using a DMC approach. However, in their study the pyrolysis vapours are treated as a single component where the fluid properties are calculated based on the initial composition of the mixture.

From the previous discussion on the existing literature, it becomes evident that there is a complete lack of computational models that tackle the multiphase multicomponent nature of the pyrolysis vapours and that can provide spatiotemporal information about their fractional phase change in the condensation unit. The current study specifically focuses on the development of a computational approach that will enable the modelling of the condensation of pyrolysis vapours in different types of condensers. The key target of the model is to provide information on the way that different compounds behave inside the condensing equipment and to study the effect of condenser design and size on the final conversion of pyrolysis vapours into liquid bio-oil.

2.5 Summary

Chapter 2 presents a review on the liquid collection systems used in the pyrolysis process and introduced its requirements for better efficiency. It also includes a discussion about the experimental works from leading laboratories in the area of pyrolysis. Most of these works are focused on the fractional condensation of the bio-oil. This is the most preferred way of improving the quality of the bio-oil with less capital cost. Moreover, unlike conventional petroleum liquids, distillation of bio-oil is not feasible due to some of its highly reactive constituents, while it undergoes thermal degradation when it is heated which results in a solid

residue. Very few experiments have been focused on the design parameters of the liquid collection system.

An extensive review of the design methods available in the open literature was also presented. Due to the complexity of the flow physics involved in liquid collections system, the general design rules are not applicable in specific cases especially in the case of pyrolysis. Some models have been developed based on thermodynamic principles but can only provide overall results while they fail to give necessary details for the designers which are useful in designing efficient equipment.

It was also observed that very few computational models are available on phase change with respect to pyrolysis process. Some of these models were based on the continuous thermodynamic theory while others made use of the discrete component method (DCM). To the best of the author's knowledge only one study has been identified in the computational (CFD) modelling of the condensation of pyrolysis vapours, however with significant limitations

Chapter 3 CFD Methodology

This chapter introduces the fundamental equations necessary to solve the multiphase-multicomponent flows. It highlights the available multiphase models and provides justification on the selection of the models for the liquid collection system. All the models used in subsequent chapters follow the methodology explained here unless otherwise stated in the relevant chapters. In order to implement and solve these equations, commercial CFD code ANSYS Fluent with versions 13.0, 14.5 was used. This code utilises the numerical algorithms to compute the flow parameters over a domain of interest. ANSYS Fluent adopted finite volume method to solve the numerical equations and this was accomplished by dividing the domain into small control volumes or cells of known shapes. Using boundary conditions defined at the domain boundaries, flow variables within these control volumes are solved using iterative methods.

3.1 Multiphase models

The understanding of the flow behaviour is of significant importance in the CFD modelling of gas-liquid flows. CFD modelling needs to describe the physical process with a required level of accuracy. This essentially requires the identification of physical phenomena that has to be taken into account and formulation of mathematical models which can be used to describe it. It is essential that the various characteristics and physics of two phase flow should be modelled and formulated on a rational basis and supported by detailed scientific experiments. However, the derivation of such models for two-phase flow is considerably

more complicated than for single phase flow. The complex nature of two-phase flow arises from the existence of multiple, deformable and moving interfaces. As a result, specific models have to be developed to take account of flow regime-dependent characteristics.

In general, multiphase regimes are classified into different categories namely gas-liquid or liquid-liquid flows, gas-solid flows, liquid-solid flows, and gas-liquid-solid flows. In the liquid collection system, the gas –liquid flow regime is expected by neglecting the presence of solid particulates under the assumption that the cyclone separates the char particles with 100% efficiency. Baker [125] first worked on the simultaneous flow of oil and gas by classifying the flow into different regimes and developed the Baker chart to identify them which is shown in Figure 3.1.

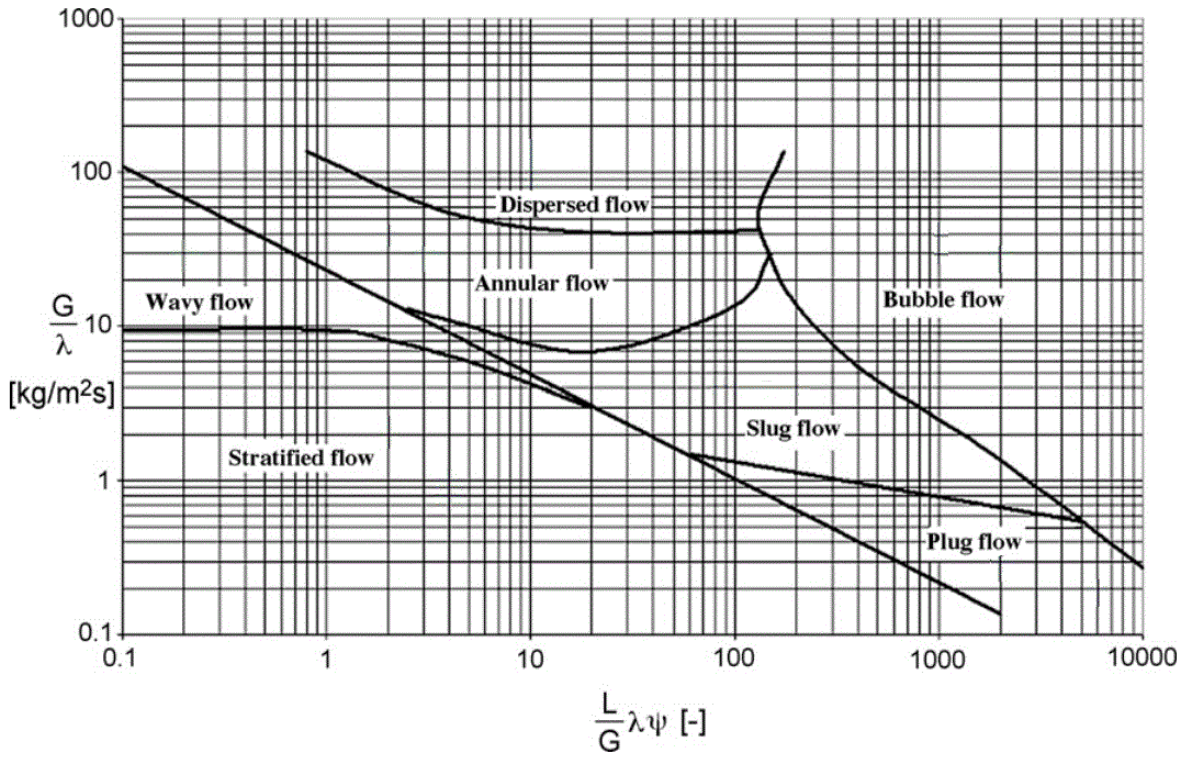

Figure 3.1– Liquid gas flow regimes (Baker chart).

Seven different flow regimes in a horizontal tube are identified by S.C.K. De Schepper et al. [126] as follows.

- **Stratified flow:** A complete separation of the two phases is expected at low liquid and gas velocities. The two phases are clearly separated by an undisturbed interface.
- **Wavy flow:** When the velocity of the gas increased under stratified flow conditions, liquid–gas interface is in the form of wave pattern. The height and frequency of the waves depends on the relative velocity between the two phases and the properties of the fluids.
- **Plug flow:** Liquid is separated by elongated gas bubbles when the gas flow rate is low. However the liquid phase is continuous as the diameters of these bubbles are usually smaller than the flow passage.
- **Slug flow:** In this regime, the interface between the liquid slugs and the elongated gas bubbles becomes less sharp as result of increased gas flow.
- **Annular flow:** Higher gas flow rates will cause the liquid to form a continuous film and the interface disturbed by small amplitude waves. Dispersed liquid droplets are expected in the continuous gas phase.
- **Bubble flow:** Gas bubbles are dispersed in the continuous liquid flow.
- **Spray or dispersed flow:** Discrete liquid droplets are dispersed in the continuous gas phase

The Baker chart in Figure 3.1 shows that the boundaries of various flow regimes are functions of the superficial velocity of the gas phase G, and the ratio of superficial velocities of the liquid and gas phase L/G. The dimensionless parameters λ and ψ shown in equations (3-1), (3-2) were introduced to make the chart in general form. Under the standard combination, where water (W) and air (A) flow at atmospheric pressure and at room temperature, the parameters λ and ψ are equal to unity.

$$\lambda = \left[\left(\frac{\rho_g}{\rho_A}\right)\left(\frac{\rho_l}{\rho_W}\right)\right]^{0.5} \tag{3-1}$$

$$\psi = \frac{\sigma_W}{\sigma}\left[\left(\frac{\mu_l}{\mu_W}\right)\left(\frac{\rho_l}{\rho_W}\right)^2\right]^{1/3} \tag{3-2}$$

Liquid collection systems possess all the above mentioned regimes. However the focus of this study is specific to quenching columns, hence the dispersed flow (spray) modelling was not considered here. It was observed that different flow regimes are present at different locations of the equipment depending on the liquid and vapour flow rates. For this reason a robust multiphase model is necessary to capture all the previously mentioned regimes. The most popular multiphase models are the volume of fluid (VOF) and the Eulerian models which address most of the gas liquid flow regimes.

3.1.1 The volume of fluid (VOF) model

The VOF model is used when accurate representation of interface between two immiscible fluids is needed. This is achieved by solving a single set of conservation equations while the volume fraction is tracked for each fluid throughout the flow domain. However, the VOF formulations assume that the two fluids are not interpenetrating. All field variables and properties are shared by the various phases and represent volume averaged values. VOF is not appropriate if the interface length is smaller than the computational cell length. This makes the model expensive in terms of number of computational cells needed to capture the interface even though it has less number of equations to solve. Moreover, the VOF method has certain limitation in modelling flooding as it solves one set of Navier-Stokes equations shared by two phases which makes momentum exchange between them is hard to obtain.

Furthermore, the phase change due to condensation induces a misty phase in the domain which is very hard to capture with the VOF model.

3.1.2 Eulerian model

The Eulerian- Eulerian model is used for the modelling of multiple phases which are interacting and interpenetrating in nature. The phases can be gases, liquids and / or solids with any combination between them. In this model a single pressure is shared by all phases. Continuity and momentum equations are solved for each phase while tracking the volume fractions of each phase in the particular cells. The interphase drag force modelling mostly affects the computational accuracy especially when flooding occurs within the quenching column. A general model which is closer to the actual physics, less empirical and independent of geometry is missing for the drag force modelling. Moreover, this model has a limitation in tracking the interface accurately as VOF model.

3.1.3 Multi fluid – VOF model

The Multi-fluid VOF model provides a method to couple VOF and Eulerian multiphase models. This makes the usage of the model more suitable for both sharp and dispersed interface regimes. This also overcomes the limitations of the VOF which is based on shared velocity temperature formulation. This model is more suitable as a multiphase model due to its robustness in terms of handling both dispersed and free surface flows as well as combination of two. Moreover, there is no limitation in creating finer grids to capture finer volume fractions of the phases accurately. The applicability of the models can be seen in Figure 3.2.

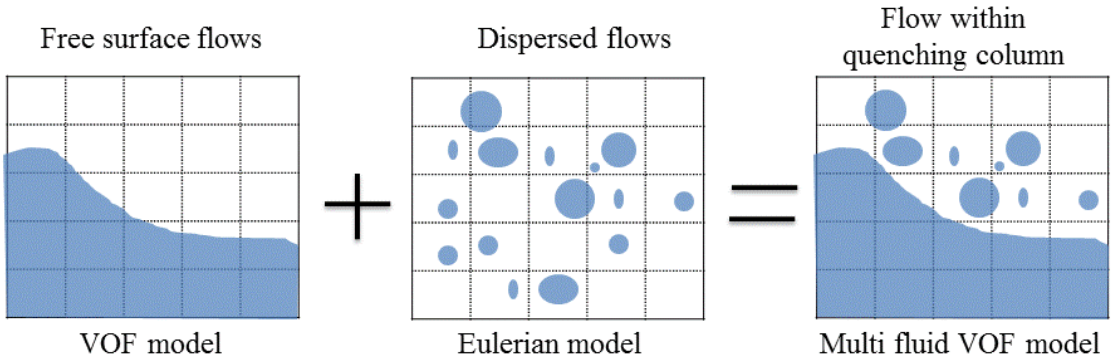

Figure 3.2– Flow regimes and recommended multiphase models.

3.2 Transport equations for multiphase systems

The basic assumption for the derivation of the transport equation in the multiphase system is that the system consists of a sufficient number of particles so that any discontinuities can be neglected, or in other words the phases are continuous. This implies that, the derivatives of the various properties of the system exists and are continuous.

As explained before, the fluid dynamics modelling approach in this study is based on the immiscible Eulerian model (Multi-fluid VOF model), which is able to track the interface between two immiscible phases, while providing a solution of the governing equations for each phase. The major advantage of this modelling approach over the standard VOF method developed by Hirt et al. [127], is that the solution of the conservation equations for each phase can provide information about the slip velocity at the interface of the two phases, which consequently leads to a more accurate prediction of the heat transfer computations. The commercial CFD package ANSYS Fluent was used as the computational platform for the simulation of the quenching column hydrodynamics.

3.2.1 Mass conservation equation

In continuum mechanics, the general form of a mass conservation law is expressed by using the continuity equation. The Navier-Stokes equations are derived by applying Newton's second law to fluid motion and govern the flow of the Newtonian fluid. They describe the unsteady and three dimensional nature of the flow. The mass continuity equation specific to multiphase systems is as follows

$$\left(\frac{\partial}{\partial t}\left(\alpha_p \rho_p\right) + \nabla \bullet \left(\alpha_p \rho_p \overline{v_p}\right)\right) = \left(\dot{m}_{qp} - \dot{m}_{pq}\right). \tag{3-3}$$

The continuity equation which provides the mass balance for phase *p* can be given in terms of volume fraction α_p and its density ρ_p. In equation (3-3) the mass source terms $\dot{m}_{qp} - \dot{m}_{pq}$ correspond to mass transfer from phase *p* to phase *q* and vice versa. In step one (section 5.2) studies the mass source term was kept as zero as the condensation model is not included in that model.

The mass transfer from the vapour phase to the bio-oil phase corresponds to the sum of the individual species mass transferred to the bio-oil. This is calculated based on the vapour liquid equilibrium (VLE) conditions as described in section 4.2. In this study, the mass transfer between the coolant and other phases is neglected.

In addition to the continuity equation, an additional equation for the volume fraction is solved. The volume fraction of each fluid is defined in equation (3-4). The volume fraction α_p is solved only for secondary phases. The primary phase volume fraction is calculated based on the fact that the sum of all phase volume fractions in the particular cell is equal to 1 as shown in equation (3-5)

$$\alpha_p = \frac{V_p}{V} \tag{3-4}$$

$$\sum_{p=1}^{n} \alpha_p = 1. \tag{3-5}$$

The secondary phase volume fraction equations are solved using an explicit scheme which uses a finite-difference interpolation method. This type of discretisation allows the usage of the Geo-Reconstruct method to get a clear interface without numerical diffusion. Since it uses the previous time step values as the basis for calculating current time step values, it does not require an iterative solution during each time step. The explicit formulation is time dependent and discretisation of volume fraction is done as shown in equation (3-6) .

$$\frac{\alpha_p^{n+1}\rho_p^{n+1} - \alpha_p^n \rho_p^n}{\Delta t} V + \sum_f (\rho_p U_f^n \alpha_{p,f}^n) = \left[\sum_{q=1}^{n} (\dot{m}_{qp} - \dot{m}_{qp})\right] V. \tag{3-6}$$

Here, $\alpha_{p,f}^n$ is the face value of the p^{th} phase volume fraction, whereas U_f^n represents the volume fluxes through the faces. The indices of the current and previous time steps are represented with n and n+1.This was computed with a compressive scheme when the interface involves the liquid coolant. In the case of an interface between bio-oil and pyrolysis vapour, the calculations were performed by using a second order upwind scheme.

3.2.2 Momentum conservation equations.

The momentum conservation equation for phase p is given in equation (3-7)

$$\frac{\partial}{\partial t}(\alpha_p \rho_p v_p) + \nabla \bullet (\alpha_p \rho_p v_p \bar{v}_p) = -\alpha_p \nabla P + \nabla \bullet \bar{\bar{\tau}}_p + \alpha_p \rho_p \bar{g} + \bar{R} + F_\sigma + \bar{M}_{s,p}. \tag{3-7}$$

where $\bar{\bar{\tau}}_p$ is the stress-strain tensor, $\bar{R}$ is the interaction force between two phases calculated by using equation (3-8)

$$\bar{R} = K_{pq}(\bar{v}_q - \bar{v}_p). \tag{3-8}$$

The interphase momentum exchange coefficient K_{pq} defined as

$$K_{pq} = \frac{\rho_{pq} f}{6\tau_{pq}} d_p A_q. \tag{3-9}$$

In this study, the drag function f used is based on Schiller-Naumann drag model [128] and is defined as $C_D Re/24$. The drag coefficient C_D is given by equation (3-10). At high Reynolds number, a constant value 0.44 was used for drag coefficient following Michaelides [129]. The relative Reynolds number Re is given in equation (3-11).

$$C_D = \begin{cases} 24\,(1 + 0.15\,Re^{0.687})\ /Re & Re \le 1000 \\ 0.44 & Re > 1000 \end{cases}. \tag{3-10}$$

$$Re = \frac{\rho_{pq}\,|\bar{v}_p - \bar{v}_q| d}{\mu_{pq}} \tag{3-11}$$

The particulate relaxation time τ_{pq} used in equation (3-11), is defined as

$$\tau_{pq} = \frac{\rho_{pq} d^2}{18\mu_{pq}}. \tag{3-12}$$

The subscript pq denotes the volume averaged properties for density and viscosity. The interfacial area A_q shown in equation (3-9) is estimated based on algebraic relation between interfacial area concentration and specific bubble diameter. This relationship is explained in

equation (3-13). The symmetric model is employed for the calculation of the interface between the coolant and vapours. In the case of vapours and bio-oil where some mist flow is expected, the particle model was used. However, for the computation of the drag forces, the symmetric drag model was utilised. This model is recommended when the dispersed phase in one region becomes a continuous phase in another region of the domain, this is true between vapours and liquid coolant.

$$A_q = \begin{cases} \frac{6\alpha_q}{d_q} & particle\ model \\ \frac{6\alpha_q(1-\alpha_q)}{d_q} & symmetric\ model \end{cases} \tag{3-13}$$

The diameter of the dispersed phase q is represented by d_q, where in this work has been set equal to 0.0001m which is 10 % of the minimum grid length scale. The term F_σ used in equation (3-7) is a source term, which represents the surface tension forces at the interface. The formulation for the surface tension is based on the work of Brackbill et al. [130]. Surface tension forces mainly arise as a result of attractive forces between molecules in a fluid at the interface. The surface force F_σ mentioned in equation (3-7) is computed using the equation (3-14) and equation (3-15) for two-phase and three-phase flows respectively.

$$F_\sigma = \sigma \frac{\rho_{pq} k_p \nabla \alpha_p}{0.5(\rho_p + \rho_q)}. \tag{3-14}$$

$$F_\sigma = \sum_{Pairsi,j,i<j} \sigma_{ij} \frac{\alpha_i \rho_i k_j \nabla \alpha_j + \alpha_i \rho_j k_i \nabla \alpha_i}{0.5(\rho_i + \rho_j)}. \tag{3-15}$$

In equation (3-14), k_p is defined as the curvature and is computed from the unit normal which is defined as the gradient of the volume fraction of the liquid phase given in equation (3-16).

$$k_p = \nabla \bullet \frac{n}{|n|}, \tag{3-16}$$

$$n = \nabla \alpha_p \tag{3-17}$$

The momentum source $\bar{M}_{s,p}$ is calculated based on the mass exchanged between the phases i.e. from vapour phase to bio-oil phase as shown in equation (3-18). This is enabled in the computational model where the phase change models are implemented.

$$\bar{M}_{s,p} = \dot{m}_{qp}(\bar{v}_q - \bar{v}_p). \tag{3-18}$$

Here $\dot{m}_{pq}$ is equal to the sum of all the individual species mass sources condensed to form the bio-oil and is computed as $\dot{m}_{pq} = \sum_i \dot{m}_c^i$.

3.2.3 Species transport equation

The discrete component model was chosen in this work as a means to represent pyrolysis vapour composition. In order to solve the conservation equations for individual chemical species within the vapour phase, the convection-diffusion equation of the ith species as shown in equation (3-19) is used.

$$\frac{\partial}{\partial t}(\rho y^i) + \nabla . \rho \bar{v} y^i = -\nabla . \bar{J}^i + S^i. \tag{3-19}$$

The diffusion flux $\vec{J}^i$ of the component *i* is computed based on Fick's law which states that mass diffusion is due to concentration gradients. The mass diffusion coefficient is assumed to be a default constant value in the mixture which is 2.88×10^{-5} m^2/s. S^i is the source or sink term based on the mass exchange between species belongs to different phases or within the same phase. Equation (3-19) solved for N-1 species where N being the total number chemical species

present in the fluid phases. The N[th] mass fraction is determined by subtracting the sum of N-1 species mass fractions from one. In order to minimise the numerical errors associated while solving, species having the largest mass fraction was chosen as the N[th] species, in this case it is the transport gas (Nitrogen) used for transporting pyrolysis vapours.

3.2.4 Energy conservation equation

The energy conservation for phase p is given as

$$\frac{\partial}{\partial t}\left(a_p \rho_p h_p\right) + \nabla.\left(a_p \rho_p \bar{v}_p h_p\right) = -a_p \frac{\partial P_p}{\partial t} + \bar{\bar{\tau}}_p : \nabla \bar{v}_p - \nabla.\bar{q}_p + Q + H_{s,p}. \tag{3-20}$$

In equation (3-20), h_p is the specific enthalpy of the phase p. $q_p$is the heat flux and Q is the volumetric rate of energy transfer between two phases as defined in the equation (3-21).

$$Q = h_{pq}\left(T_q - T_p\right) \tag{3-21}$$

The heat transfer coefficient h_{pq} between two phases was estimated based on the Ranz-Marshall correlation [131]. The heat source due to phase change $H_{s,p}$ mentioned in equation (3-21) is computed by

$$H_{s,p} = \begin{cases} \sum_i \left(-\dot{m}_c^i H_p^i\right) & for\ \ the\ vapour\ phase \\ \sum_i \dot{m}_c^i \left(H_p^i - \Delta H_v^i\right) & for\ the\ bio-oil\ phase \end{cases} \tag{3-22}$$

The terms H_p^i& ΔH_v^i are the enthalpy and latent heat of vaporisation of the species *i*.

3.2.5 Turbulence modelling

Most of the flows in the engineering fields fall within the turbulent regime. Turbulent flows are unsteady in nature. Flow properties within these types of flows fluctuate randomly. These quantities can be expressed as the sum of the mean and the fluctuating components, e.g. summation of the $u_i$velocity component can be seen in equation (3-23).

$$u_i = \bar{u}_i + u'_i \tag{3-23}$$

The fluctuating velocity component u' in equation (3-23) gives an additional term in the Reynolds averaged Navier Stokes equation. This term expressed through velocity gradients and turbulent viscosity μ_t as shown in equation (3-24).

$$-\rho_m \overline{u'_i u'_j} = \mu_t \left(\frac{\partial \bar{u}_i}{\partial x_j} + \frac{\partial \bar{u}_j}{\partial x_i} \right) \tag{3-24}$$

Prandl [133] proposed an expression for turbulent viscosity as given in equation (3-25) called Prandtl's mixing length model.

$$\mu_t = C l_m^2 \left| \frac{\partial u}{\partial y} \right| \tag{3-25}$$

When the one dimensional structure of a flow breaks down the 'mixing length model' is no longer suitable. Hence, the two-equation models were proposed. The k-ε model is the most popular model and has been successfully used by many researchers over the years. This model is implemented in the indirect contact condenser model where turbulent flow is expected. In this model, two quantities are introduced: k, the turbulent kinetic energy and ε the rate at which the turbulent kinetic energy is dissipated to compute the turbulent viscosity term as shown in the equation

$$\mu_t = C_\mu \rho \frac{k^2}{\varepsilon} \tag{3-26}$$

Two transport equations are solved for k and ε as below.

$$\frac{\partial}{\partial t}(\rho_m k) + \nabla \bullet (\rho_m \bar{v}_m k) = \nabla \bullet \left(\left(\mu_m + \frac{\mu_{t,m}}{\sigma_k} \right) \nabla k \right) + G_{k,m} - \rho_m \epsilon \tag{3-27}$$

$$\frac{\partial}{\partial t}(\rho_m \varepsilon) + \nabla \bullet (\rho_m \bar{v}_m k\varepsilon) = \nabla \bullet \left(\left(\mu_m + \frac{\mu_{t,m}}{\sigma_\varepsilon} \right) \nabla \varepsilon k \right) + \frac{\epsilon}{k}\left(C_{1\varepsilon} G_{k,m} - C_{2\varepsilon} \rho_m \varepsilon \right) \tag{3-28}$$

The mixture properties mentioned in equations (3-27) and (3-28) are defined in below set of equations from (3-29) to (3-31).

$$\rho_m = \sum_{p=1}^{N} a_p \rho_p \tag{3-29}$$

$$\mu_m = \sum_{p=1}^{N} a_p \mu_p \tag{3-30}$$

$$\bar{v}_m = \frac{\sum_{p=1}^{N} a_p \rho_p \bar{v}_p}{\sum_{p=1}^{N} a_p \rho_p} \tag{3-31}$$

The turbulence kinetic energy $G_{k,m}$ is calculated from the equation (3-32).

$$G_{k,m} = \mu_{t,m}(\nabla \bar{v}_m + (\nabla \bar{v}_m)^T) : \nabla \bar{v}_m \tag{3-32}$$

Chapter 4 Condensation model

This section provides the details of the condensation model which was implemented on the liquid collection system CFD models in the subsequent chapter. It outlines the physics involved behind the process and also shows how the mass transfer between phases can be estimated with certain limitations. This section also gives some details about estimation techniques of pyrolysis vapour and bio oil properties. The computational equations required to perform this kind of simulations are also mentioned.

4.1 Discrete component method (DCM)

Pyrolysis vapours consist of more than 100 compounds. It is computationally very demanding to model the complete spectrum of species found in the pyrolysis vapours. There are two popular approaches to model the phase change dynamics of the pyrolysis vapour components available in the literature, as mentioned in the section 2.4.2. One is the continuous thermodynamics approach while the other one is the discrete component approach. Unlike the continuous thermodynamics approach, if the vapour contains or can be represented by few components, it is more desirable to track the mole fraction of the each component during the condensation process.

Vapours obtained from pyrolysis reactor contain different compounds and it will vary greatly with the type of reactor and type of feed stock and it highly depends on the operating parameters. It is hard to obtain a universally acceptable composition for the pyrolysis

vapours. In fact, many approaches have been reported in the literature in order to separate the bio-oil into fractions [134 - 137]. This kind of fractioning or grouping is very useful in modelling phase change and reactions as well as developing upgrading strategies. Garcia-Perez et al. [138] developed a characterisation approach to determine bio-oil chemical compositions in terms of macro-chemical families. These families are highlighted in the Table 4-1.

Table 4-1– Typical bio oil chemical families

Macro-chemical family	Chemical compounds (example)
Volatile non-polar compounds	Ethylbenzene
Volatile polar compounds	Cyclopentanol
	Tetrahydro-2-furanmethanol
Mono- lignols	Alkylated and methoxylated phenols
	Benzenediol
Polar compounds with moderate volatility	5-methyl-2-furaldehyde
Sugars	Levoglucosane
Extractive-derived compounds	Fatty and resin acids
	Paraffins
Heavy non-polar compounds	
Heavy polar compounds	

The chemistry of the pyrolysis oils are qualitatively well expressed by Hallet and Clark.[121]. The main components for the pyrolysis compounds are organic acids, phenols, aldehydes, pyrolytic lignin, ketones, levoglucosan and water typically between 15-25%. Brett et al. [123] utilised a similar composition in their DCM model for bio-oil evaporation modelling. Moreover, this composition was later utilised by Papadikis et al. [124] to develop a

condensation model. The condensation model used in the present work is an analytical improvement of the work of Papadikis et al. [124] model. In contrast with the uniform vapour composition presented in that study the current model treats each individual species as a separate compound that is condensed according to its individual saturation vapour pressure. In this way, fractional condensation modelling is enabled and the prediction of the bio-oil composition at each condensation stage becomes possible, once the initial vapour composition is known. The pyrolysis vapours are modelled by using a discrete representation of 11 chemical species dominant in bio-oil. The chemical species are listed in Table 4-2.

Table 4-2 – Pyrolysis vapour composition.

Name	Initial Volume fraction	Molecular weight (g/mol)	Critical Temperature (K)	Critical pressure (atm)	Critical volume (cm3/mol)	Acentric factor	Critical compressibility factor
Acetic acid	0.037	60.05	594	57.1	171	0.454	0.2
Butanal	0.109	72.11	524	40	278	0.352	0.26
Butyric acid	0.011	88.11	628	52	292	0.67	0.295
Coniferyl alcohol	0.19	180.2	569.9	33.6	482	1.155	0.346
Formic acid	0.042	46.02	580	57.34	120	0.368	0.1445
Guaiacol	0.108	124.14	696.8	46.613	338	0.563	0.275
Pentanal	0.021	86.13	554	35	333	0.4	0.26
Phenol	0.054	94.11	694.2	60.5	229	0.44	0.24
Propanal	0.144	58.08	496	47	223	0.313	0.26
Propionic acid	0.017	74.08	612	53	230	0.536	0.242
Water Vapour	0.267	18.01	647.3	217.6	56	0.344	0.229
Nitrogen			126.19	33.53	90.1	0.037	0.292

The representative composition with chemical structure can be seen in Figure 4.1

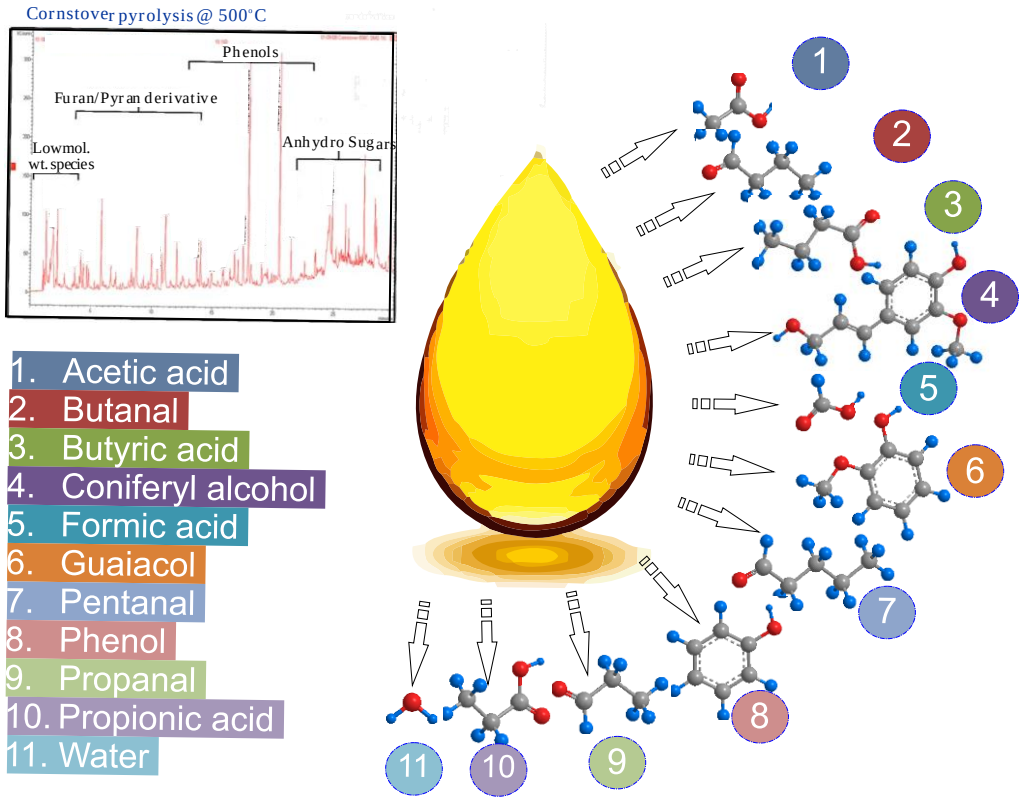

Figure 4.1– Bio-oil composition simplified.

4.2 Vapour liquid equilibrium (VLE)

4.2.1 Equation of state

The physical properties of every chemical compounds depends on the nature of the molecules present in it. However, there is a significant gap in understanding the molecule behaviour completely. Early experimental observations of the Charles and Gay-Lussac laws together with Avogadro's hypothesis formed the ideal gas law PV=NRT which formed the basis for the concept of the equation of state (EOS). By definition, an equation of state is a thermodynamic equation which is used to describe the state of the fluid under a given set of

physical conditions. It is useful in providing the relationship between two or more state functions like temperature volume and pressures.

As pointed out by the Poling et al.[141] the following points are important while choosing the appropriate method for estimating physical properties.

- Provide reliable estimation of physical properties for pure substances and mixtures.
- Indicate the thermodynamic state of the substance.
- Use minimum data for inputs.
- Optimise error while estimating.
- Indicate the error magnitude.
- Computationally easy.

Many molecular theories are available and useful for data correlation; the law of corresponding state is particularly useful. This law generalises and relates the critical properties in a universal way. In this study most of the simulations have been solved using ideal gas law. However, most of the properties are estimated using different estimation techniques explained in section 4.3. In many practical situations this may induce error in predicting quantities accurately. Engineers and researchers need to take proper justification when using the appropriate equation of state. For this reason, results obtained from real gas model Peng-Robinson equation of state were compared with the results obtained from Ideal gas laws (section 5.3.5).

There are several equations of state available in the open literature. Lawal et al.[139] introduced a more general equation of state which can accommodate different equation of state by simply replacing its coefficients as mentioned in Table 4-3. The Lawal- Lake-Silberg (LLS) equation developed by Lawal et al. [139] is given in equation (4-1).

$$P = \frac{RT}{\upsilon - b} - \frac{a(T)}{\upsilon^2 + \alpha b\upsilon - \beta b^2} \tag{4-1}$$

Where α and β are the coefficients of the quadratic and are given in the Table 4-3 for different equations of state.

Table 4-3 – LLS equation coefficients

EOS	year	Coefficient of the quadratic		
		α	β	α − β
Two constant equations:				
Van der Waal	1873	0	0	0
Redlich - Kwong	1949	1	0	1
Peng - Robinson	1976	2	1	1
Three constant equations				
Clausius	1881	2c/b	c^2/b^2	1 (c=b)
Patel - Teja	1982	(b+c)/b	c/b	1
Yu -Lu	1987	3+ ω	ω	3
Four-constant equations:				
Lawal -Lake -Silberberg	1983	α	β	α − β
Adachi- Lu	1983	$(b^2+ b^3)/b$	$(b^2b^3)/b^2$	1
Trebble -Bishnoi	1987	(b+c)/b	$(bc-d^2)/b^2$	1

Among all the EOS mentioned in the table, the Peng Robinson EOS has become more popular and widely used in petroleum industry. It is better suited to gas condensate systems. The P-R Equation of state can be written in terms of compressibility factor as given in equation (4-2).

$$Z^3 - [1 + (1 - \alpha)B]Z^2 + [A - \alpha B - (\beta + \alpha)B^2]Z - [AB - \beta(B^2 - B^3)] = 0 \quad (4\text{-}2)$$

Where α and β are taken as 2 and 1 respectively as shown in the Table 4-3. Cubic equation coefficients A and B are calculated as shown in equations (4-3) and (4-4).

$$A = \frac{a(T)P}{(RT)^2} \quad (4\text{-}3)$$

$$B = \frac{bP}{RT} \quad (4\text{-}4)$$

The coefficients 'a' and 'b' are made functions of critical properties of the species by imposing critical conditions on the cubic equation. They are defined as follows.

$$a = \left[1 + (0.37464 + 1.54226\omega - 0.26992\omega^2)\left(1 - \sqrt{T_r}\right)\right]^2 \left(0.45724 \frac{R^2 T_c^2}{P_c}\right). \quad (4\text{-}5)$$

$$b = 0.0778 \frac{RT_c}{P_c}. \quad (4\text{-}6)$$

4.2.2 Saturation pressure

When condensation or evaporation takes place in an enclosed volume, escaping molecules from the vapour accumulate as liquid and vice versa. As the molecule exchange between vapour and liquid reaches equilibrium, the vapour is said to be saturated and vapour pressure, density and temperature at that point is constant and there is no further change observed [142]. When the vapour phase of the fluid is in equilibrium with its liquid phase, the equality of the chemical potential, temperature and pressures gives the well-known Clapeyron equation.

$$\frac{dP_{Vp}}{dT} = \frac{\Delta H_v}{T\Delta V_v} = \frac{\Delta H_v}{\left(RT^2/P_{Vp}\right)\Delta Z_v} \tag{4-7}$$

$$\frac{d\ln P_{Vp}}{d(1/T)} = -\frac{\Delta H_v}{R\Delta Z_v} \tag{4-8}$$

In the equations (4-7) and (4-8), ΔH_v and ΔZ_v corresponds to the difference in enthalpies and compressibility factors of saturated liquid and vapours. Most of the estimation techniques for the vapour pressure come from integration of equation (4-8). The simplest of these is given in the equation (4-9), which assumes ΔH_v / ΔZ_v is constant and independent of temperature.

$$\ln P_{Vp} = A - B/T. \tag{4-9}$$

The above equation holds for small temperature ranges. However it suffers at large temperature ranges and near critical point regions. Antoine [143] proposed a simple modification of the above equation which can be used in limited temperature ranges. Wagner [144] used a statistical method to develop an equation. More recently, Mejbri and Bellagi [145] developed a generalised three parameter corresponding states correlation for vapour pressure. In this correlation, the natural logarithm of the reduced saturated vapour pressure and acentric factor ω^i are in linear relation as shown in equation (4-10) with an average relative deviation between data and estimated values is about 0.16% and maximum being around 0.3%.

$$\ln(P_r^i) = f_0\left(\tau^i\right) + \omega^i f_1\left(\tau^i\right), \tag{4-10}$$

where τ^i is the inverse of the reduced temperature T_r^i of the i^{th} species and is equal to $1/T_r^i$. The functions f_0 and f_1 are given by equations

$$f_0(\tau^i) = \gamma_1(\tau^i - \exp(1-\tau^i)) + \gamma_2((\tau^i)^{\gamma_3} - \exp(1-\tau^i)) \quad (4\text{-}11)$$

$$f_1(\tau^i) = \gamma_4(\tau^i - \exp(1-\tau^i)) + \gamma_5((\tau^i)^{\gamma_6} - \exp(1-\tau^i)) \quad (4\text{-}12)$$

The values of the six universal γ coefficients which are used in the above two equations are listed in Table 4-4.

Table 4-4 – Coefficients of equation (4-11) and (4-12).

k	γ_k
1	-5.53357241
2	11.0210515
3	-0.51243147
4	-10.6722729
5	29.4364927
6	-0.44101891

For estimating vapour pressures with equation (4-10), the critical pressures and temperatures are needed along with the acentric factor. If the acentric factor is not available, Mejbri and Bellagi [145] recommended estimating it using the boiling temperature T_b^i by using equation (4-13).

$$\omega^i = \left(0.013162987 - \ln P_c^i - f_0\left(\tau_b^i\right)\right)/f_1(\tau_b^i) \tag{4-13}$$

where τ_b^i is the ratio between critical and boiling temperatures i.e. $\tau_b^i = T_c^i/T_b^i$. The critical pressure P_c^i used in equation (4-13) is expressed in bars.

The condensation rate is governed by the magnitude of the relative saturation value which is the ratio of the vapour fugacity f_v^i to the saturated vapour fugacityf_l^i. Under the vapour liquid equilibrium (VLE) conditions, the relative saturation will be unity. The vapour fugacity in this case is the partial pressure of the particular species in the system as given in equation (4-14).

$$f_v^i = \phi^i P^i = \phi^i x^i P \tag{4-14}$$

where P^i is the partial pressure of the species 'i' and P is the total pressure of the mixture. x^i is the mole fraction of the ith species within the vapour mixture. The saturated vapour fugacity computed from the reduced saturation pressure obtained from equation (4-12) as shown in equation (4-15).

$$f_l^i = \phi_{sat}^i P_r^i P_c^i \tag{4-15}$$

Here the fugacity coefficients $\phi^i$and ϕ_{sat}^i which measure the departure from ideal behaviour are assumed as 1 and hence the saturated vapour pressure is considered the same as the saturated vapour fugacity. This is especially true when the system is not under high pressures and is evident from equation (4-14)

$$\lim_{p \to 0} \quad \ln \phi^i = 0 \tag{4-16}$$

4.3 Thermodynamic properties

4.3.1 Viscosity

In a confined fluid subjected to shearing stress, the fluid will move with certain velocity gradient. The ratio obtained between the shear stress and the velocity gradient at that location is defined as the viscosity of the fluid. It is a measure of internal fluid friction. It is a function of thermodynamic state of the fluid like density. However it is referred to as non-equilibrium property. Viscosity is independent of the magnitude of applied shear stress or velocity gradient in the Newtonian fluids which is the case in liquid collection system flows. In order to estimate the viscosity of gases at low pressures, a number of corresponding states methods are available and most of them use the relation shown in equations (4-17)and (4-18).

$$\mu = \frac{f(T_r)}{\xi} \tag{4-17}$$

$$\xi = 0.176 \left(\frac{T_c}{M^3 P_c^4}\right)^{1/6} \tag{4-18}$$

ξ is inverse viscosity and expressed in μP^{-1} .

The viscosity of the vapour mixture is estimated based on the Dean and Stiel [146] relation which is a function of the reduced mixture temperature. Mixture viscosity in equation (4-19) is expressed in micro poise.

$$\mu_m = \begin{cases} 3.4\, T_{rm}^{8/9}/\xi_m & T_{rm} \leq 1.5 \\ 16.68\,(0.1338\, T_{rm} - 0.0932)^{5/9}/\xi_m & T_{rm} > 1.5 \end{cases} \tag{4-19}$$

$$\xi_m = \left(\frac{T_{cm}}{(M_m{}^3 P_{cm}{}^4)}\right)^{1/6} \tag{4-20}$$

The reduced mixture temperature T_{rm} is expressed as the ratio between temperature of the vapour phase and mixture critical temperature. Here the mixture critical temperatures and mixture molecular weight were calculated by mass fraction weightage basis i.e. $\sum y^i T_c^i$, $\sum y^i M^i$ respectively. The mixture critical pressure P_{cm} expressed in atmospheres is calculated using equation (4-21). The universal gas constant R is equal to 82.05746 (atm. cm^3/ mol K).

$$P_{cm} = \frac{R\left(\sum_i y^i Z_c^i\right)}{\sum_i y^i V_c^i} T_{cm} \tag{4-21}$$

4.3.2 Thermal conductivity

Due to lack of the group contribution data, in this analysis, the more accurate correlations like Chung et al. [147] are not considered for calculating the thermal conductivity. The famous Eucken correlation offers a simple method to estimate the mixture's thermal conductivity,

$$k_m = \left(1.32 + \frac{1.77}{\left(C_{p_m}/R - 1\right)}\right)\left(\frac{\mu_m(C_{p_m} - R)}{M_m}\right) \tag{4-22}$$

where k_m is the thermal conductivity of the vapours, C_{p_m} is the heat capacity of the vapours, which is calculated based on a mass fraction average, i.e. $\sum w^i C_p{}^i$.

4.3.3 Heat capacity

The specific heat capacities of the individual species are given in Table 4-5. These values are obtained from Reid et al. [148] and Stull et al.[149]. Group contribution using Constantinou and Gani (CG) method [150, 151] was employed when the data for the heat capacity were missing.

Table 4-5 – Heat capacities of individual components present in pyrolysis vapours.

Chemical compound	Cp = A1+A2T+A3T2		
	A1	A2	A3
Acetic acid	195.74849	3.5237048	-0.001545339
Butanal	245.97362	4.4604585	-0.001734686
Butyric acid	229.03995	3.9854485	-0.001549761
Coniferyl alcohol	527.97236	3.1066709	-0.000768719
Formic acid	326.7	2.5160000	-0.00105
Guaiacol	531.24523	3.0758568	-0.000739824
Pentanal	202.39221	4.7575163	-0.001883003
Phenol	-158.75528	4.9638417	-0.002442437
Propanal	240.36658	4.2292475	-0.001671269
Propionic acid	164.9201	4.0156030	-0.001735477
Water Vapour	1779.0173	0.1717701	0.000362651

4.3.4 Heat of vaporisation/condensation

The enthalpy of condensation is equal to the enthalpy of vaporisation by definition except that it has opposite sign. An enthalpy change in case of vaporisation is positive (taken by the fluid), whereas in condensation it is negative (given by the fluid).

The heat of vaporization for each chemical species within the vapour is estimated based on the law of corresponding states. The relationship of the heat of vaporisation with the acentric factor ω^i, and the reduced temperature T_r^i shown in equation (4-23) is an analytical representation of the Pitzer's [152] correlation.

$$H_v^i = \left(7.08\left(1 - T_r^i\right)^{0.354} + 10.95\omega^i\left(1 - T_r^i\right)^{0.456}\right) R\, T_c^i \tag{4-23}$$

4.4 Bio-oil properties

In this work, the bio-oil is treated as a homogeneous compound and hence its composition is not varied spatially or temporally. Representative bio-oil properties were sourced from the recent works of Oasmaa et al. [153 – 155]. The bio-oil properties along with the coolant liquid and the transport gas are shown in Table 4-6.

Table 4-6 – Fluid properties.

Fluid	Density (kg/m^3)	Specific heat capacity (J/kg·K)*	Thermal conductivity (W/m·K)*	Dynamic viscosity (kg/m·s)*	Surface tension (N/m)
Nitrogen	Ideal gas	979.043 + 0.4179639 T – 0.001176279 T^2 + 1.674394 e-06 T^3 – 7.256297 e-10 T^4	0.004737109 + 7.271938 e-05 T – 1.122018 e-08 T^2 + 1.454901 e-12 T^3 – 7.8712 e-17 T^4	7.473306 e-06 + 4.083689 e-08 T – 8.244628 e-12 T^2 + 1.305629 e -15 T^3 – 8.177936 e-10 T^4	
Octane	722.32	2127.812	0.13415	0.000769	0.024088
Bio-oil	1200	3200	0.386	12.9881-0.080204T +0.000124T^2	-

The pyrolysis vapour and liquid bio-oil properties are subjected to errors associated with the estimation techniques and experimental values used for their computation. However, there is great confidence that the deviations from reality will not significantly affect the final results of the numerical model as the previously mentioned correlations and experimental values have been widely used and accepted by the chemical industry for several years.

Chapter 5 LCS model – Results and discussion

The fifth chapter provides a brief outline about the existing quenching column design and its operating conditions which forms the platform for this work. The rest of the section primarily divided in to four parts following each of the steps in detail as outlined in section 1.3. The current chapter is entirely dedicated to the results obtained from steps 1 to 3. The first part of the analysis presents the quenching column design optimisation on the basis of hydrodynamic modelling. In step 2, the model is tested for fractional condensation and validated with experimental results. In addition, in step 2A, a real gas model is also investigated and compared against the results obtained from the ideal gas model. Finally in step 3, a combined model obtained from steps 1 and 2 is applied in the quenching column with the detailed mass transfer mechanism associated with three distinct multi-component phases. The impact of the number of disc and donut stages of the column in the overall conversion of the pyrolysis vapours into liquid bio-oil is also investigated and analysed.

5.1 Quenching column Design and Operating condition

The liquid collection system of the pyrolysis rig comprised of a quenching column coupled with an electrostatic precipitator. The pyrolysis reactor is designed to operate at a biomass feeding rate of 5 kg/hr; however, the feeding rate was limited to 3 kg/hr. due to feeder limitations.

The original (baseline) design of the quenching column is shown in Figure 5.1. The equipment has been designed for a total gas (i.e. gases plus pyrolysis vapours) flow rate of 0.0044 m^3/s with a temperature of 400^OC. The gaseous composition consists of 87% N_2, 7% water vapour, 4% non-condensable gases and 1.5% organics, by volume. The design specifications of the discs and donuts inside the quenching column are given in Table 5-1. The dimensions of the quenching column are based on the maximum intended gas flow rates from the pyrolysis reactor, as well as the flooding factors.

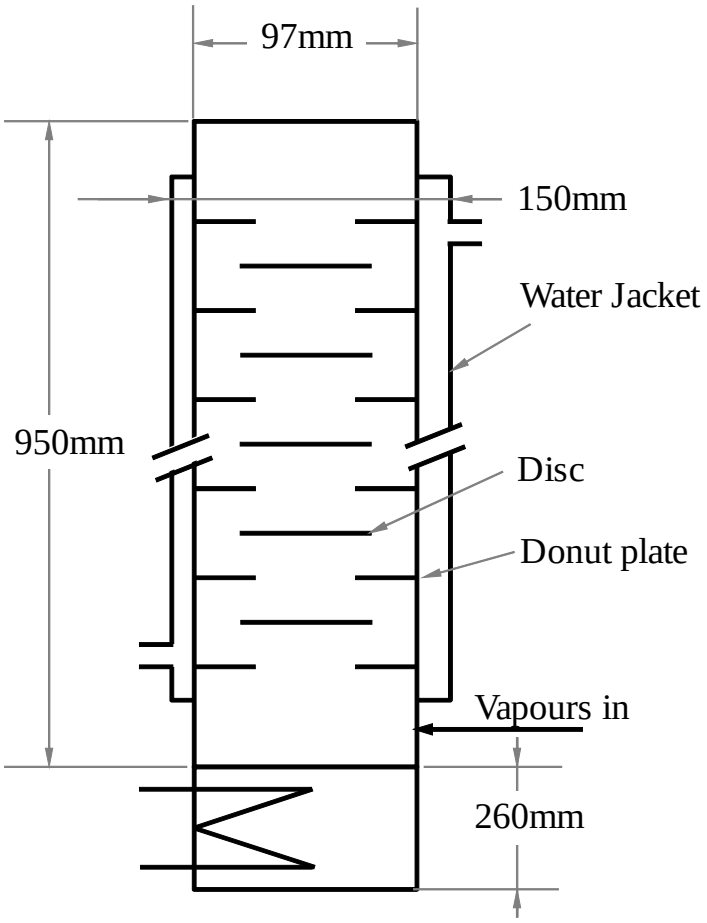

Figure 5.1– Sketch of experimental quenching column.

Table 5-1 – Quenching column design parameters

Parameter	Experiment
Volumetric flow rate, m^3/s	0.0044
Temperature, OC	400
Column diameter, cm	9.7
Donut inner annular diameter, cm	3.4
Disc diameter, cm	9
Spacing between disc and donut , cm	2
Number of discs	18
Number of donuts	19

Octane at $-5^{O}C$ has been used as the direct contact cooling medium because of its immiscibility with the highly oxygenated hydrocarbons present in the final liquid bio-oil product. The experimental findings reported flooding of the quenching column at the design gaseous flow rate of 0.0044 m^3/s. The problem was finally resolved by lowering the liquid coolant flow rate and by reducing the diameter of the discs. However, these modifications severely affected the quenching capacity of the equipment. It was also reported that the original quenching column design could only operate normally when the gaseous flow rate was reduced to 10% of its original design value. Flooding was reported in the thesis [17] for any gas flow rate above this value. All of the previously mentioned issues set the platform for resolving the problems associated with the operation of quenching columns.

5.2 Step1 - Quenching column hydrodynamics

In this study, an attempt on the modelling of the hydrodynamic and heat transfer phenomena with the aim of eliminating the flooding issues of the previously mentioned quenching

column is presented. The gas liquid interactions are simulated using the immiscible Eulerian – Eulerian approach (multi-fluid VOF). The CFD studies validated the flooding phenomena, occurring at 50% of the design gas flow rate, while it is shown that the column can normally operate at 10% of the design gas flow rate. Both of these conditions were reported in the experimental investigations [17]. Under these considerations, four alternative design configurations are presented and modelled. The results are thoroughly analysed and discussed in terms of both hydrodynamic and heat transfer performance.

5.2.1 Model assumptions

The implementation of the hydrodynamic model is based on the following assumptions.

I. Nitrogen has been used to represent the total gaseous flow rate in the column. The current model does not take into account the phase change of the condensable vapours present in the gaseous mixture. The small concentration of the condensable vapours compared to the dominant presence of non-condensable gases (especially N_2 as the fluidising gas) was considered not to play an important role in the development of the hydrodynamic characteristics of the quenching column.

II. For the previously mentioned reasons, the heat transfer calculations were assumed to be governed solely by the presence of N_2.

III. Buoyancy induced laminar flow conditions were assumed inside the quenching column since the Rayleigh number of the flow is well below the 10^8 value. It has also been previously reported that laminar flow assumptions give better predictions for this type of flow [28].

5.2.2 Initial conditions and Boundary conditions

Initially 2D models were considered as these will give quick insight into the physics. However, due to flow which is highly unsymmetrical and random in nature, 3D transient analysis was adopted for this modelling task.

The initial volume fraction of the coolant was set to zero and the entire equipment was filled with nitrogen at room temperature i.e. at 25^{O}C. The initial velocity and pressure were set to zero (gauge) in the whole domain. A mass flow rate of 0.025 kg/s of octane is supplied at the coolant inlet at -5^{O}C. The initial run was continued until the coolant liquid reaches the bottom surface of the equipment.

Once the liquid flow was developed, Nitrogen was injected from the vapour inlet at 400^{O}C. The initial flow rate supplied is about 10% of the designed flow rate. The designed flow rate for this equipment is $0.0044 m^3/s$, since the detailed chemical components of the pyrolysis vapours not included and the flow is assumed to be governed by nitrogen, the calculated mass flow rate is about 0.002232 kg/s based on its density at 400^{O}C. For the baseline model two studies conducted with different flow rates one at 10% flow rate and another one at 50% flow rate. The modified models were run with 50, 75 and 100% flow rates respectively.

The quenching column wall was considered as adiabatic and heat transfer from it is neglected. Atmospheric pressure outlet was maintained at the gas outlet. The coolant outlet is modelled as a mass flow inlet with a negative flow rate. Based on the liquid levels at the bottom, the flow rate changes to either '0' or '-0.025'kg/s in order to avoid rising the liquid coolant beyond specified levels.

5.2.3 Baseline model

The baseline model was constructed based on the existing experimental quenching column dimensions which were shown in Table 5-1. The sketch of the experimental quenching column is shown in Figure 5.1. The original design has 18 sets of disc and donuts. Flooding is caused by choking flow near the flow area either at disc plates or donut plate's i.e. up flow of the vapour restricts the down flow of the liquid coolant [84]. In order to assess this phenomenon in the computational model, it is sufficient to consider the bottom three stages of donut arrangement as the maximum expected flow rates of the vapour is expected in this

area. For this reason, a three donut and two disc plate arrangement is considered in the baseline model as shown in Figure 5.2.

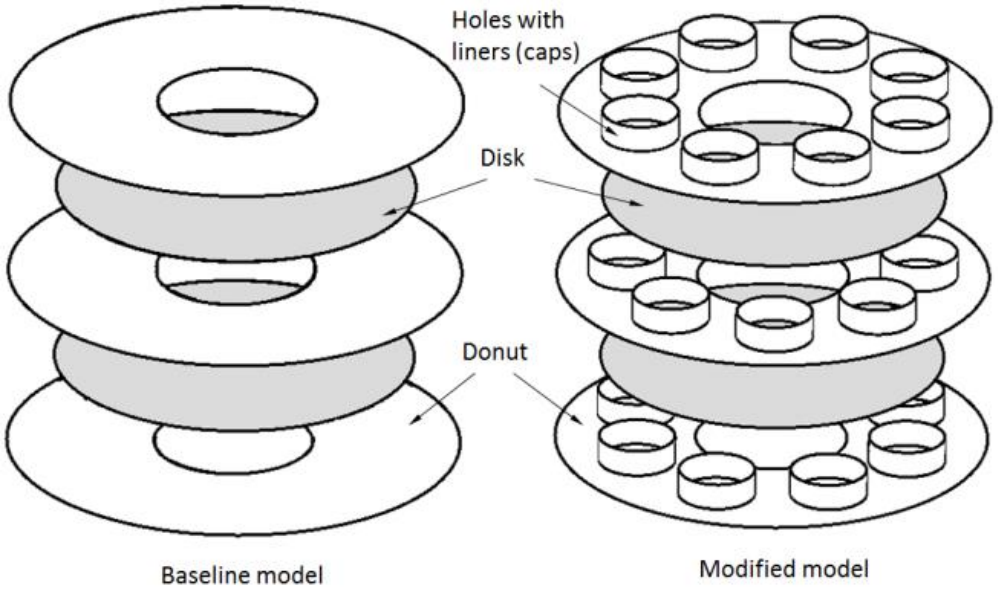

Figure 5.2– Disc and Donut plate arrangement.

Based on the observations from the results of the baseline model, a new design was proposed at this stage and modelled. The modified design is identical to the baseline model except for the donut plate configuration. In this model, eight holes with liners (herein after called caps/weirs) were placed circumferentially. The pitch circle diameter for these holes is the same for all donut plates. However the holes are arranged in an alternate pattern as seen in Figure 5.2. This is to facilitate bypassing of some gas to the next stage and at the same time not allowing vapours to escape directly in the vertical direction. The lining was about 5mm in height.

Due to the size of the quenching column (Figure 5.3) and its complexity of the flow behaviour, the grid size was chosen as 1.5 mm with uniform spacing. Hexahedral cells were

used for the domain discretisation as they give better accuracy than tetrahedral cells when computing surface tension effects.

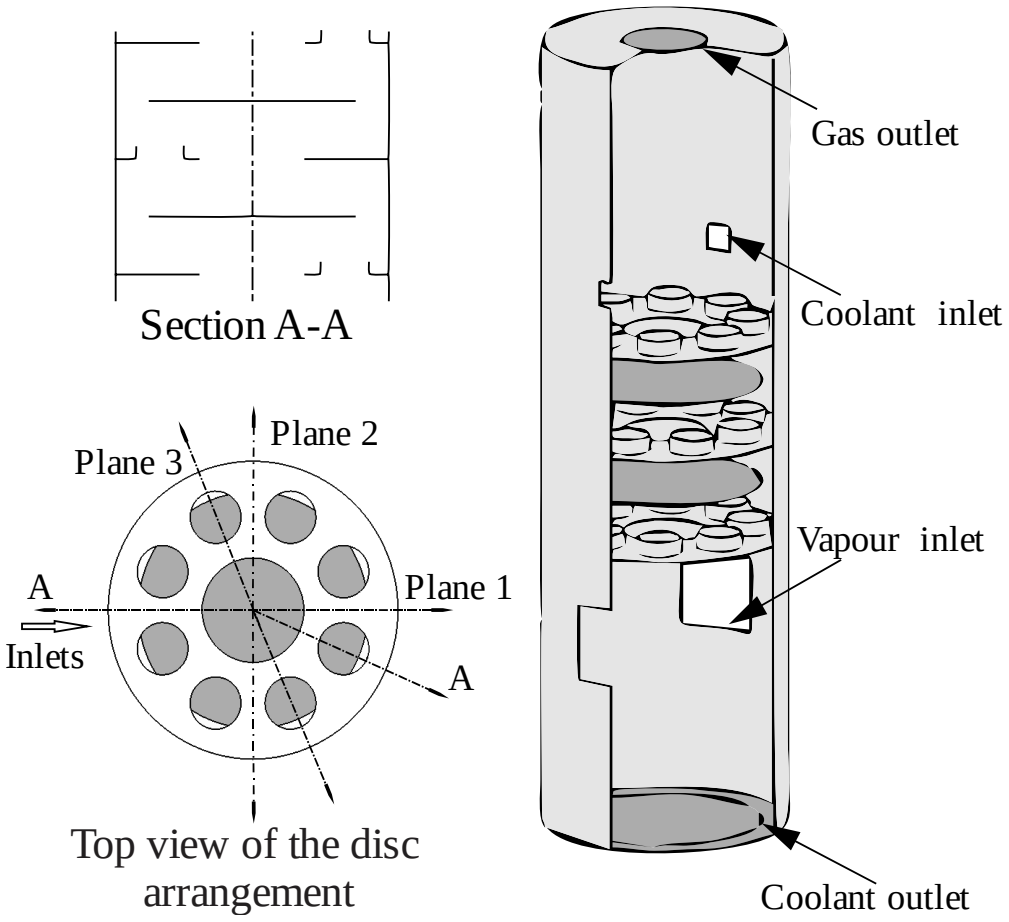

Figure 5.3– CFD Domain - Quenching column.

The section of the meshed model is shown in Figure 5.4. The total number of cells for the baseline model is 0.66 million whereas for the modified design model is 0.73 million.

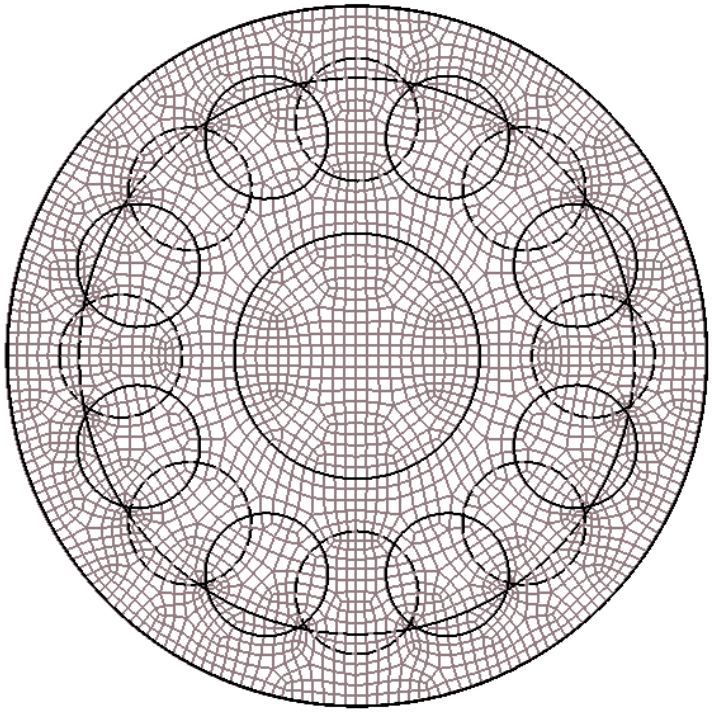

Figure 5.4– Grid spacing – section taken at mid height.

5.2.4 Validation study results

All the models started with 0.001 s time step which was found to be the optimal in this kind of simulation and grid size. Moreover, the global courant number is well below the value 1 when this time step was used. After monitoring the gas temperatures at the exit and the liquid flow rate at the intermediate section which was located in between the disc plate and the donut, the nearly stable state was achieved after 8s maximum in all cases. The exception to this is the baseline with 50% gas flow case, where the stable state solution for these flow rates has not been achieved due to flooding of the coolant. The presented data in this part corresponds to data obtained after this time. Figure 5.5 shows the coolant liquid inside the domain for the baseline case. According to this figure, the coolant liquid is clearly flowing towards the bottom stages for the 10% flow case (10% to the designed flow rate condition). It

also clearly shows that in 50% flow case flooding is occurring at the top donut plate as it has been also reported in the experimental procedure.

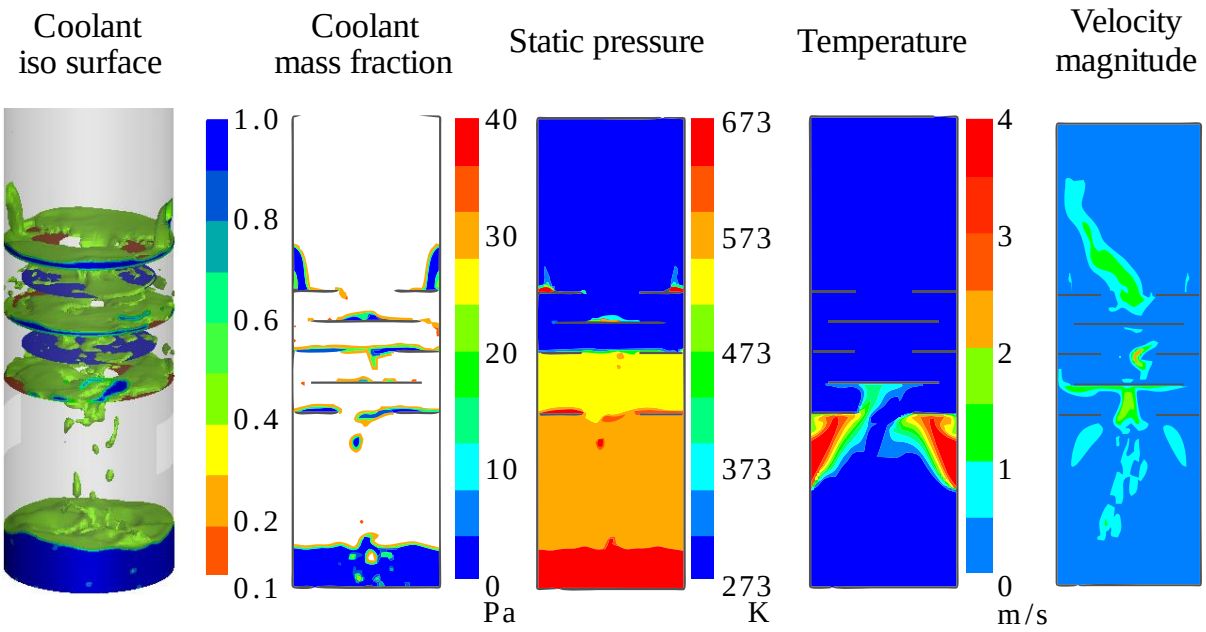

(a) Baseline model with 10% flow condition

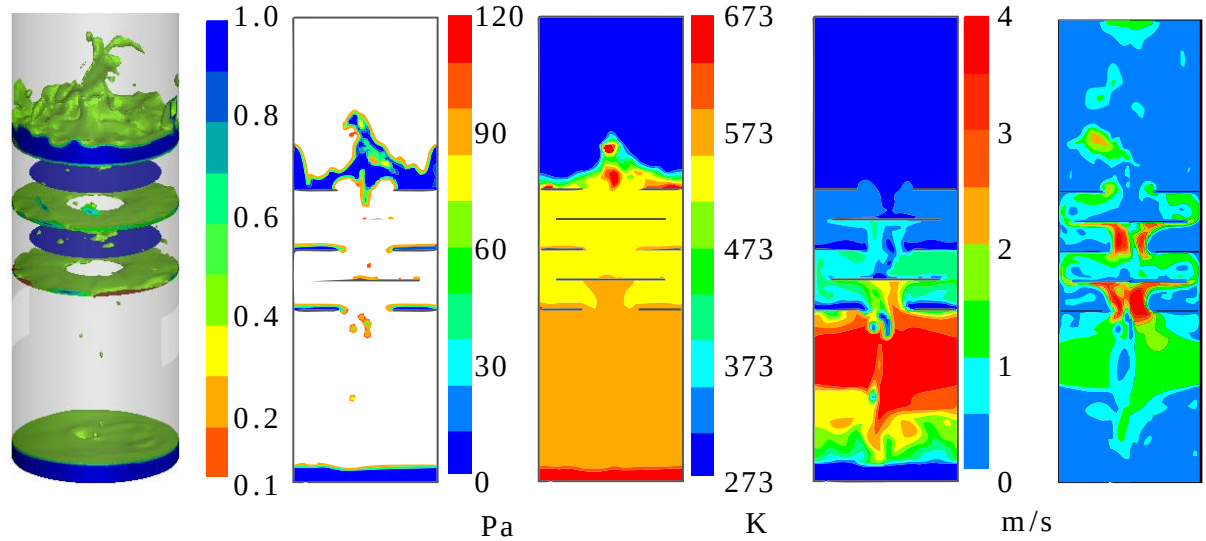

(b) Baseline model with 50% flow condition

Figure 5.5– Instantaneous contours and iso-surface plots for the baseline models.

The coolant liquid level is constantly rising on the donut whilst a very small quantity is flowing towards the bottom stage as this is evident from the liquid level at the bottom for these two cases. The liquid is forced to move upwards through the donut due to the higher pressure exerted by the gases from the lower stages. Moreover, the accumulation of the liquid coolant at the top of the donut caused by the choked flow of gases causing further increase of the resistance from the coolant on smooth passage of the gas. This prevents the smooth flow of the coolant to the lower stages of the column and eventually leads to flooding at high gas and liquid flow rates.

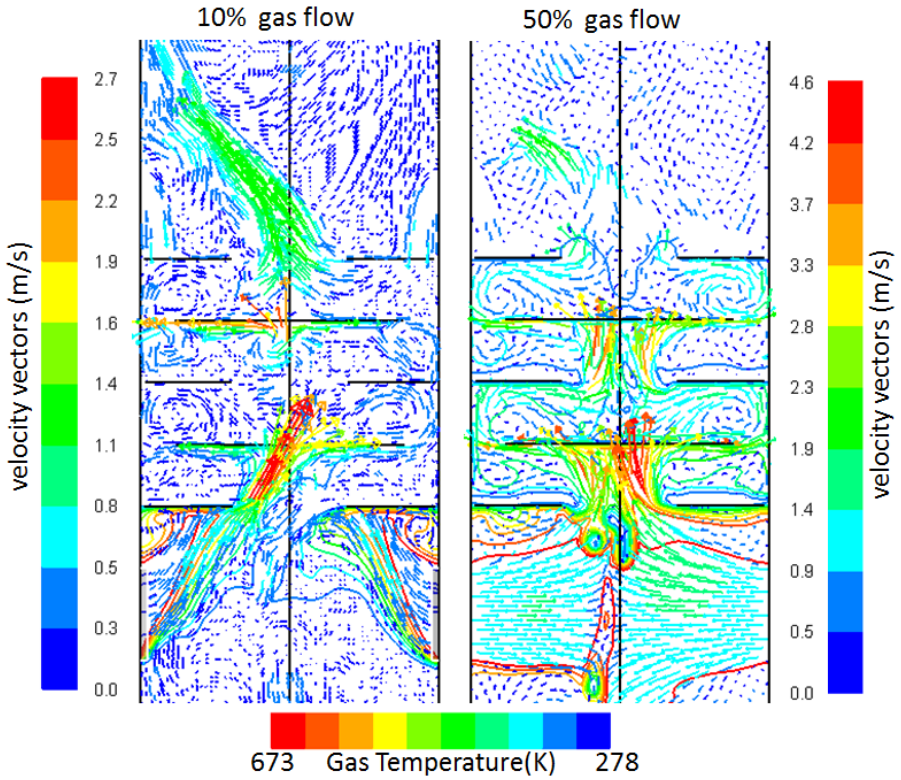

Figure 5.6– Instantaneous velocity vectors in baseline models.

The velocity vectors for the gas combined with temperature contours varying from the maximum 400^{O}C to minimum -5^{O}C are presented in Figure 5.6. This section was created by slicing the equipment vertically at the centre which passes through the vapour inlet. From

this, it can be observed that in the 50% case of the base line model, the maximum velocity reached by the vapour is about 5m/s which is well below the permissible velocity mentioned in the literature based on which the equipment was designed. Since flooding is observed at 50% flow of the designed flow rate, simulation of the 100% flow case on the baseline model was not conducted.

As observed in Figure 5.6, the flow is highly unsymmetrical. It is also observed from the transient simulation that the flow is fluctuating from one side to the other over time. Based on the results of the baseline model, it was observed that the main issue lies with the donut plate design. The flow area for the donut plate is less than the flow area available for disc in the baseline model. In order to obtain the same open area for the disc and donut plates, eight holes with liners were introduced on the donut plate. The liners on the hole aimed to allow only the passage of the vapours through them so that the flooding can be avoided.

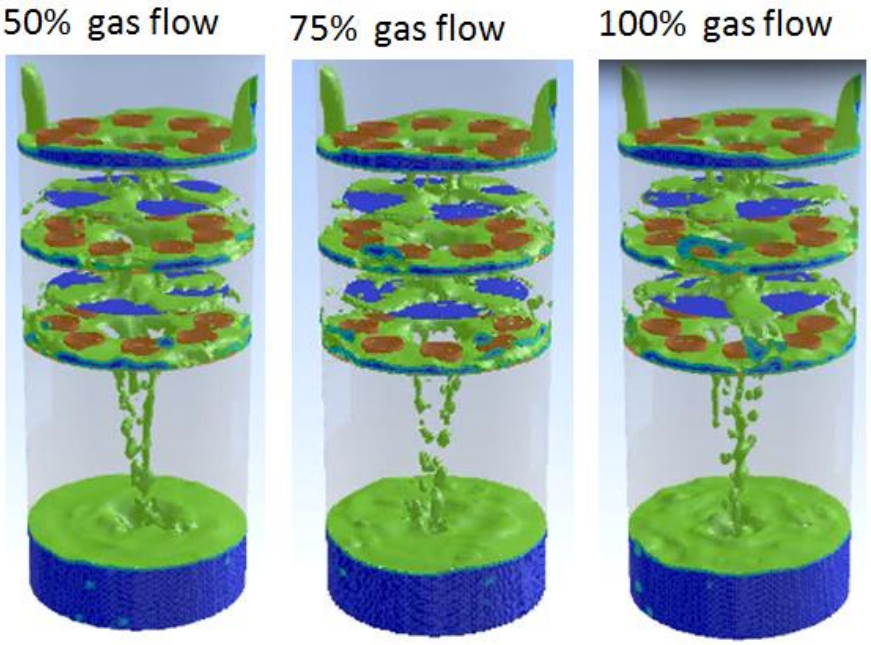

Figure 5.7– Iso-surface with 0.4 volume fraction for oil showing coolant under different vapour flow rates.

Figure 5.7 shows the coolant liquid flow pattern in the modified model for different flow conditions. From this picture it is evident that the flooding is avoided completely by this new configuration and is able to perform up to its designed limits. It was also observed that the disc plates are not fully wetted by the coolant where rivulet patterns can be observed. As this is expected to reduce the heat transfer considerably, it would be preferable that liners are provided for the disc plates as well so that a constant level of coolant will be always maintained on the disc plates.

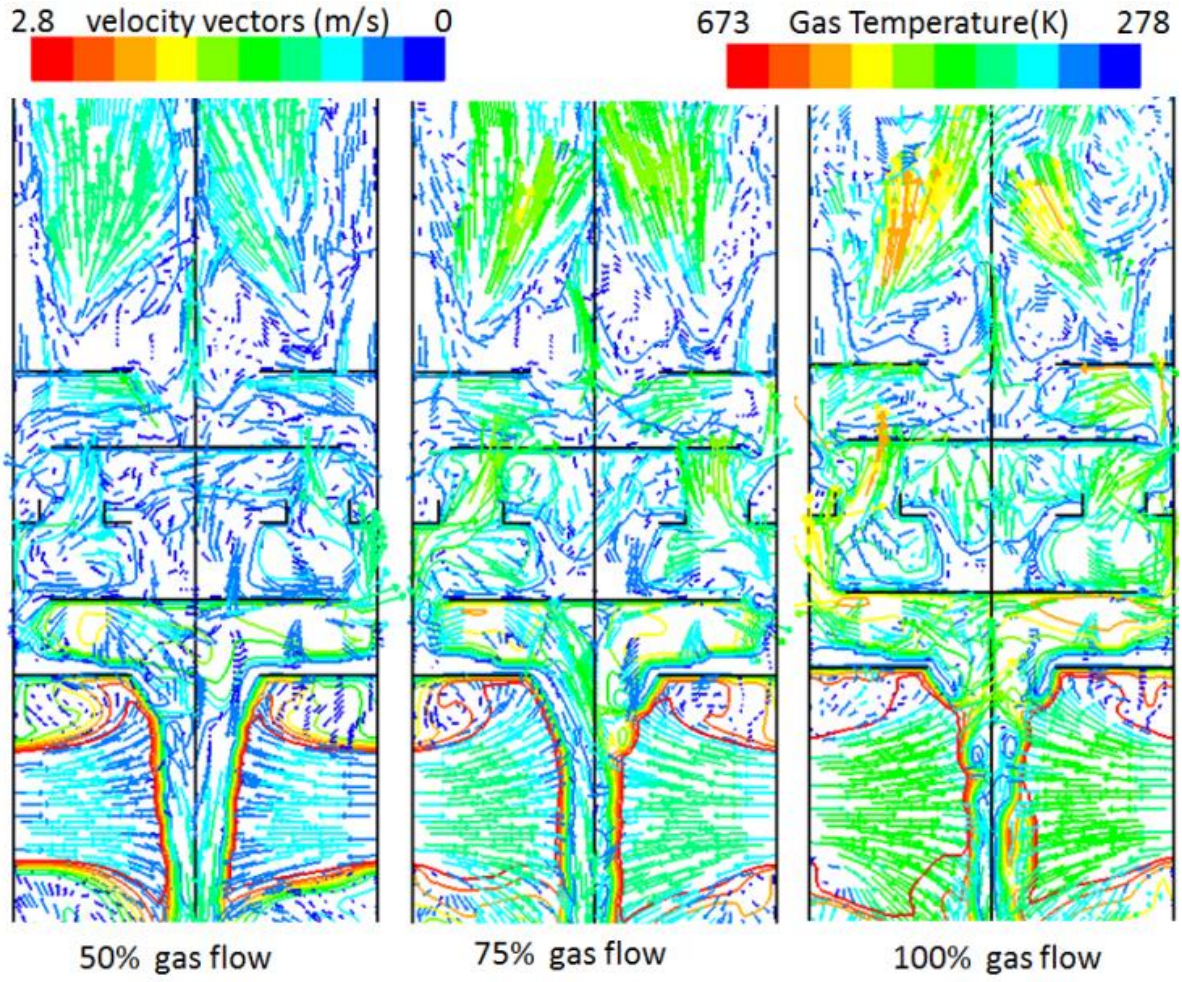

Figure 5.8– Velocity vectors and temperature under different vapour flow rates.

Figure 5.8 shows the combined plot of velocity vectors coloured by velocity magnitude and the temperature contours for the all three cases of the modified model. It is evident that a part of the vapour is bypassing through the holes provided on the donut plates. The holes act as nozzles which direct the vapour towards the disc plates. As the vapours come in contact with the disc plates a vapour recirculation towards the donut plate is observed, thus increasing the contact time with residing coolant while maintaining the high heat transfer rates and higher effectiveness. It is also observed that the flow directions/vectors are unchanged irrespective of the flow conditions and this gives the equipment a scope for scaling up.

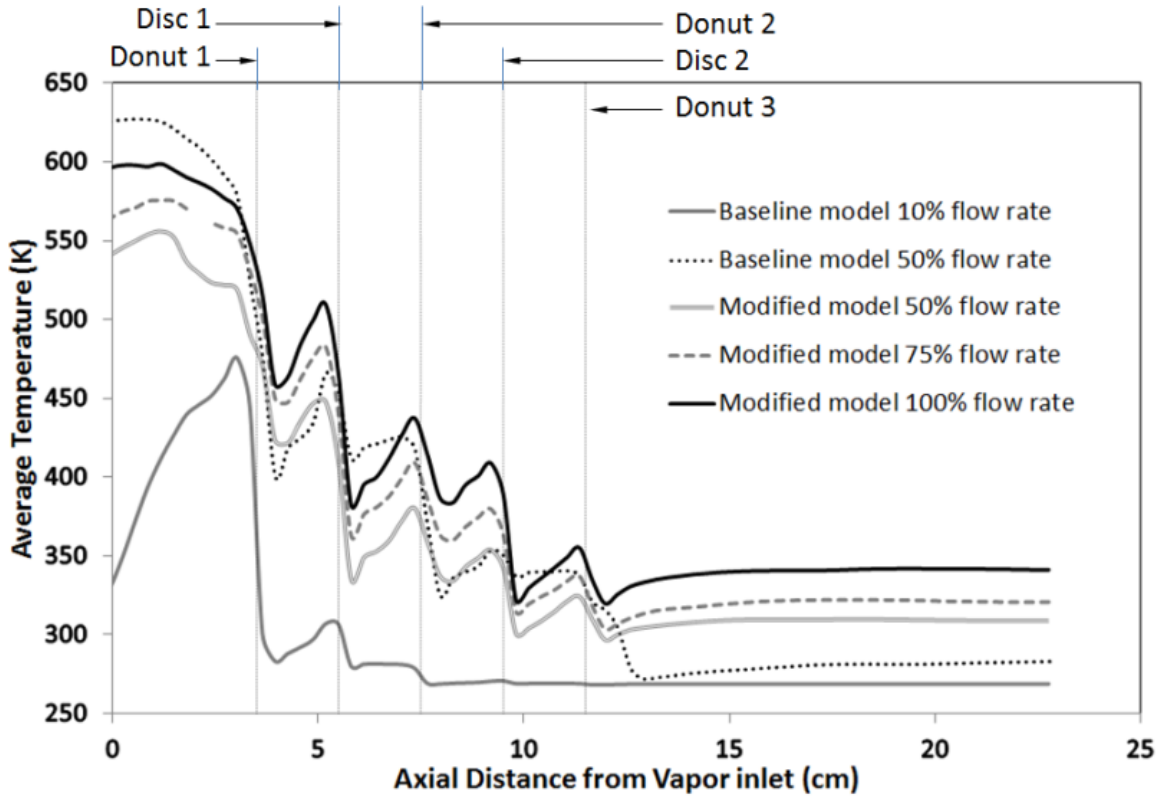

Figure 5.9– Average temperature of the gas along the quenching column height.

The average temperatures of the gas for the different flow cases are presented in Figure 5.9. For the modified model at 100% flow condition, the minimum temperature attained was about 68^{O}C which indicates that a significant amount of cooling can be achieved simply by

just three stages. Further cooling can be achieved if more stages are introduced inside the column. This depends on the nature of the process and the degree of cooling that is required. From this graph it is noted that the major cooling occurs at the disc plate section as it presents two types of cooling. The first one is impingement cooling which refers to indirect cooling and the second is direct contact cooling. After the passage through the holes of the donut plate the vapour are directed towards the disc plate which is highly desired for faster heat transfer.

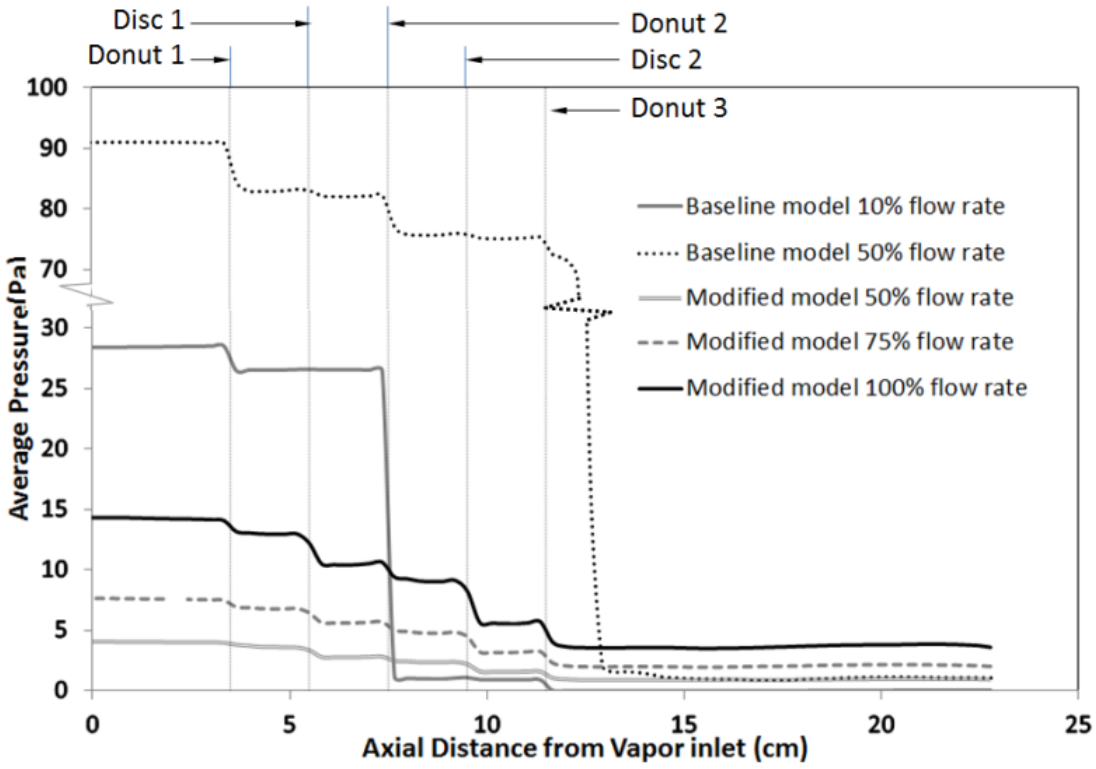

Figure 5.10– Average pressure of the gas along the quenching column height.

Figure 5.10 shows the pressure plot along the length of the quenching column for different simulations. I it is evident that in the baseline model 50% flow case, a large pressure drop occurs at the top most donut section which is 12 -13 cm from the vapour inlet. This is due to the increasing levels of the coolant over the vapour due to flooding. In the case of 10% gas

flow, the maximum gas flow rate occurs at the bottom donut plate level as the temperature of the vapour is high and hence the pressure drop is high at that location. In the modified models the maximum pressure drop was limited to approximately 11 Pa compared to 90 Pa in the baseline case.

The gas flow residence times for the different cases are tabulated in Table 5-2. The top row shows the per cent of the total inlet flow which directly pass through the outlet within a given time. 85% of the flow in the modified model is reaching the outlet within 1 second and thus rapid cooling of pyrolysis vapours can be achieved.

Table 5-2 – Gas residence times (sec) under different vapour flow rate conditions

CFD Run	**% of inlet flow**				
	25%	**50%**	**75%**	**80%**	**85%**
Baseline model with 10%	8.25	-	-	-	-
Modified model with 50%	-	1.18	1.76	1.86	-
Modified model with 75%	-	0.83	1.13	1.26	-
Modified model with 100%	-	0.65	0.84	0.89	0.97

5.2.5 Design variants

Based on the previous study and understanding, four new design variants for the quenching column were developed. The dimensions were chosen based on curtain and window velocities calculated near the bottom of the column where the maximum gas flow rate is expected. Correlations for these velocities are shown in equations (2-1) and (2-2). The values of 1.15 and 0.58 are the recommended Souders-Brown coefficients [85].

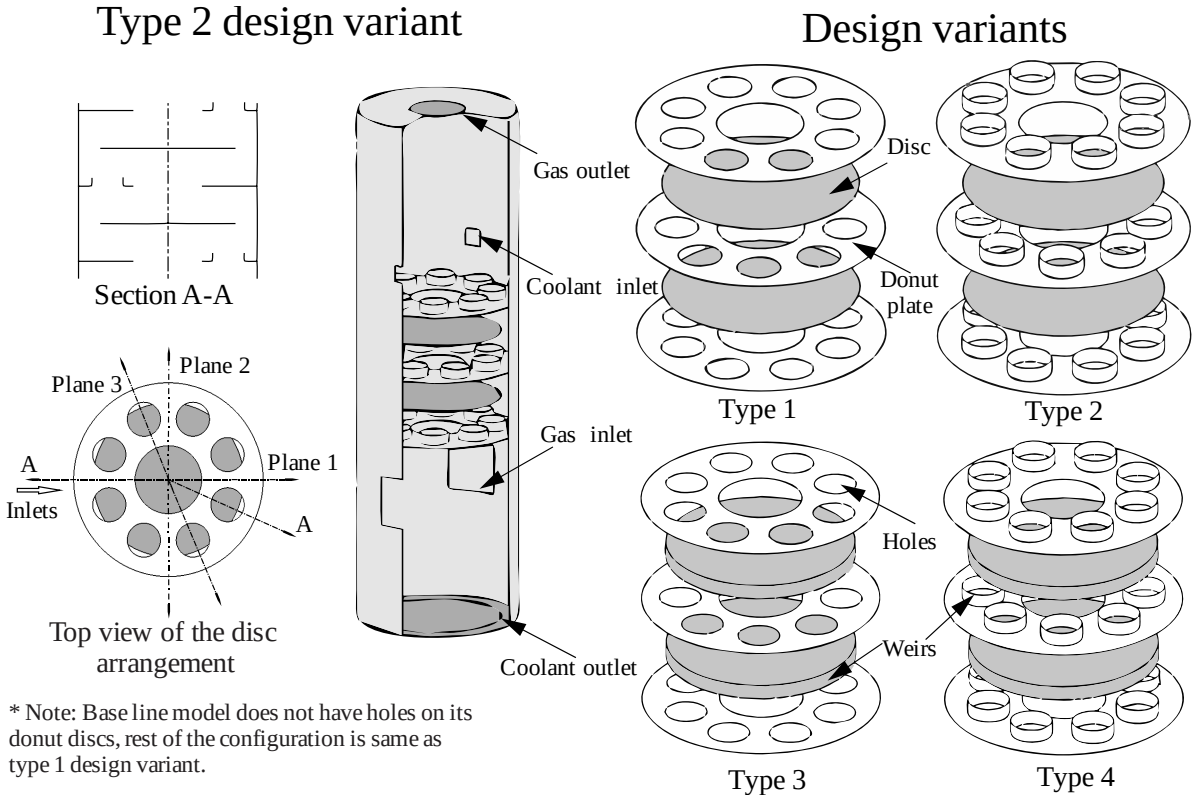

Figure 5.11– Design variants and their disc and donut plate configurations.

The modified designs are identical to the baseline model except for the donut and disc plate configurations. Eight holes of 17 mm in diameter were placed circumferentially on the donut plates. This was done to facilitate the bypassing of a certain quantity of gas to the next stage and thereby reducing the window velocities to the desired range. The four new variants are different among them in terms of the placement of weirs on the disc and donuts. This can also be seen in Figure 5.11, whereas the height of each weir is approximately 5mm. The grid for the four design variants consists of approximately 0.73 million hexahedral cells and maintained a similar grid as shown for baseline model.

The four design variants were numerically investigated at the design flow rate of 0.0044 m^3/s (100% flow condition). Figure 5.12 shows the pressure, temperature and velocity contours, as

well as the liquid coolant iso-surfaces for all cases. It is clearly demonstrated that the flooding phenomena have been completely eliminated in all configurations.

Figure 5.12 shows a magnified view of the velocity vectors for all design variants at different planes. A description of the planes can be seen in Figure 5.11. It is evident that the gas flow pattern differs significantly among the various design configurations. There are certain similarities between the types 1 and 3, while the flow pattern is also quite similar for types 2 and 4, indicating a clear correlation between the structure of the weirs in the donut plates and the resulting gas flow pattern in the quenching column. In cases 1 and 3, no weirs have been incorporated on the donut plate openings; hence the liquid spreading on top of the donut plates affects the gas flow structure in a similar way. The same applies for the types 2 and 4, where weirs have been incorporated on the donut plates of both configurations. However, the liquid flow pattern presents some differences for all configurations, something that has to do with the presence of the weirs on the disc plates of types 3 and 4. In those cases, the presence of weirs on the disc plates, forces the liquid coolant to be accumulated on top of them, providing constant cooling to the plate as well as controlling the downward flow of the coolant in a more uniformly distributed manner. This is clearly evident in Figure 5.12 when one compares the liquid flow pattern, at the disc plate, in types 1 and 2, with the much more uniform flow occurring in types 3 and 4 due to the presence of the weirs.

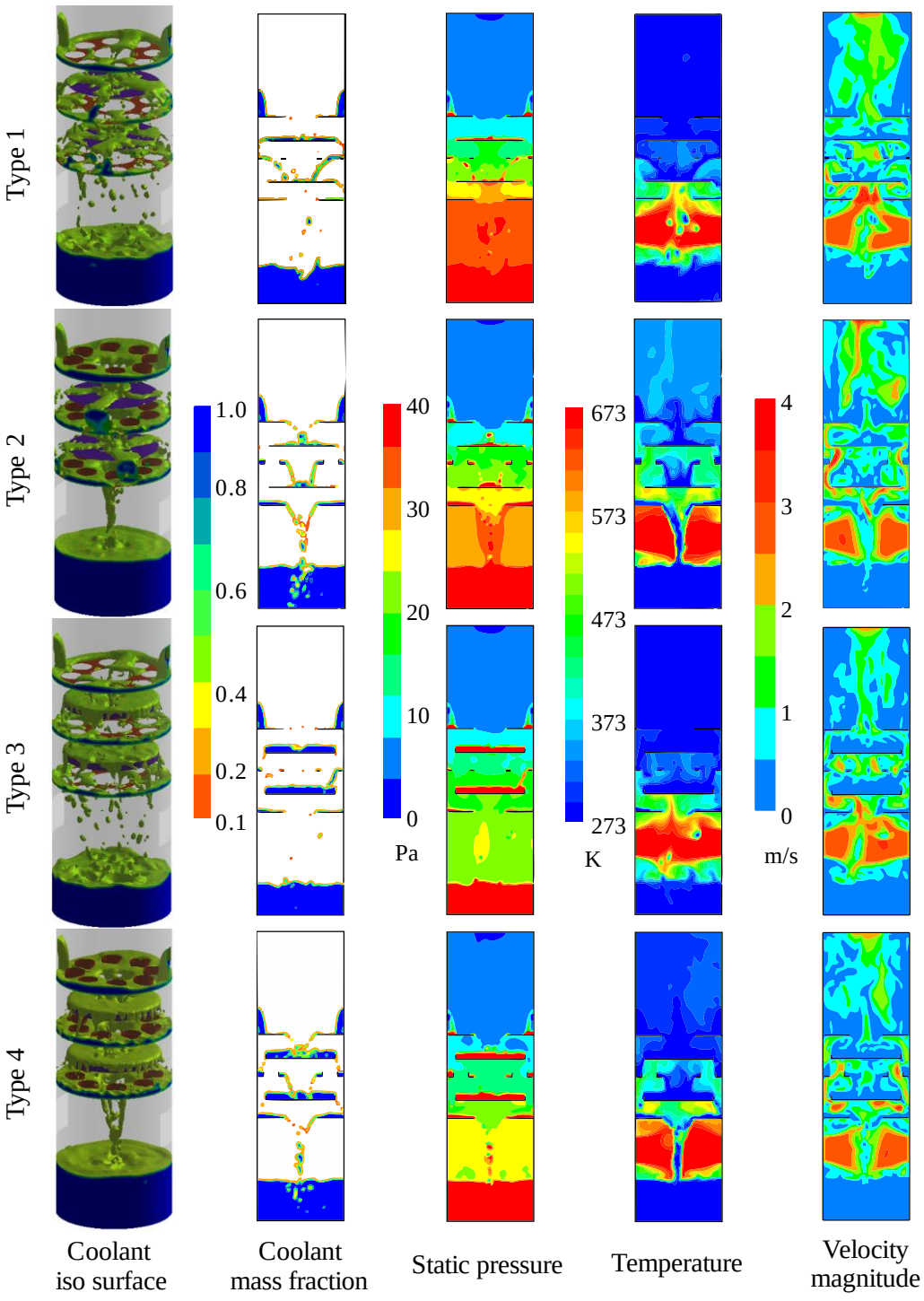

Figure 5.12– Contours and iso-surface plots for the four design variants.

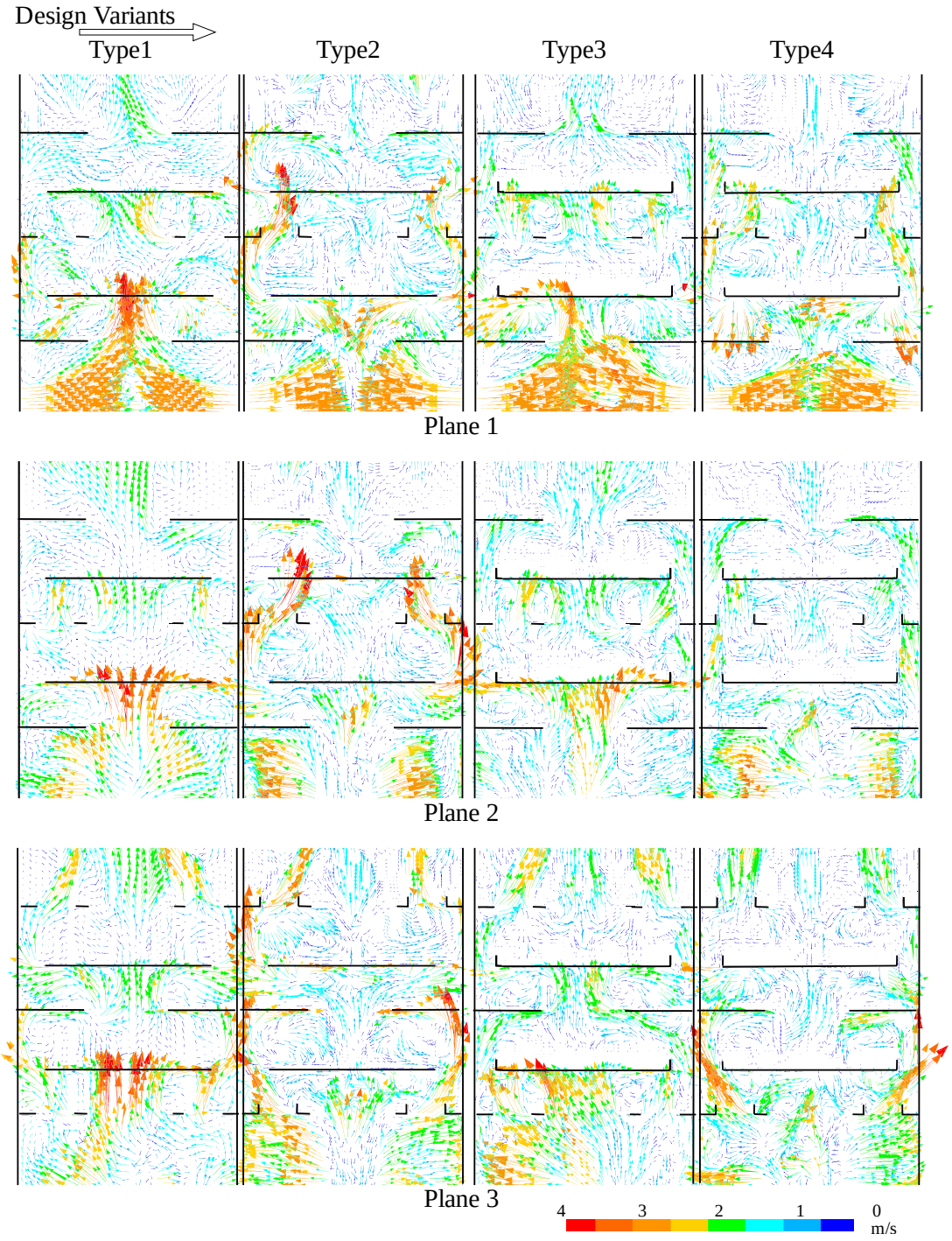

Figure 5.13– Velocity vectors at three different planes for the four design variants.

This has also a huge impact on the liquid flowing from the bottom donut plate, in which an atomised liquid flow pattern is present compared to a more uniform liquid jet flow pattern present in types 2 and 4. Looking at the temperature plot (Figure 5.14) it is clearly evident that the atomised liquid flow pattern of types 1 and 3 provides rapid cooling to the inflowing gases, resulting to a much lower gas temperature of approximately 260^{O}C near the gas inlet region. This large temperature drop is a result of the higher heat transfer surface area provided by the liquid droplet flow pattern in cases 1 and 3, compared to the uniform liquid jet present in types 2 and 4 (gas inlet region temperature of approximately 320^{O}C).

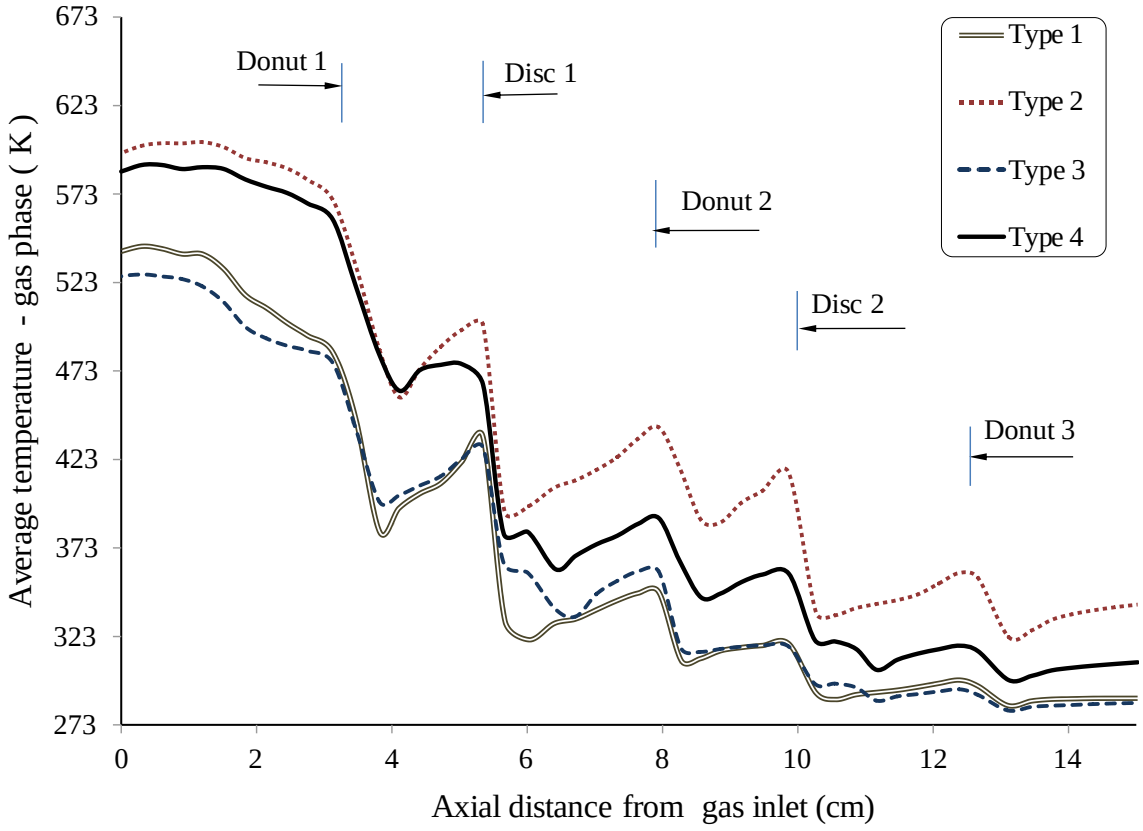

Figure 5.14– Average gas temperatures - Design variants.

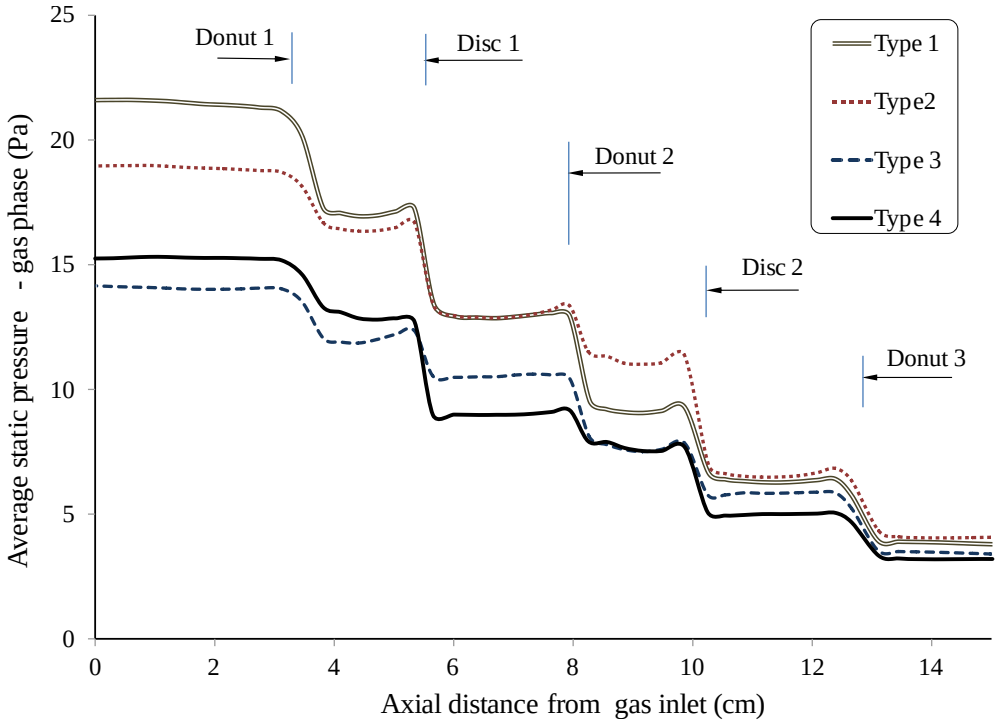

Figure 5.15– Static (gauge) pressure for the four design variants.

Figure 5.15 shows the variation of static pressure along the various stages of the quenching column. It is shown that types 1 and 2 present a much higher pressure build up because of the absence of flow control weirs in their disc plates. In these cases, the momentum contained in the liquid cannot be dissipated by the presence of weirs (like in types 3 and 4), thus allowing the liquid to fully cover the disc openings resulting in higher pressure build up in the quenching column (see Figure 5.12, liquid flow pattern for types 1 and 2). From the industrial application point of view, this means that configurations 1 and 2 are more susceptible to flooding when the coolant flow rate is increased. These issues are not as severe in cases 3 and 4 where the presence of weirs on the disc plates results in a much more uniform and controlled liquid flow from the disc plate to the following donut plate. The uniform liquid curtain present on these two types allows the gas to smoothly transit from a donut plate to the disc plate right above it, without significant flow restrictions, which consequently lead to pressure rise in the column.

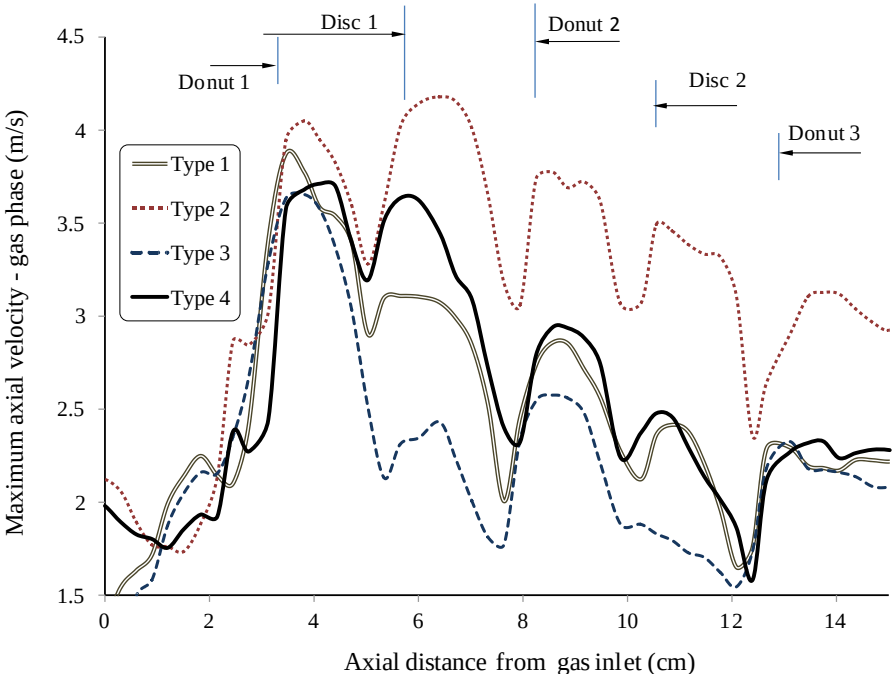

Figure 5.16– Maximum axial velocities for the four design variants.

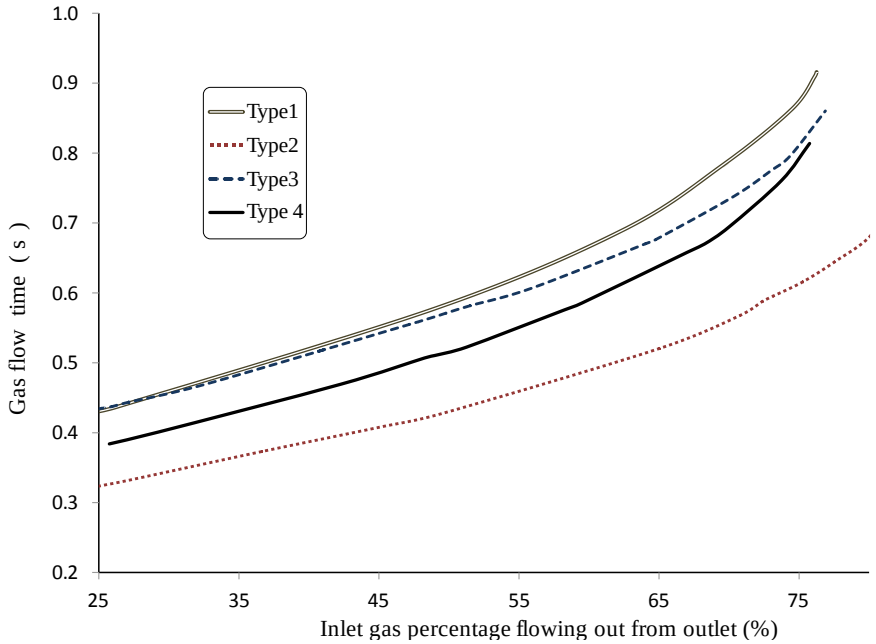

Figure 5.17– Gas residence time in the quenching column – Design variants.

Figure 5.16 and Figure 5.17 show the mean axial velocities and vapour residence times for all design configurations. It is clear that type 2 presents the higher mean axial velocity which results in the lower residence time of the gases into the column. However the lower residence time in type 2 leads to a lesser interaction time between gas and coolant liquid which leads to an inefficient heat transfer between them. Types 1, 3 and 4, present similar velocity patterns, apart from small deviations between disc 1 and donut 2. This results in a similar gas residence time for the three types.

Considering all of the above observations, one can state that the type 4 design is the most suitable design for more flexible and efficiently continuous operation of the quenching column. The fourth type of quenching column might not be able to provide a rapid initial cooling as can be seen in types 1 and 3, however, the uniform hydrodynamic conditions and efficient gas-liquid contact at the subsequent stages, results in the final gas temperature similar to types 1 and 3. Type 4 design also demonstrates a minimum pressure build up in the quenching column, something that makes it more flexible in changes of the liquid coolant flow rates. Types 1 and 2 present higher pressure build up for the same coolant flow rate, something that makes them more susceptible to flooding at higher liquid flow rates or at higher gas flow rates. Overall, it has been shown that the incorporation of weirs on both disc and donut plates result on a smooth and uniform liquid flow pattern inside the quenching column, providing efficient gas-liquid contact and thus significantly improving the heat transfer rates.

5.2.6 Hybrid design

The hybrid design is a combination of the Type 3 and Type 4 design variants as it is proposed in section 5.2.5. The main features of the hybrid design is that it offers the atomisation pattern present in the Type 3 variant at the bottom stage of the column, while it maintains the uniform flow characteristics of Type 4 variant for the rest of the column stages. This

configuration provides a rapid cooling on the pyrolysis vapours as they enter the quenching column, while it minimises the pressure build up and eliminates any flooding phenomena.

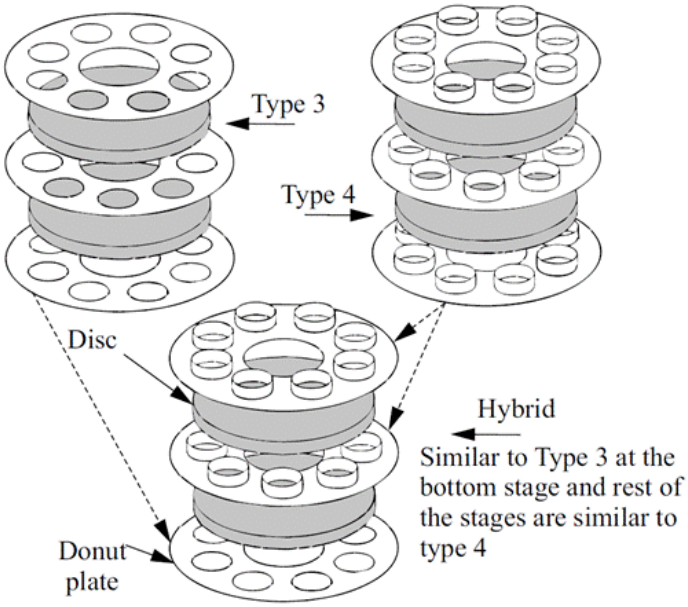

Figure 5.18– Hybrid design of the quenching column.

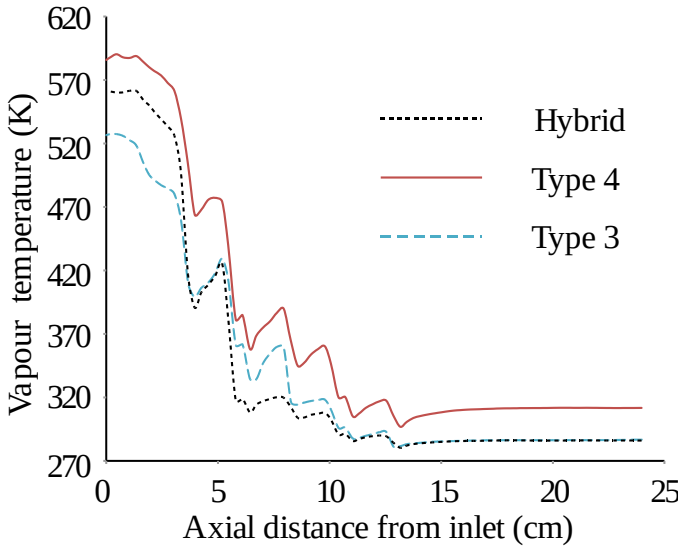

Figure 5.19– Instantaneous average axial temperature plot- quenching column.

The hybrid design shown in Figure 5.18, presents better inlet heat transfer characteristics than Type 4 variant whereas Type 3 variant provides the most rapid cooling at the inlet point mainly due to the increased heat transfer area resulting from the intense coolant atomisation. However, as the vapours flow through the first (i.e. between 3.5 and 5.5 cm) stage of the column, a sudden drop in the vapour temperature is observed in the hybrid design shown in Figure 5.19 is due to the combined effects of the coolant atomisation at the bottom donut plate and the uniform curtain flow from the upper disc plate. The vapour temperature is further decreased at the subsequent stages where it is eventually matched by the Type 3 variant towards the outlet of the column. The Type 4 variant is not able to provide as efficient vapour cooling as the Type 3 or the hybrid configuration at any stage of the column.

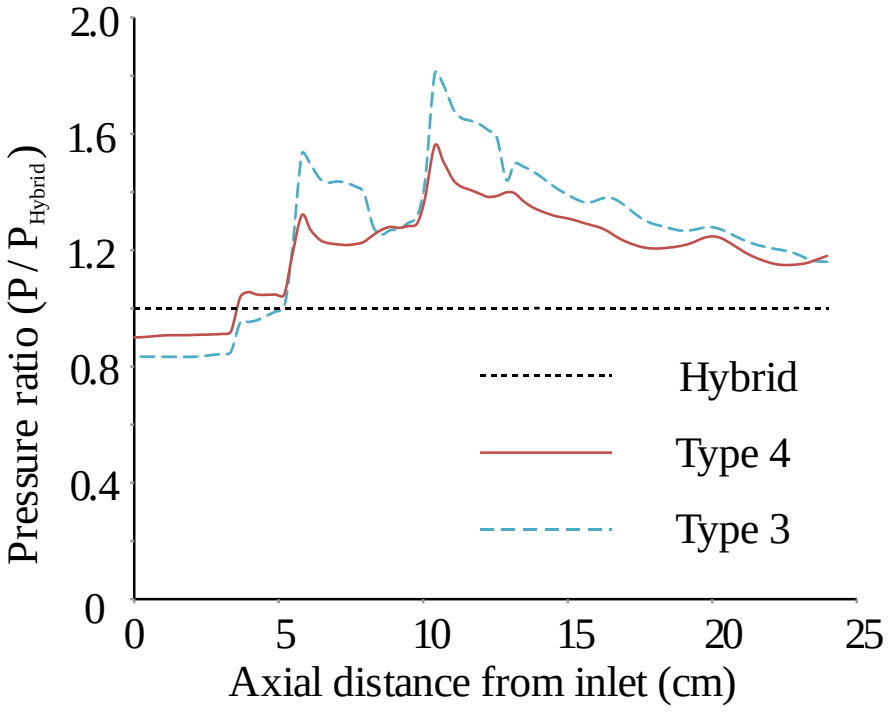

Figure 5.20– Average pressure ratio plot – hydrodynamic models.

Observing the pressure variation in the three configurations (Figure 5.20) one can see that the hybrid design presents the lowest overall pressure build up in the column compared to the

Types 3 and 4 variants. Comparing the pressure build up as a pressure ratio of Types 3 and 4 to the hybrid design, one can observe that the pressure close to the inlet is higher in the hybrid configuration, something that is expected to positively affect the rapid vapour condensation at an early stage. The column pressure significantly increases at the later stages for Types 3 and 4 compared to the hybrid case. This pressure rise is expected to improve vapour to liquid conversion at the subsequent stages; however it makes the column more susceptible to flooding phenomena.

Overall, the hybrid design has been shown to provide better heat transfer performance with rapid vapour cooling. The increased vapour pressure at the early stages in the hybrid design facilitates better condensation, whereas its uniform hydrodynamic conditions and low pressure build up at the subsequent stages greatly overcome possible flooding phenomena.

5.2.7 Conclusion

The hydrodynamic behaviour of a quenching column used for the condensation of fast pyrolysis vapours has been presented in step1 studies. The study focused on the column design optimisation for the elimination of the flooding phenomena which were reported in the experimental procedures. The effect of the design alterations on the liquid to gas heat transfer has also been investigated. The original design (baseline model) has been simulated for two different gas flow conditions of 10% and 50% design flow rates. Flooding phenomena were already observed on the 50% flow case, as also reported in the experimental procedure, thus the operation of the column at the design flow rate (100%) was not attempted.

Four new design variants, based on the Souders-Brown coefficients, were developed and simulated. It was shown that the gas flow is greatly affected by the weirs on the donut discs (gas flow similarities between types 1 and 3), while the presence of weirs on the disc plates greatly affected the liquid flow distribution at each stage. It was shown that the absence of weirs at bottom donut plate in types 1 and 3 resulted in an atomised liquid flow which has a significant impact on the initial temperatures of the gases due to the high heat transfer area.

Types 2 and 4 present a more uniform jet like type of liquid flow on the bottom donut plate, something that reduces the gas-liquid heat transfer rate which causes $50^{O}C$ higher average temperature at the first stage compared with type 1 and 3. However, it was shown that the uniform liquid flow at the subsequent stages of the column is able to provide the necessary gas-liquid contact area for efficient interphase heat transfer and subsequent cooling of the pyrolysis gases. The type 4 configuration was proved to be the more efficient and flexible design among all the cases. However, in order to maximise the rapid heat transfer, we propose the type 4 configuration combined with type 3 donut plate configuration at the bottom most stage.

In this study, the important problem of quenching column flooding and hydrodynamic behaviour was tackled and resolved. Apart from that, the pressure difference across the system has been reduced from 90Pa in the base line case to 25-15 Pa in design variants without compromising heat transfer. In all design variations, the gas flow time within the quenching column was less than 0.8 seconds signifying the rapid cooling of the vapours which is essential for higher liquid bio-oil yield.

5.3 Step2 – Condensation model for indirect contact condenser

This section presents the detailed modelling of the water cooled condenser. It also outlines the boundary and operating conditions used in this simulation. The assumptions made during the development of the condensation model are also mentioned.

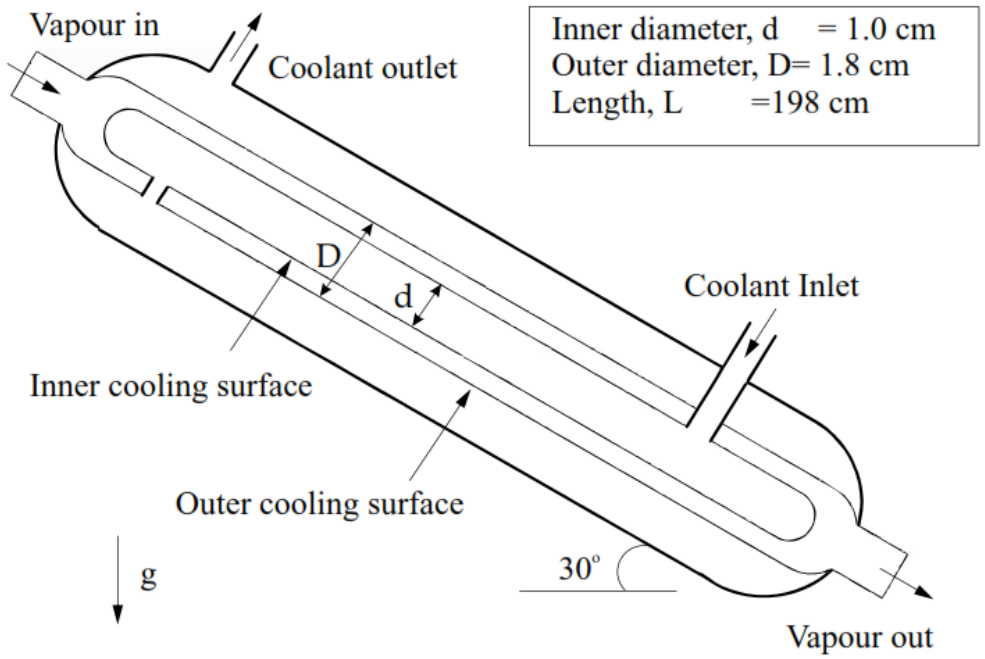

Figure 5.21– Double surface water cooled condenser.

The scope of the step 2 study is to simulate the phase change phenomena and to capture the selective condensation of the pyrolysis vapours inside the liquid collection system (LCS). The double surface water cooled condenser shown in Figure 5.24 was selected as the model condenser for validation purposes. The commercial CFD code ANSYS Fluent 13.0 has been used as the computational platform for the simulation of the condensation process. The phase change phenomena were incorporated to the code as user defined functions (explained in Appendix A).

The computational grid size is around 1.1 million and comprised of all hexahedral elements as shown in the Figure 5.22.

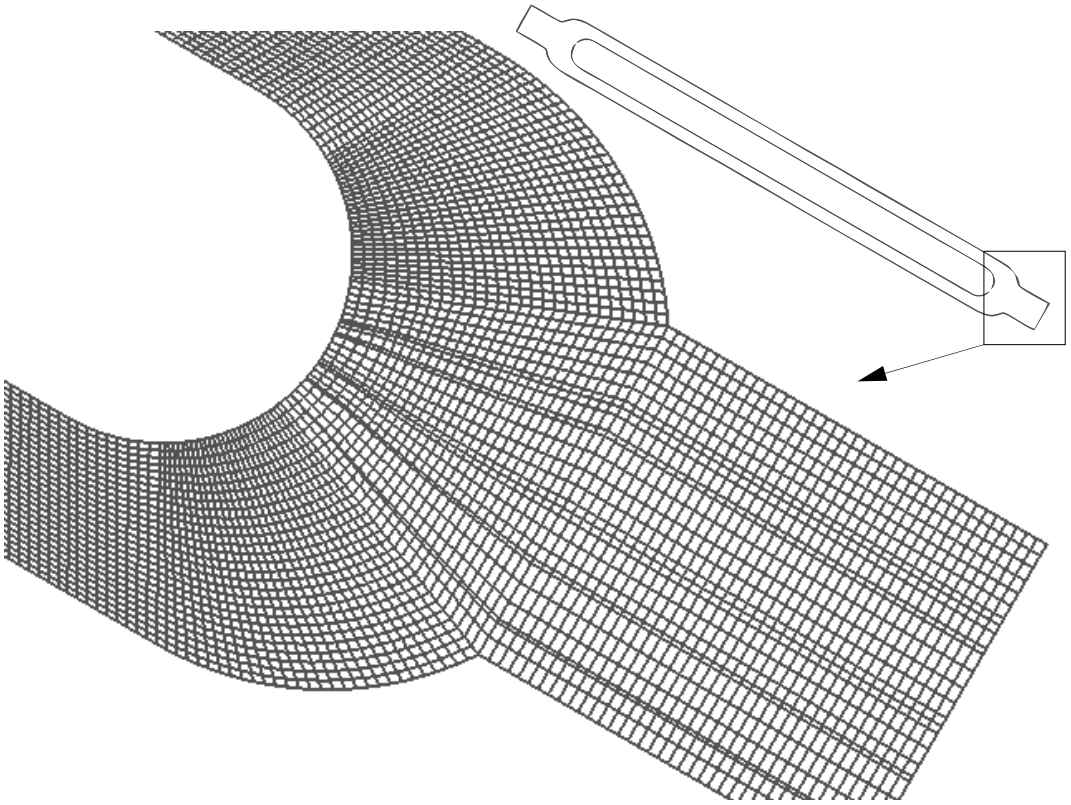

Figure 5.22– Grid - Double surface water cooled condenser.

5.3.1 Operating conditions

The double surface water condenser (Figure 5.22) was used in the experiments conducted at Aston University as a first stage condenser within the liquid collection system (LCS) [48]. According to Salter [48], the flow rate of the cooling water is 2 L/min at 15^{O}C and the vapour flow rate into the condenser 12 L/min at 500^{O}C. The vapour flow includes condensable and non-condensable gases. In the current computational model the wall surfaces, which are exposed to the water modelled with constant temperature of 15^{O}C with an assumption of marginal increase in cooling water temperature in the system.

Biomass was injected to the experimental reactor at rate of 100g/hr. According to the mass balances obtained from the experiments, the total conversion of biomass into vapours is approximately 70 wt.%, whereas the non-condensable gases amount to 15 wt.%. Nitrogen is used as the carrier gas, which is also modelled together with the non-condensable gases.

5.3.2 Assumptions

The condensation model application is based on the following assumptions.

I. The pyrolysis vapours together with the carrier gas nitrogen is treated as an ideal mixture. This is mainly due to the unavailability of the excess function data in the literature.

II. The density of the species over the computational domain was calculated based on the ideal gas assumption. However, while estimating the vapour pressures, and critical properties such as viscosity and thermal conductivity, real gas behaviour was considered.

III. Pyrolysis vapours are modelled with 11 chemical species (Table 4-2) and are assumed to represent the majority of its behaviour in terms of critical properties. This is a compromise between accuracy and the speed of the solution. In reality, pyrolysis vapours consist of more than 100 chemical compounds and it is nearly impossible to model all the species in this kind of study. The model presented here is readily scalable to different species groups based on the feedstock used for pyrolysis.

IV. Fugacity coefficients are assumed as 1. This assumption can be justified when the system is not under high pressures.

The non-condensable gases obtained from the mass balance done during the experiment are modelled as Nitrogen and clubbed with the carrier gas composition. The very low concentration of the non-condensable gas fraction produced during biomass pyrolysis, is not expected to significantly influence the thermodynamic and fluid dynamic behaviour of the system.

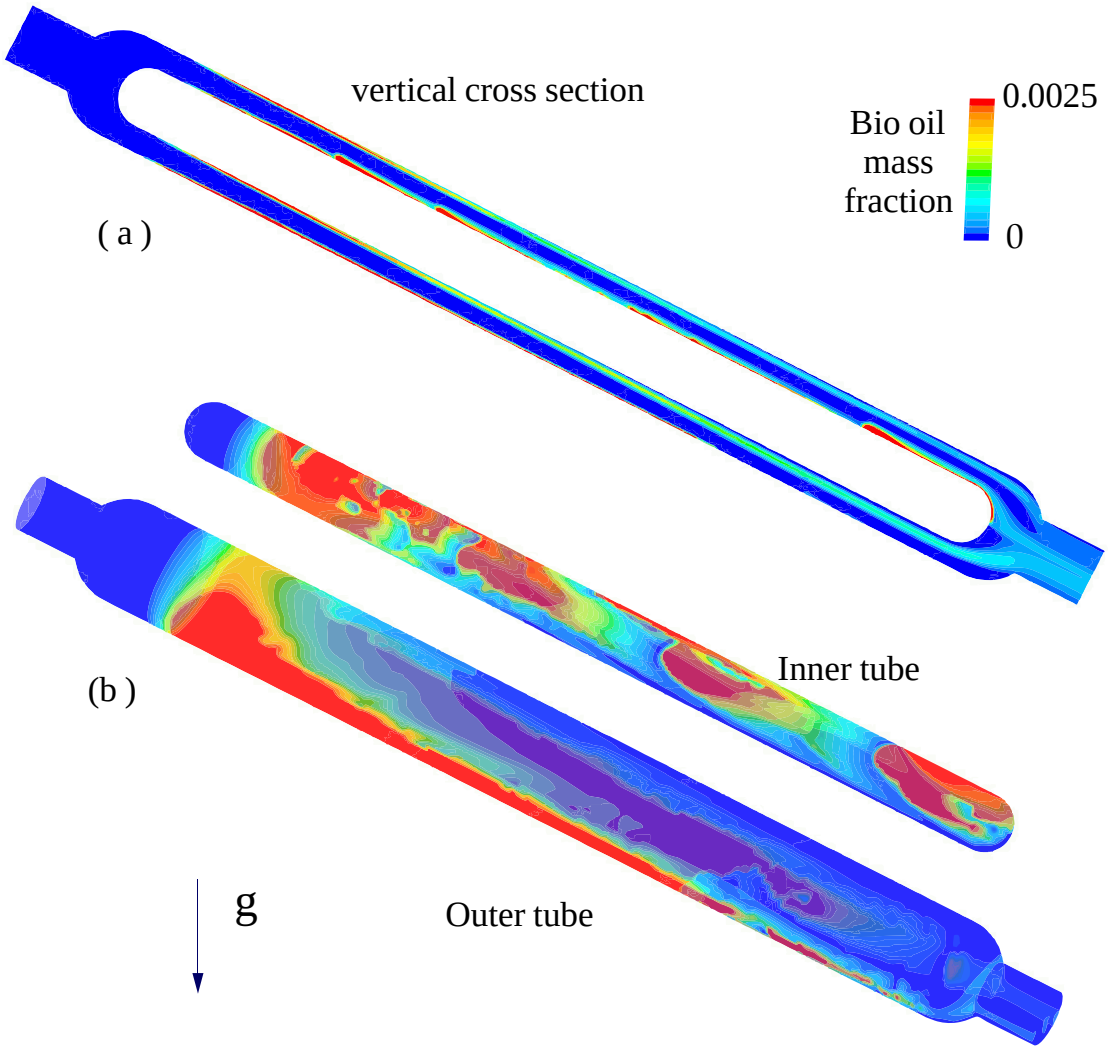

Figure 5.23– Bio-oil mass fraction contours.

5.3.3 Results and discussion

The geometry of the condenser used in the current CFD model is the same as the double surface condenser used in the pyrolysis experiments [48].

Figure 5.23 (b) shows the volume fraction of the bio oil at the outer tube and inner tube surfaces of the condenser. The contours of the bio-oil volume fractions on the vertical section of the condenser are presented in Figure 5.23(a). From this figure, it is evident that condensation is more intense at the surfaces at which the cooling water is in contact with. It also demonstrates the bio-oil droplet accumulation on the condenser during the condensation process. The dynamics of the bio-oil mist is highly influenced by the gas flow within the condenser. This is evident from the contours on the inner tube surface volume fraction as they can be seen in Figure 5.23(b), where ripple like formation is observed. In the case of the outer tube, the gas flow at the bottom side forces the bio-oil droplets into the central zone of the annular section.

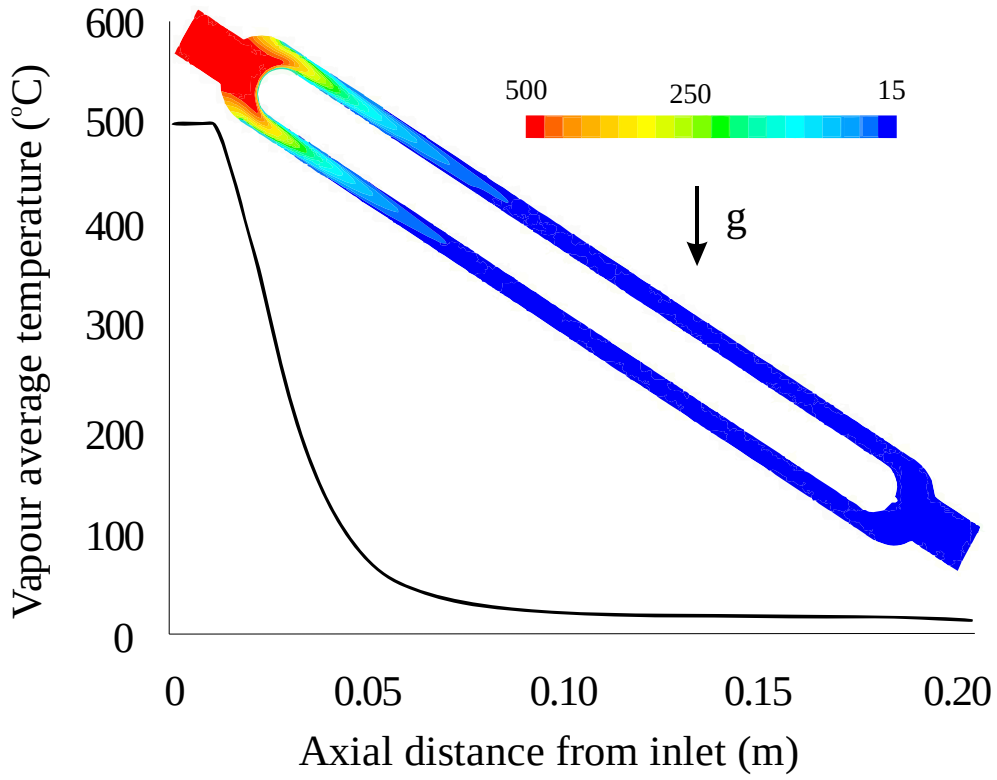

Figure 5.24–Temperature plot along the length of the condenser.

In Figure 5.24, the contours of the gas temperature are shown where it can be observed that the gas temperature is lower at the wall surfaces than in the middle zone of the annulus space between the inner and the outer tubes. The gravitational force vector is shown in the same figure as 'g'. The liquid bio-oil droplet formation discussed in the previous section is mainly due to this particular temperature profile of the gas. To have a clearer picture of the temperature variation along the length of the condenser, the average temperature, from the inlet to the outlet, is plotted in the same figure. The rapid vapour temperature drop can be seen in the same plot, where the inlet vapour temperature is approximately $500^{O}C$ and outlet temperature is around $18^{O}C$. It can be observed that the most significant region for vapour cooling is located between ≈ 0.02 – 0.07m of the length of the condenser.

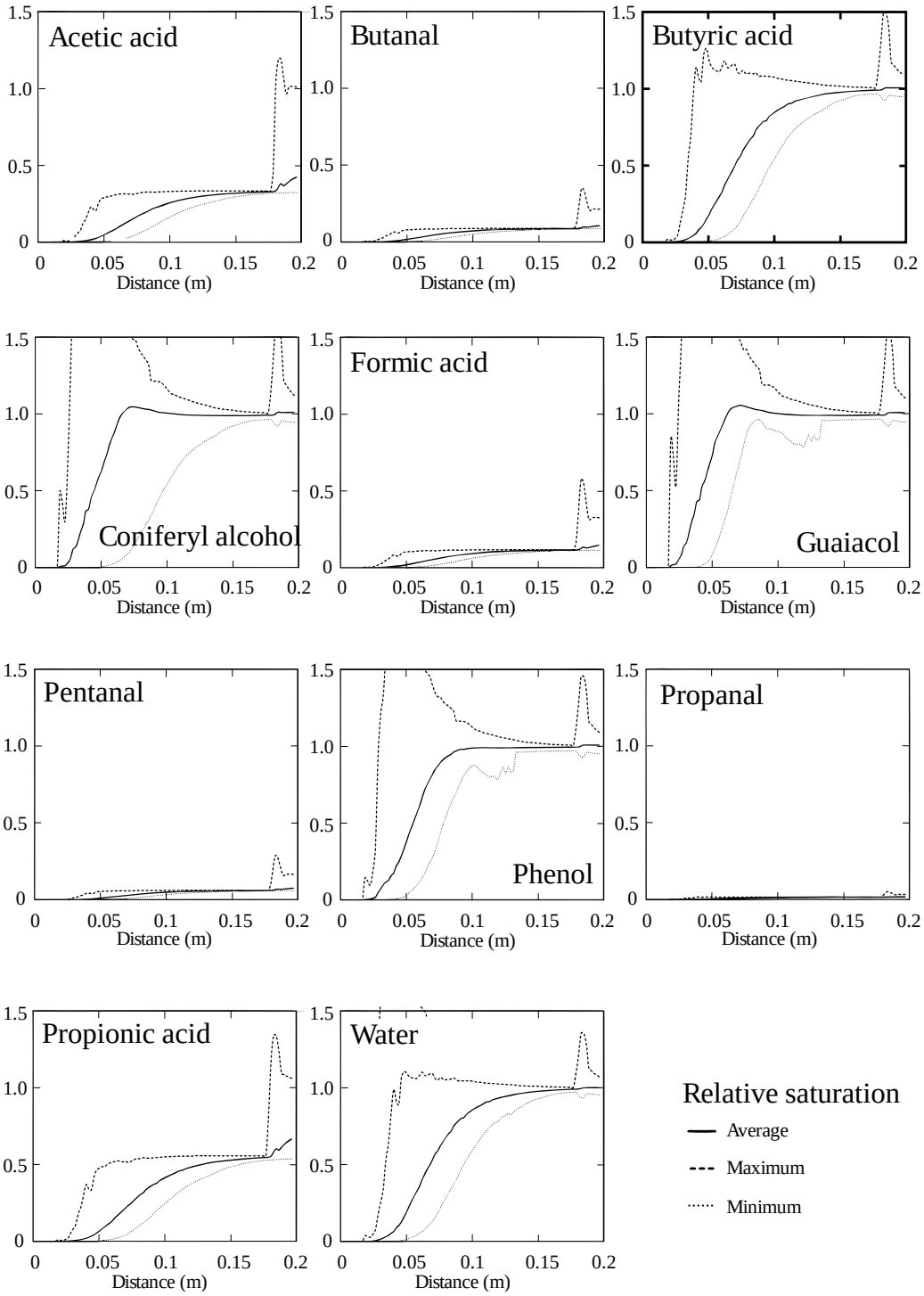

Figure 5.25– Relative saturation plot.

Figure 5.25 shows the variation of the relative saturation of the different compounds along the length of the condenser. The dashed lines represent the maximum and minimum values at the different sections, while the continuous line represents the volume averaged compound saturation at each particular section of the condenser.

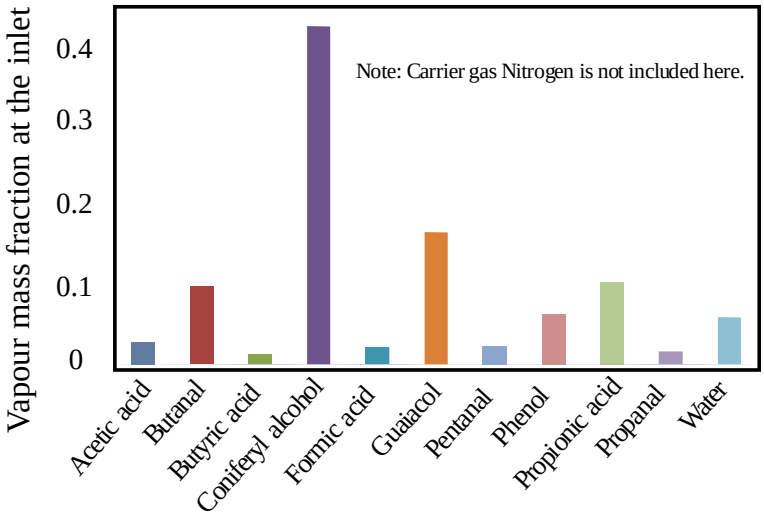

Figure 5.26– Mass fractions of the pyrolysis vapour components at inlet.

A compound will change phase (condense) when its relative saturation exceeds unity. From Figure 5.25, it can be seen that the maximum relative saturation for Butyric Acid, Coniferyl Alcohol, Guaiacol, Phenol and water reaches its maximum value before 0.1 m of length, while the curve relaxes towards its equilibrium value as the vapours continue to condense beyond this region. The maximum relative saturation occurs close to the wall boundaries due to the significantly lower temperatures at those points. The minimum relative saturation values are mainly located towards the centre of the annular section where temperatures are higher. The volume averaged relative saturation line represents the volume weighted average of the relative saturation at different sections of the condenser. It shows that the average relative saturation along the condenser has an increasing trend (approaching unity) due to the rapid cooling of the vapours and gives a very good indication of the bio-oil composition at the first stage of condensation.

One can see that for the components where the average saturation has exceeded unity, a significant proportion of them will be collected in the form of liquid bio-oil at the first stage. For some of the components with low initial partial pressures, as shown in Figure 5.26 (e.g. propionic acid), only small traces will be collected that are mainly determined by the maximum relative saturation. For those components that none of the maximum and consequently none of the average and minimum saturations have exceeded unity, no traces will be detected in the final bio-oil product.

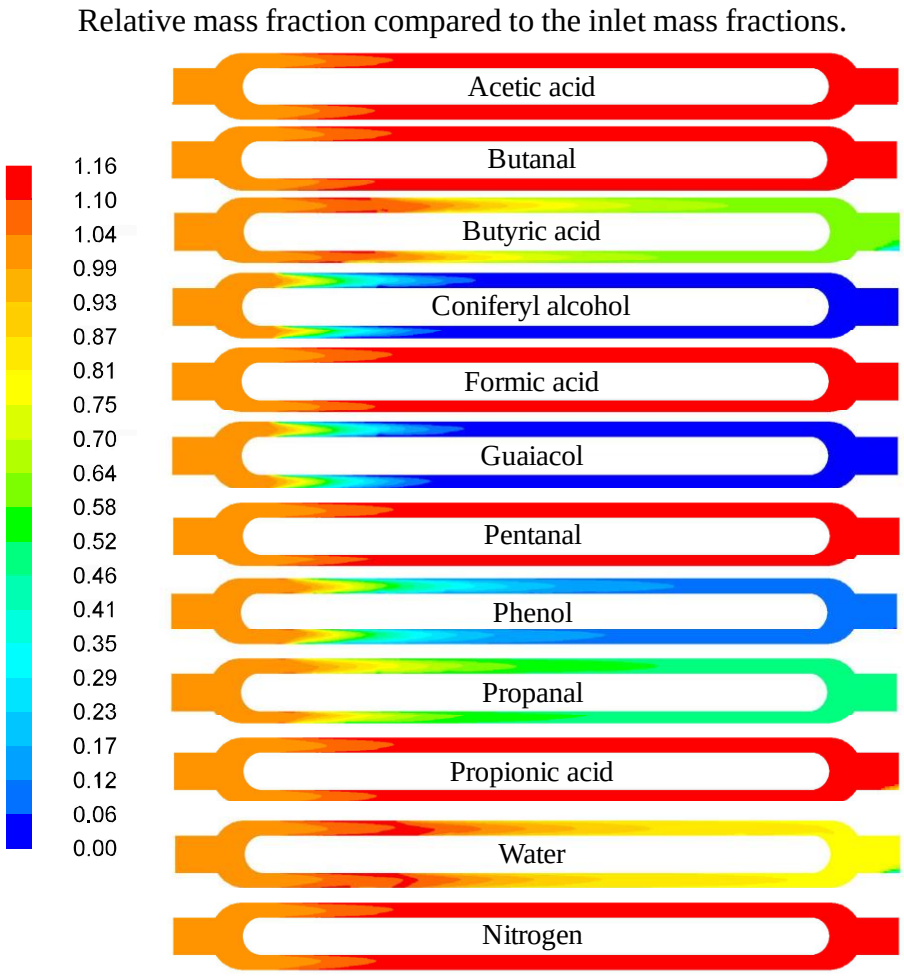

Figure 5.27– Relative mass fraction of the vapour components.

The relative mass fraction contours of each compound are shown in Figure 5.27. These contours are plotted at the vertical mid-section of the condenser. At the inlet, all the values are equal to unity. As the vapours flow through the condenser, the values of the relative mass fraction decrease or increase depending on whether the compound within the condenser changes its phase to liquid bio-oil or not. Those compounds with maximum relative saturation above unity within 0.1 m of length keep condensing as the vapours flow along the length of the condenser. The relative mass fractions of those decrease continuously. The blue colour at the outlet indicates that a particular compound is completely condensed. Light green colour indicates that those components have been partially condensed within the condenser, whereas the red colour indicates that those compounds have been slightly or not been condensed at all.

Another interesting point that can be observed in Figure 5.27 is that the values of the relative saturation increase sharply for many components at around 0.18m. This is primarily attributed to the rise in gas pressure near the exit of the condenser due to the diffuser effect at the point where the inner tube ends. As the inner tube ends, the cross sectional area increases steadily over a small distance which effectively gives a small rise in pressure.

The maximum velocity of the vapour and the average pressure within the condenser are plotted in Figure 5.28 and Figure 5.29 respectively. From Figure 5.29, it is evident that at lower temperatures, a small increase in pressure highly increases the value of the relative saturation of the components. The relative saturation values shown in Figure 5.25 indicate that at higher temperatures condensation is primarily affected by heat transfer rates whereas at later stages, where the temperature is low, they highly depend on pressure changes.

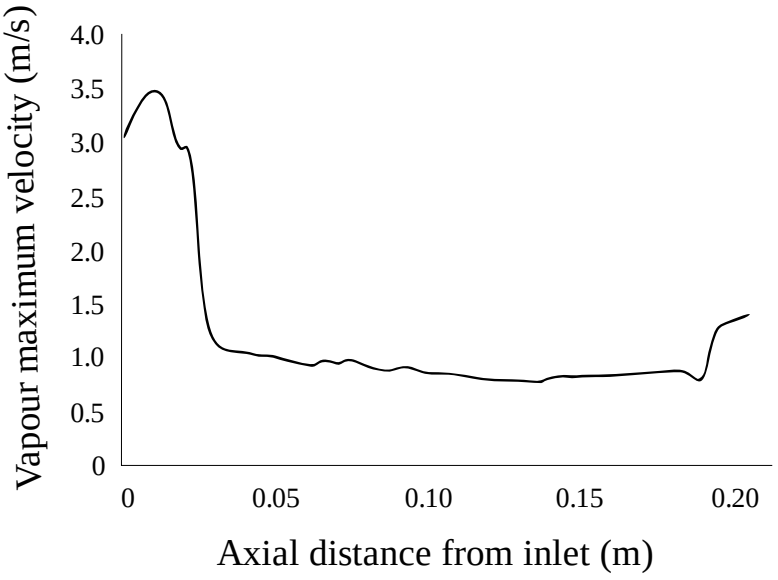

Figure 5.28– Maximum velocity plot.

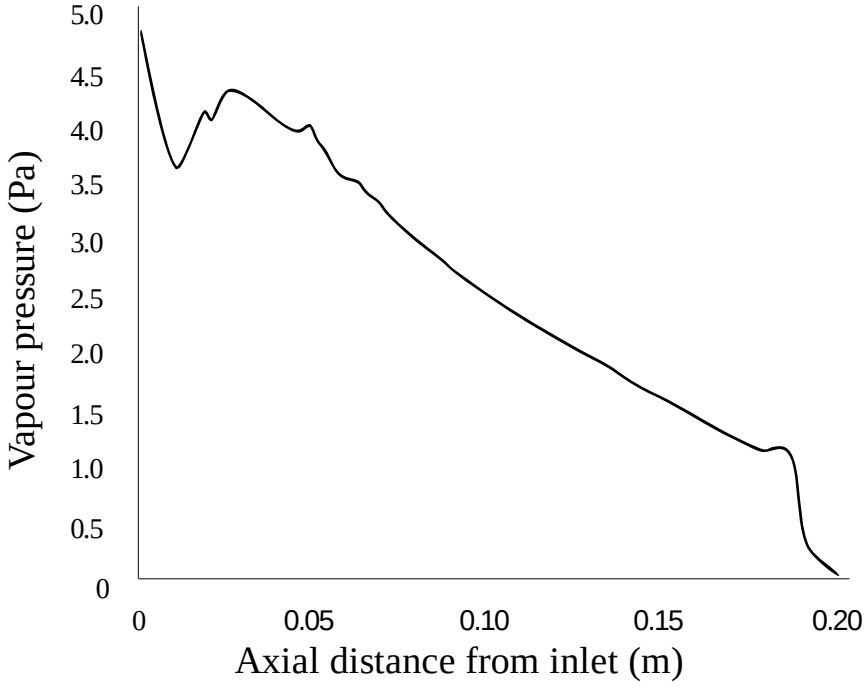

Figure 5.29– Average vapour pressure plot.

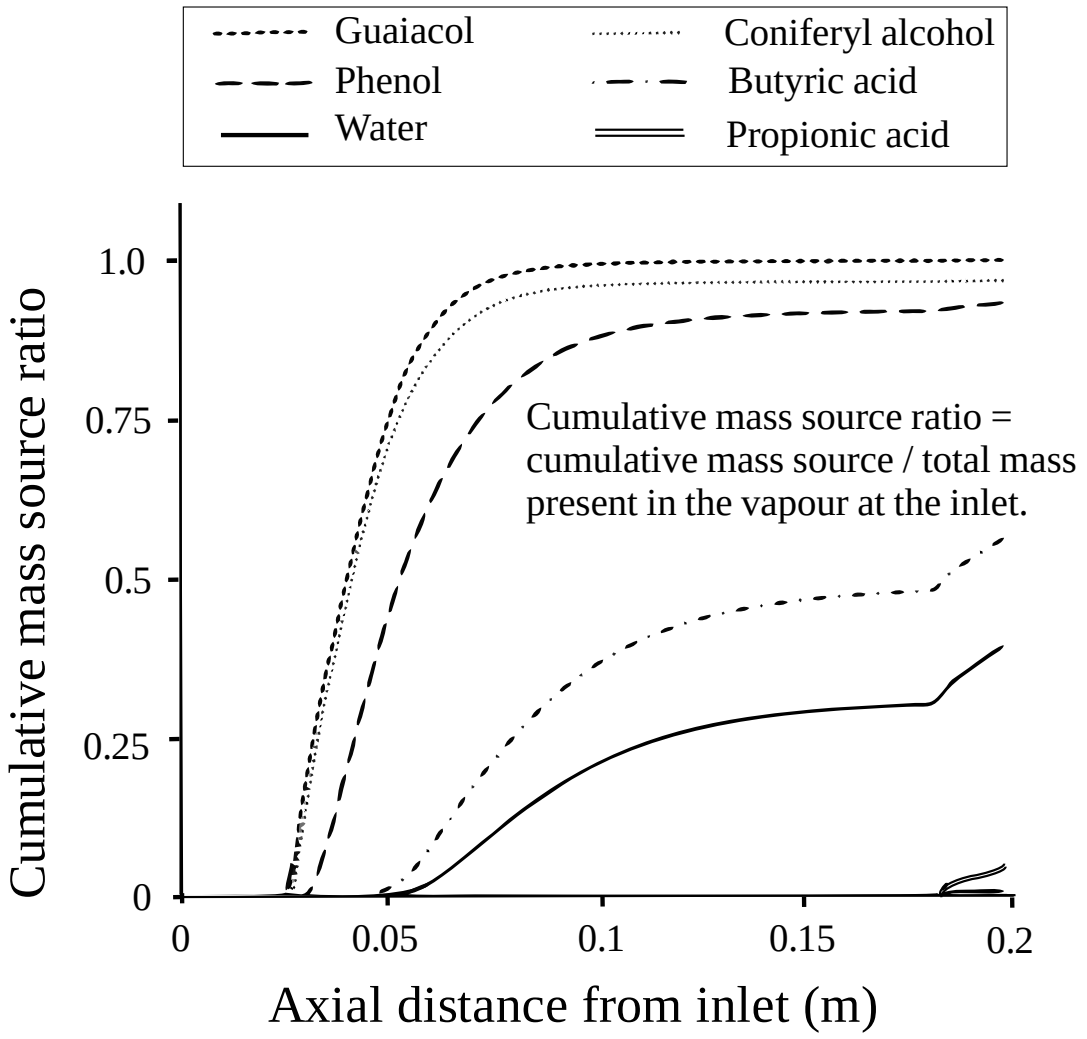

Figure 5.30– Cumulative mass source ratio plot.

Figure 5.30 shows the plot of cumulative mass source (amount of mass transferred from vapour phase to bio-oil phase) ratio along the direction of the flow. This is the ratio between the cumulative mass source of the particular component and its mass fraction at the inlet. When the value of this ratio approaches unity, it indicates the complete conversion of that particular component. From Figure 5.30 we can see that Guaiacol is the first component condensed completely followed by Coniferyl Alcohol and Phenol. It is also worth noticing

that butyric acid and water have been partially condensed within the condenser. Approximately 35% of water vapour is condensed in the bio-oil.

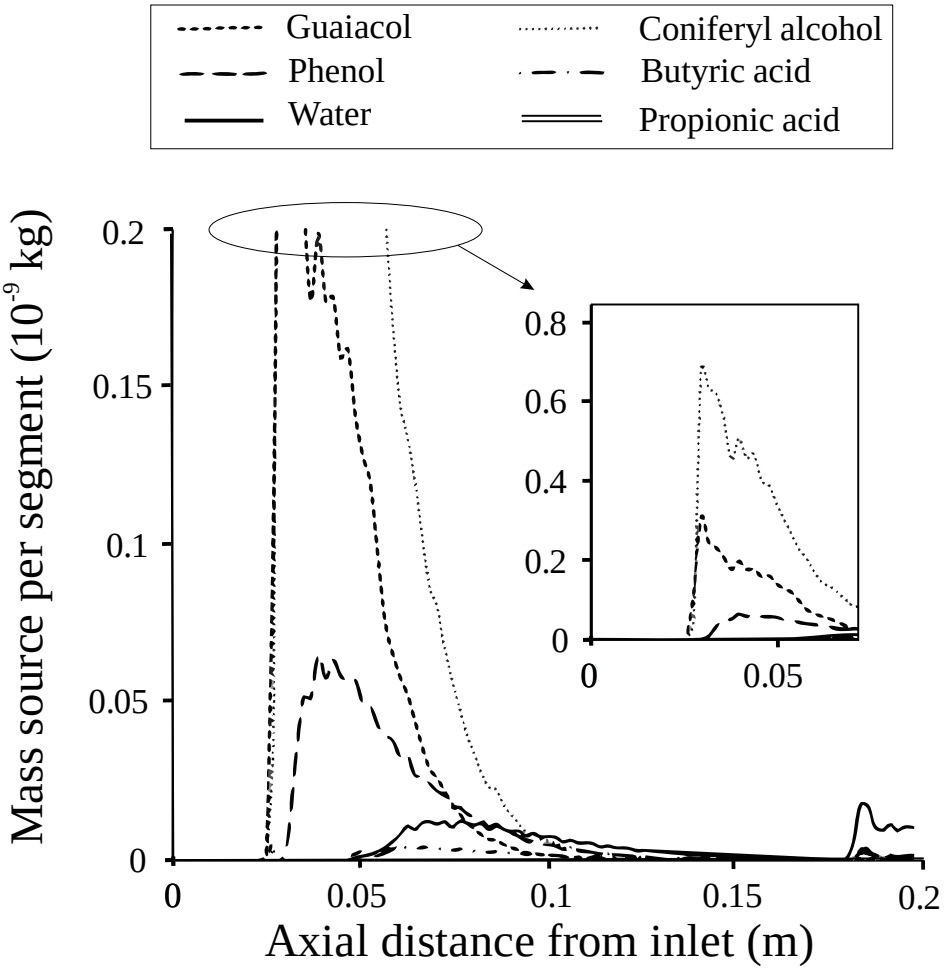

Figure 5.31– Instantaneous mass source of the condensed vapour components.

Small traces of condensation can be seen at the end of the tube for the propionic acid. Figure 5.31 shows the total mass source plot within each segment of the condenser along its length from the inlet to the outlet. The condenser has been divided into 100 equal segments along its axis and the total mass fraction shown in Figure 5.31 is summed in all the cells within the individual segments. As expected, mainly due to the high initial concentration, the mass

fraction source of Coniferyl Alcohol is the greatest among all components, followed by Guaiacol. From Figure 5.31 we can see that the condensation of Guaiacol, Coniferyl Alcohol and Phenol starts at almost the same location in the condenser (approximately 0.025 m from the inlet). The condensation of components like water and Butyric acid starts at approximately 0.05m from the inlet. In the case of water, a considerable amount is transferred from the vapour phase to liquid bio-oil phase near the outlet region. This is mainly due to increased pressure at lower temperatures. From Figure 5.31 we can safely conclude that most of the condensation takes place between 0.025 to 0.1 m of the condenser.

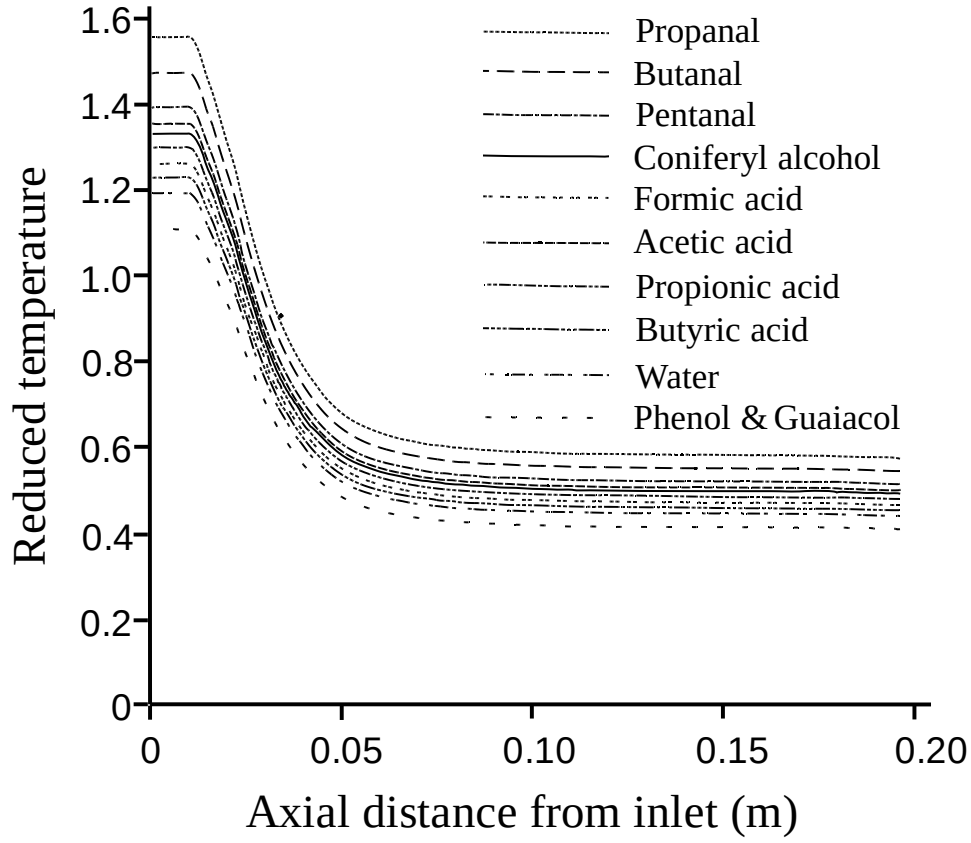

Figure 5.32– Reduced temperature.

The reduced temperature variation of all components within the vapour phase can be seen in Figure 5.32. The reduced temperature, which represents the ratio between the vapour temperature and the corresponding component's critical temperature, varies between 1.5 and 0.4. More importantly between the lengths 0.025 m and 0.1 m where maximum condensation taking place, the reduced temperatures vary between 1.0 and 0.6. This is an essential condition for using the enthalpy of condensation relationship mentioned in equation (4-23).

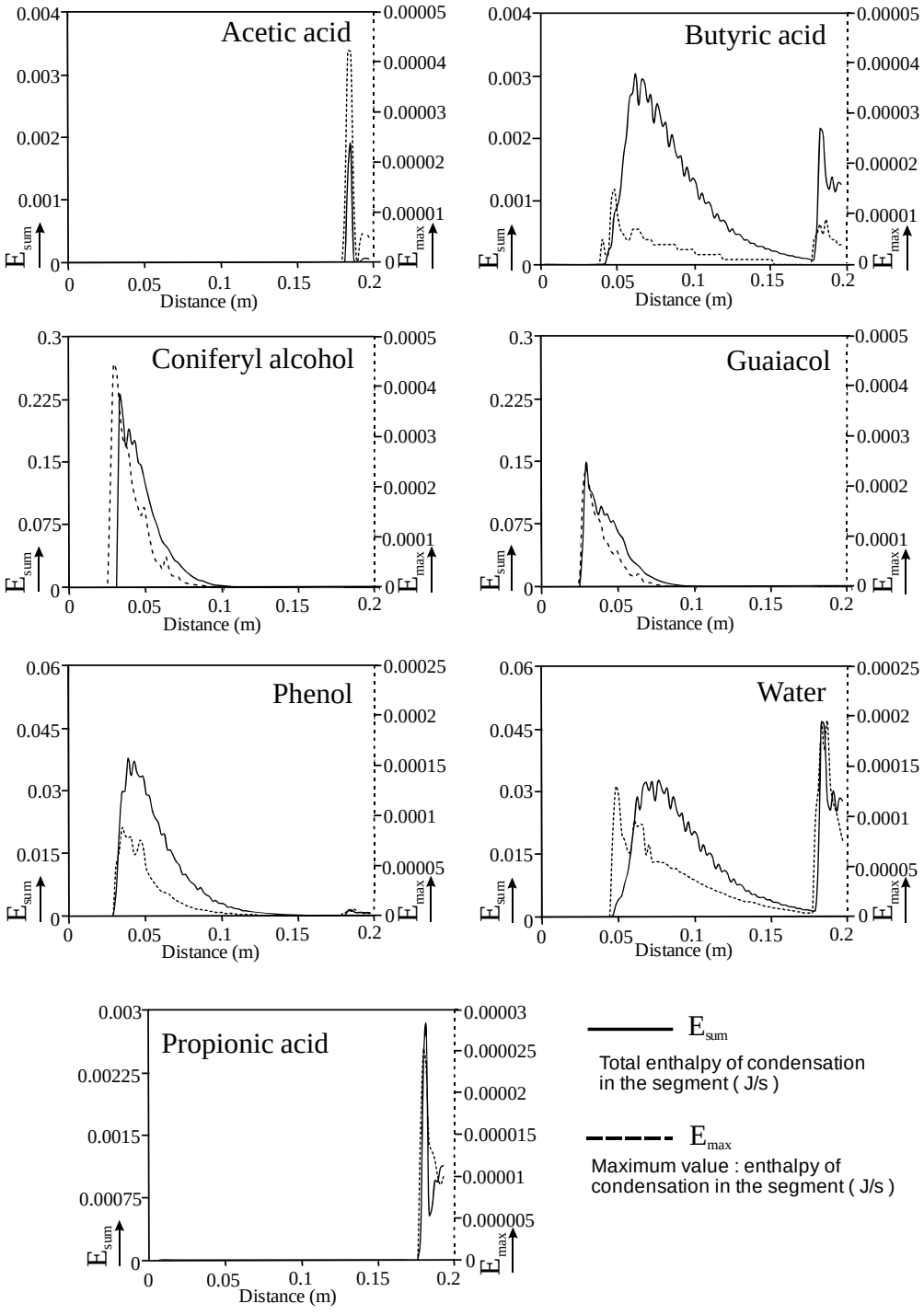

Figure 5.33– Enthalpy source due to the condensation.

The enthalpy of condensation for each condensed component is plotted separately in Figure 5.33. The continuous line represents the total enthalpy of vaporisation within each axial segment of the condenser. The plot follows a similar trend as mass sources plot shown in Figure 5.31. The enthalpy of vaporization values are embedded into solver as energy source terms and are removed from the bio-oil phase. Dotted lines represent the maximum value of the enthalpy of condensation within a particular segment. The maximum enthalpy of condensation both in terms of total and maximum value is observed for Coniferyl Alcohol and followed by Guaiacol. One order of magnitude lower values are observed in the case of water and Phenol in comparison to Coniferyl alcohol. The rest of the acids contributed relatively negligible amounts of enthalpy towards the outlet region of the condenser.

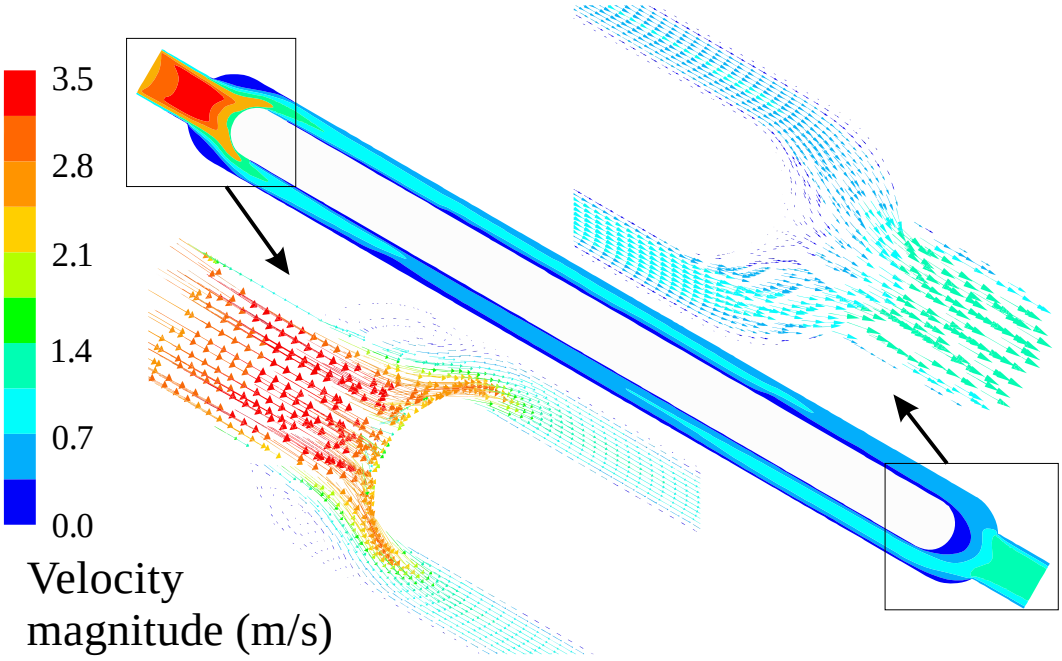

Figure 5.34– Velocity of the pyrolysis vapour.

From the experiments it has been observed that the exit temperature is around 23^{O}C whereas in the numerical simulation an average outlet temperature of approximately 18^{O}C is predicted. The numerical simulations slightly over predict the heat transfer as the Ranz-

Marshal correlation assumes that the secondary phase forms spherical droplets in the primary one. Moreover, the temperature at the outlet varies spatially over entire section so it was not clear at what location the actual measurement has been taken. Fivga's [47] experiments, in which the same equipment has been used, also showed that the water vapour partially condensed in this stage of the liquid collection system. In the experiments, the condensed water percentage varies between 45 to 30% of the total water content. It is also mentioned that the pH value of the first stage condensed bio-oil is higher than the subsequent collection stages. This is primarily due to the condensation of the acid components at the later stages. In this numerical study, we also observed a similar trend where acids like formic acid and acetic acid are not condensed in the present condenser.

It is worth commenting that the vapour thermochemical properties and in turn the condensation patterns of it will vary if a different initial vapour composition is used. In the real cases, the bio-oil and pyrolysis vapour composition is much more complex than the one described in this work. However, the numerical predictions of our simulation showed a very good agreement with the experimental results. Based on the type of biomass and type compounds present in it, the composition can be modified or further simplified and the properties can be estimated accordingly. In this way, this model can be utilised during the designing stage of biomass specific or function specific heat exchangers/condensers.

5.3.4 Conclusion

A species transport model has been implemented within the Eulerian multiphase approach to model the fractional condensation of bio-oil. The generalised corresponding states method has been used to estimate the saturation vapour pressure of the individual components. In this study, 11 discrete chemical compounds were selected to represent the pyrolysis vapours composition, together with Nitrogen which represents the carrier gas and the non-condensable fraction. The mixture of pyrolysis vapours was treated as an ideal gas mixture. From the simulations, it was observed that only few components condensed completely in

this stage of the condenser something that it is in good agreement with the experiments. According to Fivga's [47] experimental study, only 30% of the water vapour was condensed. Guaiacol, Coniferyl Alcohol and Phenol components were completely condensed within the first half of the length of the condenser. It is also observed that the marginal increase in the pressure at the lower temperature towards the outlet of the condenser resulted in the increase of relative saturation of water and other acidic components. The reduced temperatures within the condensing region for most of the components fall in the range of 1 to 0.5, which is the recommended range for using the Pitzer correlation for estimating the enthalpy of condensation. The model can be utilised for the design and optimisation of condensers and/or heat exchangers used in bio-oil liquid collection systems.

5.3.5 Step 2A - Real gas effects on vapour temperature and pressure

In this step, the condenser model was simulated by using real gas model and compared with ideal gas model temperature predictions. The Peng Robinson real gas equation of state was used for calculating vapour mixture properties.

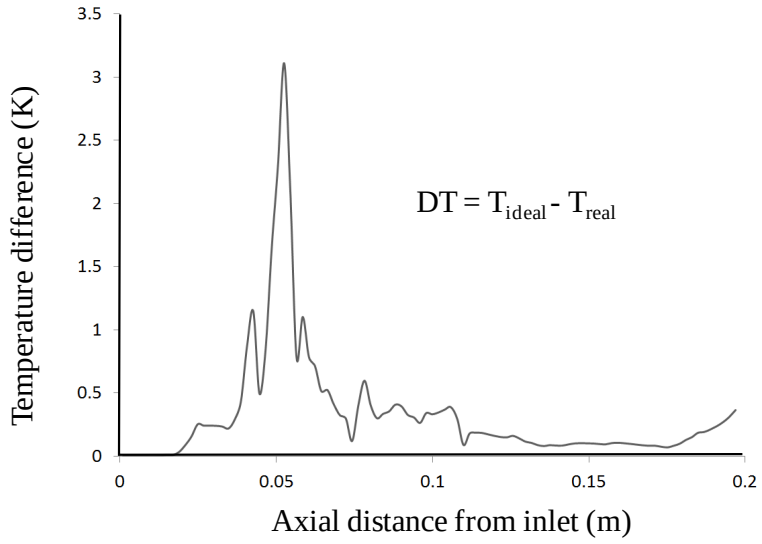

Figure 5.35– Vapour temperature difference between ideal real gas model predictions.

From Figure 5.35, it is evident that there is a marginal decrease in the vapour temperature when the real gas model is used. The maximum temperature difference observed was around $3^{O}C$ which can be safely considered as insignificant in terms of condenser operating temperatures.

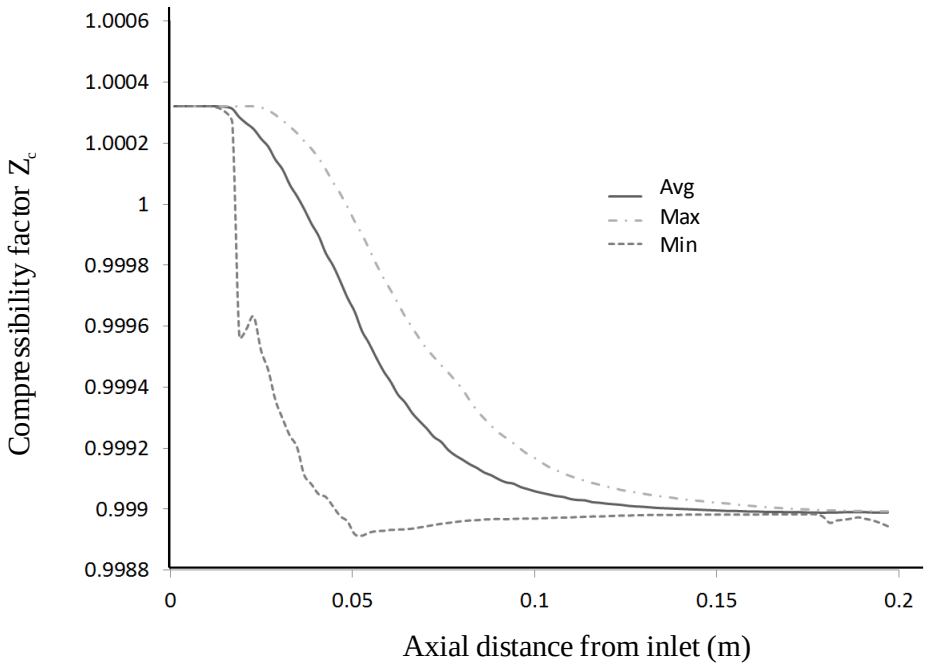

Figure 5.36– Compressibility factor for vapour mixture.

The departure from the ideal behaviour of the real gases can be estimated by determining the compressibility values of the real gas. For that reason, the compressibility factor for the mixture was examined. From Figure 5.36, it is evident that the compressibility factor is very close to unity indicating that the behaviour of the vapour mixture can be considered ideal. This is expected when the equipment is operated at low pressures. However, usage of a real gas model is necessary when the condenser operates at higher pressures. Therefore, it can be concluded that the assumption of ideal gas behaviour of the pyrolysis vapour mixture does not significantly affect the accuracy and validity of the condensation model.

5.4 Step3 - Quenching column phase change model

The aim of the step 3 study is to model the phase change phenomena due to condensation occurring within a quenching column. The gas-liquid interactions are simulated using the immiscible Eulerian – Eulerian approach. The selection of the quenching column design was based on the assessment of its hydrodynamic performance that was presented in the Step 1 studies. The chemical thermodynamics governing the condensation process have been incorporated in user-defined subroutines to account for the flow regimes within the quenching column. The numerical model has been applied for the determination of the optimum number of stages and their effect on the condensation of individual species. The CFD results clearly show the impact of the number of stages, temperature and pressure on the relative saturation of the individual compounds. In addition, the effect of the species volatility on the phase change characteristics is thoroughly analysed and discussed

5.4.1 Geometry

The existing experimental quenching column dimensions are given in the Table 5-1. The original configuration includes 9 stages (pairs) of discs and donuts. However, in order to assess the effects of the number of stages on the condensation of pyrolysis vapours, the hybrid design (Figure 5.37) is modelled with 3, 5 and 9 stages respectively.

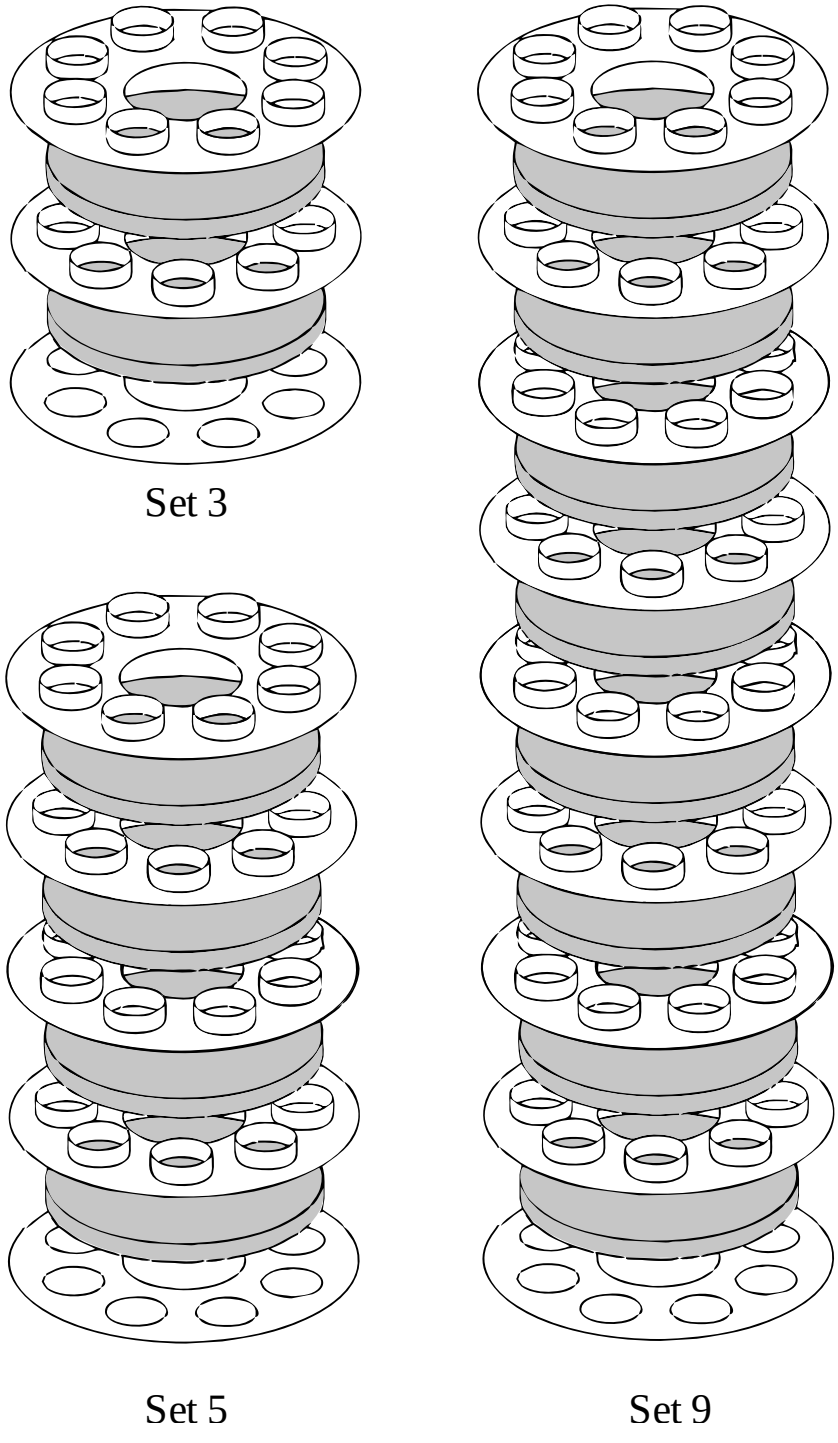

Figure 5.37– Donut and disc configuration for 3, 5 and 9 stage models.

5.4.2 Model assumptions

The implementation of the condensation model is based on the following assumptions.

I. The pyrolysis vapours together with the carrier gas nitrogen are treated as an ideal mixture. This is mainly due to the unavailability of the excess function data in the literature.

II. Fugacity coefficients are assumed as 1. This assumption has been justified when the system is not under high pressures as explained in section 5.3.5.

III. Uniform properties for the condensed bio-oil were assumed within the quenching column, whereas, for the bio-oil phase, a diffusive behaviour similar to a mist flow regime is assumed.

IV. Buoyancy induced laminar flow conditions were assumed inside the quenching column.

V. Interaction between bio-oil phase and coolant phase is not modelled.

5.4.3 Results and discussions

The condensation process is studied in different hybrid configurations consisting of 3, 5 and 9 stages respectively (Figure 5.37) in order to determine the optimum column size and vapour conversion efficiencies.

As shown in Figure 5.38 the number of stages as well as the different pressure build ups in the different configurations do not have a significant impact on the maximum velocities at which the vapours travel through the column. It is observed that higher velocities are achieved close to the inlet with a magnitude ranging between 6-7 m/s, whereas a significant decrease (2-3 m/s) is noted when the vapours flow through the disc and donut pairs on the column. Hence, the residence time and consequently the condensation time of the vapours will mainly depend on the geometrical aspects of the column rather than its two phase flow characteristics, which at steady state are almost identical for all three configurations.

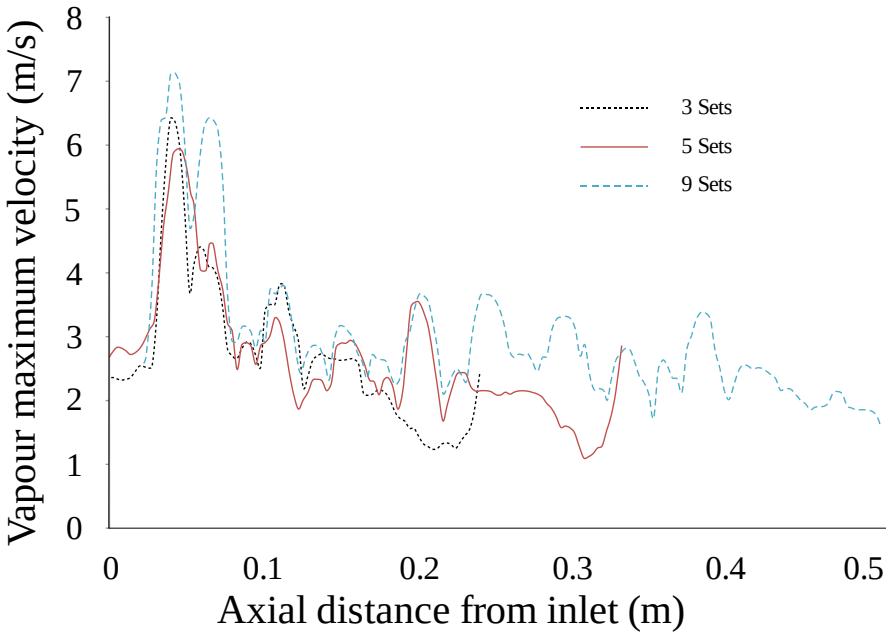

Figure 5.38– Maximum vapour velocity plot – 3, 5 and 9 stage models.

As shown in Figure 5.39, there are considerable differences in the heat transfer and pressure build up characteristics among the various column configurations. It is evident that the higher the number of stages in the column, the more rapid the vapour cooling due to higher pressure build ups. The hydrodynamics behaviour of the column is only slightly affected by the different number of stages, whereas the condensed bio-oil distribution presents significant differences due to different heat transfer and pressure characteristics. Some of the condensed bio oil is leaving the condenser in the form of aerosols as seen in the Figure 5.39. These condensed aerosols can be effectively captured by placing coolant spray at the top of the condenser which improves the area of contact significantly in the cooler regions.

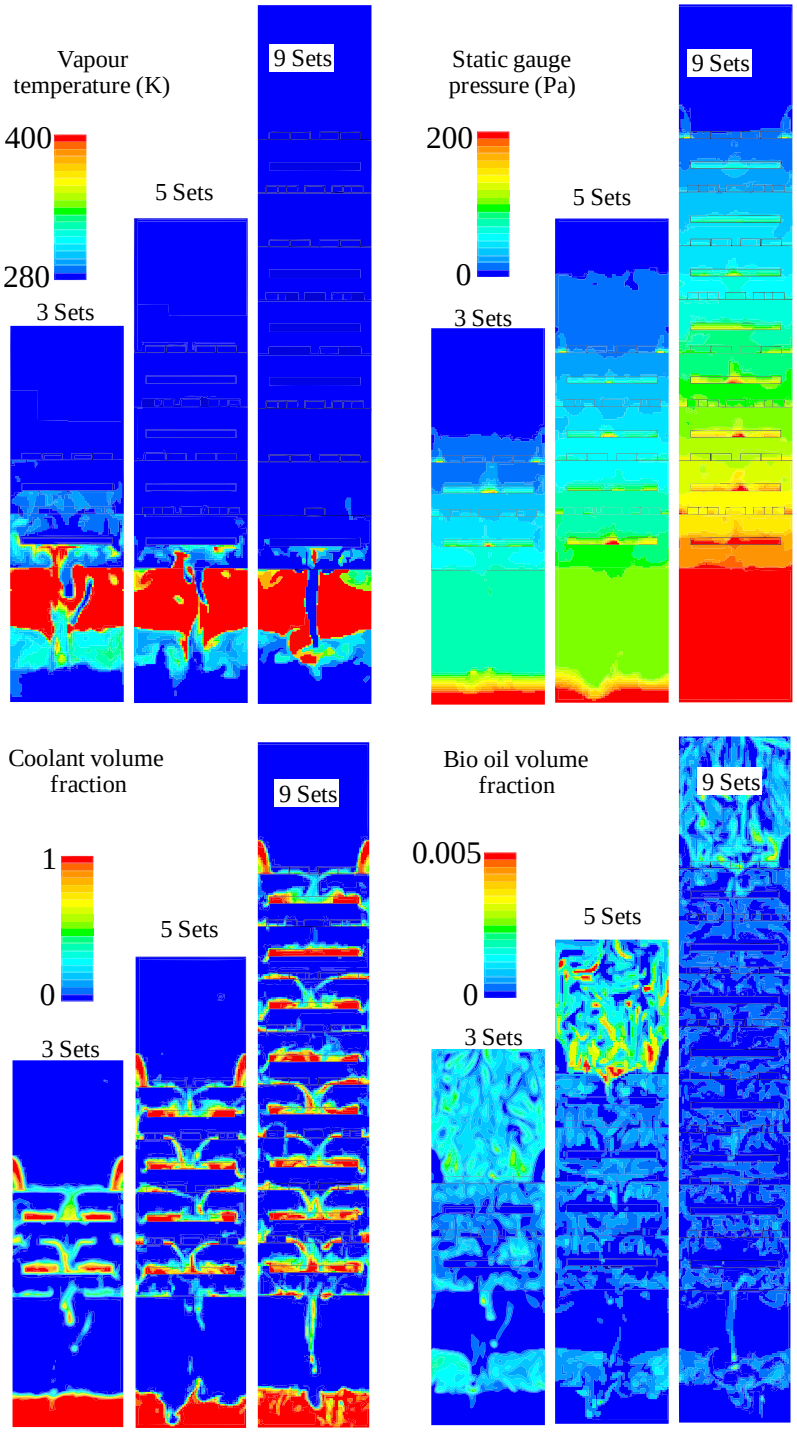

Figure 5.39– Contours of temperature, pressure and volume fractions.

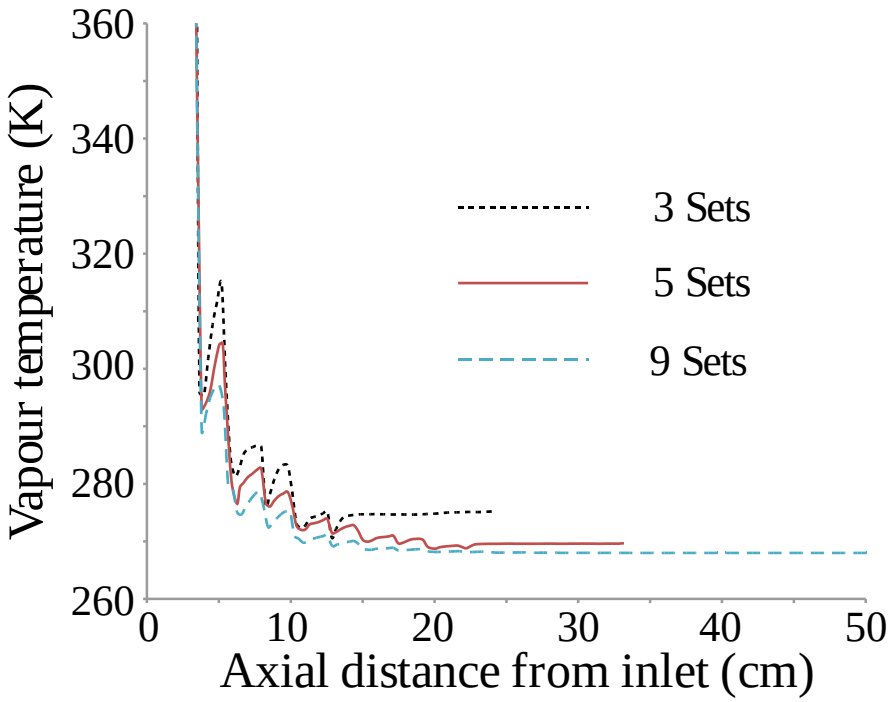

Figure 5.40– Average temperature plot – 3, 5 and 9 stage models.

It is evident from Figure 5.40 that the average temperature difference between the 3-stage and the 9-stage configuration can reach up to approximately 8-10 K at individual stages. That is mainly reflected at the regions of 5-10 cm from the inlet as well as the region beyond 15 cm from the inlet. It is also worth noting that the coolant temperature raised by 12 to 18 K within the quenching column from coolant inlet to coolant out let and maximum rise observed in set 9 configurations. The pressure difference for the same regions can exceed 100 Pa as shown in Figure 5.41 This will have significant implications on the final condensed fraction of the individual chemical compounds comprising the pyrolysis vapours in each column configuration. Higher the pressure, higher the partial pressure for the particular component and this will increase the condensation rate compared to lower pressure conditions.

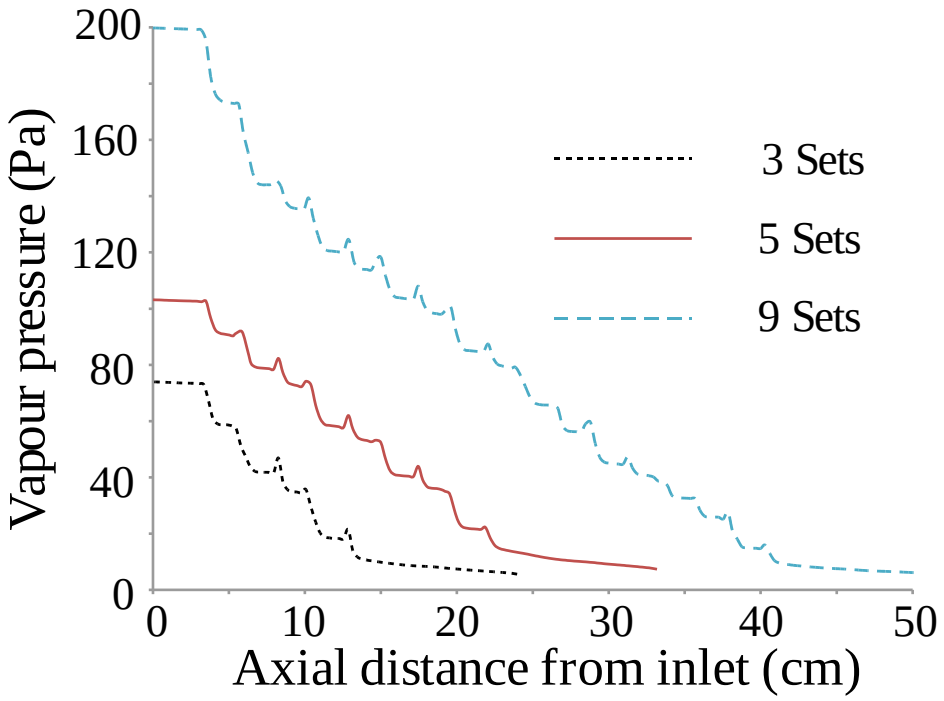

Figure 5.41– Average pressure plot – 3, 5 and 9 stage models..

As shown in Figure 5.42, the phase change behaviour differs among the various compounds. Phase change from vapour to liquid takes place whenever the relative saturation of a specific compound exceeds unity. It is evident that in all configurations, the same 7 compounds (i.e. acetic acid, propionic acid, butyric acid, coniferyl alcohol, guaiacol, phenol and water) are condensed inside the column, however at different proportions. The different temperature and pressure build up characteristics in the column significantly affect the amount of the final condensed product. The 4 compounds that remained uncondensed in all column configurations are the aldehyde group (propanal, butanal, pentanal) as well as formic acid (i.e their maximum relative saturation does not exceed unity in any stage or configuration). In the carboxylic acids group, the acetic and propionic acid have been condensed to significant proportions.

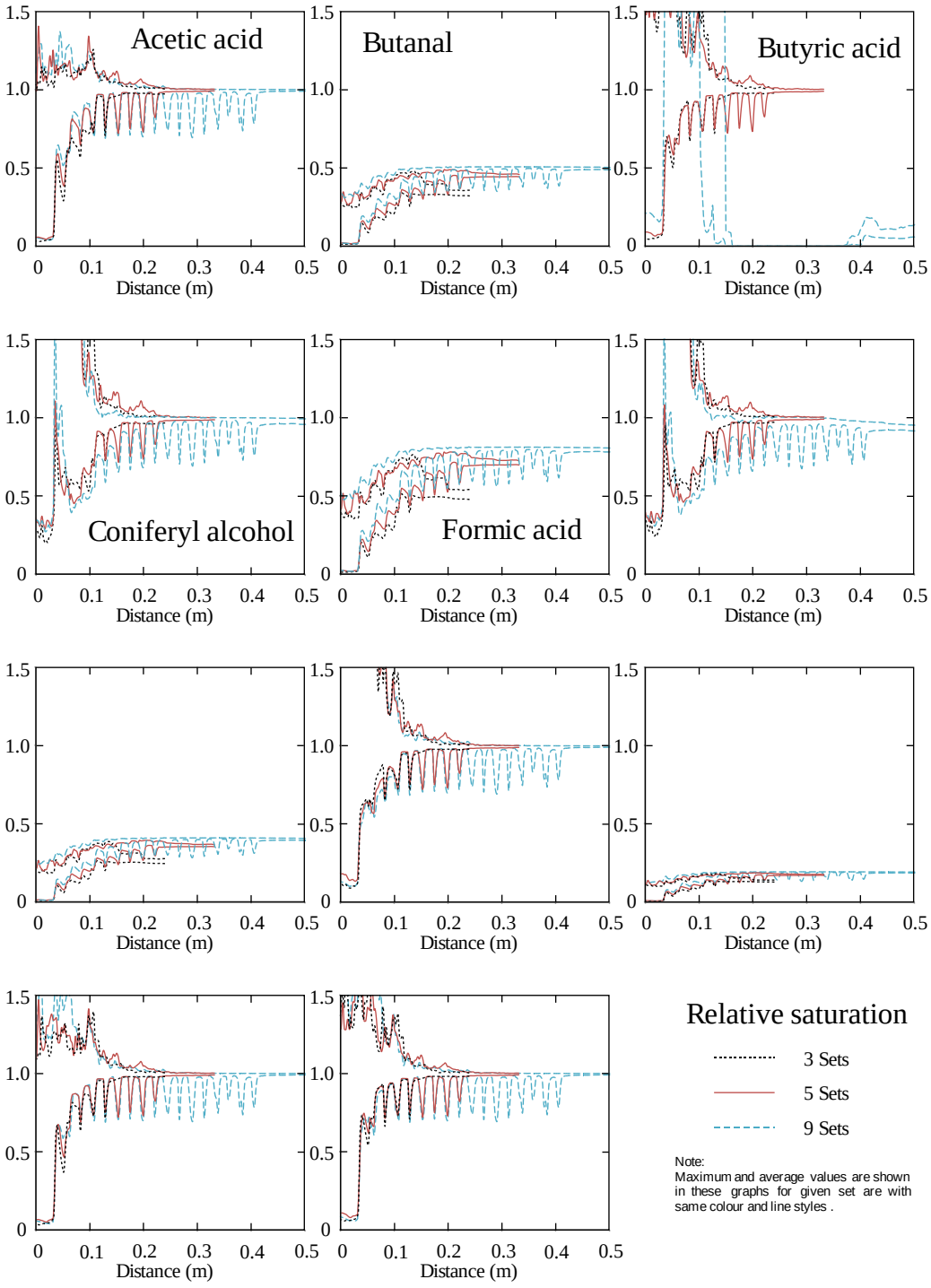

Figure 5.42– Relative saturation.

This result is in many aspects different compared to a previous study conducted in step 2, where the condensation of pyrolysis vapours was investigated in an indirect contact heat exchanger. In that study, only traces of acetic and propionic acid were condensed due to a sudden change in pressure towards the outlet of the condenser. This was also validated by the experimental observations [47]. These results are also in good agreement with the observations of Westerhof et al. [11, 12], where the light organic compounds (e.g. acetic acid) were primarily collected in the second condenser. It needs to be noted though that different operating conditions and different types of condensers (spray columns) were used in that study. It is clearly evident that the lower temperature and especially the greater vapour pressure build up in the quenching column significantly promote the phase change of the acidic components (35 to 62% for acetic acid and 66 to 81% for propionic acid as shown in Table 5-3).

In both studies however, the highly volatile compounds such as formic acid and the aldehyde group have not been condensed at all. It is worth to note that compound condensation continues to take place until the outlet of the column for all configurations. The only compound that shows significant difference in its thermodynamic behaviour between the 5-stage and the 9-stage configurations is the butyric acid. The mole fraction ratio in the vapour mixture (Figure 5.43) shows how the concentration of each of the pyrolysis vapours compound changes relative to its concentration at the inlet, as the various compounds condense in the column. A value of zero in the relative mole fraction graph indicates complete conversion of that compound. As shown in Figure 5.42 and Figure 5.43, butyric acid is completely condensed only in the 9-stage configuration due to the increased pressure build up in the column. This shows the significant role that pressure variations can play in the liquid collection system. Taking into account that coolant temperatures present a lower limit and can significantly limit phase change, the design of quenching columns needs to focus on pressure control for the optimisation of the final liquid yield. In this study, butyric acid is the perfect example of such influence of the system pressure on the thermodynamic behaviour of selected compounds. However, the upper limit for pressure gradient build up in the column is

dictated by flooding phenomena, as described in the part A of this study. Excessive condensation of the remaining six compounds, with nearly over 50% in all configurations, is also observed as shown in Table 5-3 with acetic acid being the only exception in the 3-stage configuration with 35% conversion.

Table 5-3 – Conversion of pyrolysis vapours at different column configurations

Chemical Compound	Degree of Conversion (% of inlet mass fraction)		
	3-stages	5-stages	9-stages
Acetic Acid	35	57	62
Butanal	0	0	0
Butyric Acid	35	95	100
Coniferyl Alcohol	0	100	100
Formic Acid	0	0	0
Guaiacol	100	100	100
Pentanal	0	0	0
Phenol	99	99	99
Propionic Acid	66	78	81
Water	85	90	91

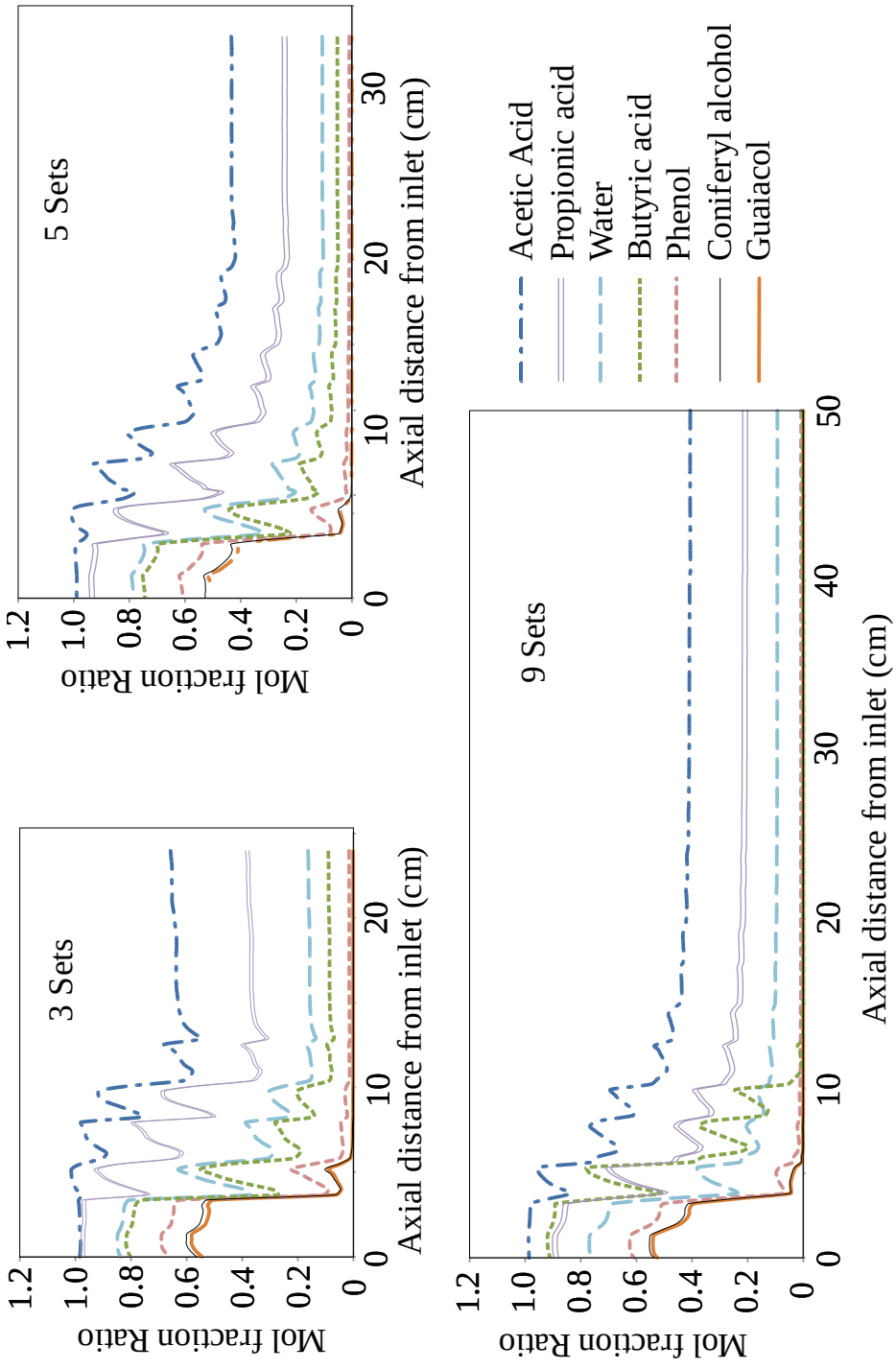

Figure 5.43– Relative mole fraction.

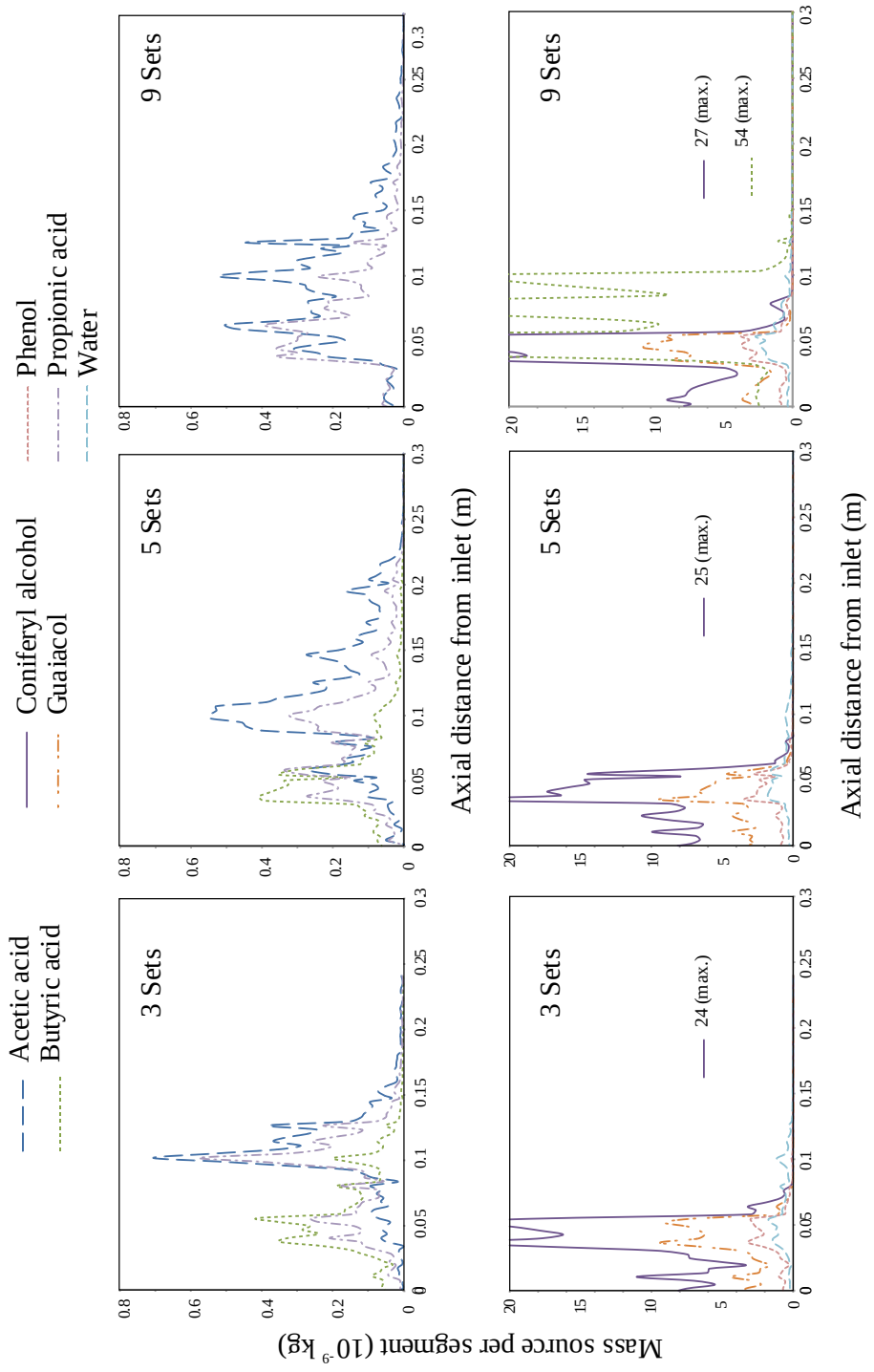

Figure 5.44– Axial mass source per segment of the column.

As shown in Figure 5.44, the higher fraction of vapour conversion occurs within the bottom 3 stages of each column configuration. This is an expected outcome if one considers that the partial pressure of the vapour compounds is significantly higher at the inlet of the column. However, the mass source of each species varies significantly depending on the degree of volatility of the corresponding compound. It is clear that compounds with lower volatility (i.e. coniferyl alcohol, phenol, guaiacol) are nearly completely condensed even at the first stage of the column, whereas the fraction with higher volatility is only partially condensed at the end of the third stage. As mentioned earlier, butyric acid behaves differently in the 9-stage configuration due to higher pressure build up in the column.

It is shown (Figure 5.44) that in the 3- and 5- stage configurations it is only partially condensed at the end of the third stage, whereas it is completely converted at the end of the first stage in the 9-stage configuration. A significant amount of water is also converted primarily in the bottom 2 stages of the column in all configurations, while its overall conversion is only slightly affected by the number of stages in the column (i.e. only 6% difference between the 3-stage and 9-stage configurations). The rate of water condensation is also found to be in line with the predictions of the thermodynamic model of Westerhof et al. [11, 12], where limited condensation is observed at for temperatures below $20^{O}C$.

The total and maximum enthalpy of condensation per segment (Figure 5.45) is directly related to the condensed mass of each species and they follow a similar trend. The enthalpy of vaporization values are embedded into the solver as energy source terms and are subtracted from the bio-oil phase. As it is the case for the mass sources of the individual compounds, the higher total as well as maximum enthalpy values are attributed to the lower volatility compounds and water, where an order of magnitude difference is observed with the rest of the condensed components. Despite its complete conversion in the 9-stage configuration, butyric acid's contribution to the total and maximum enthalpies of condensation is still low due to its higher vapour pressure.

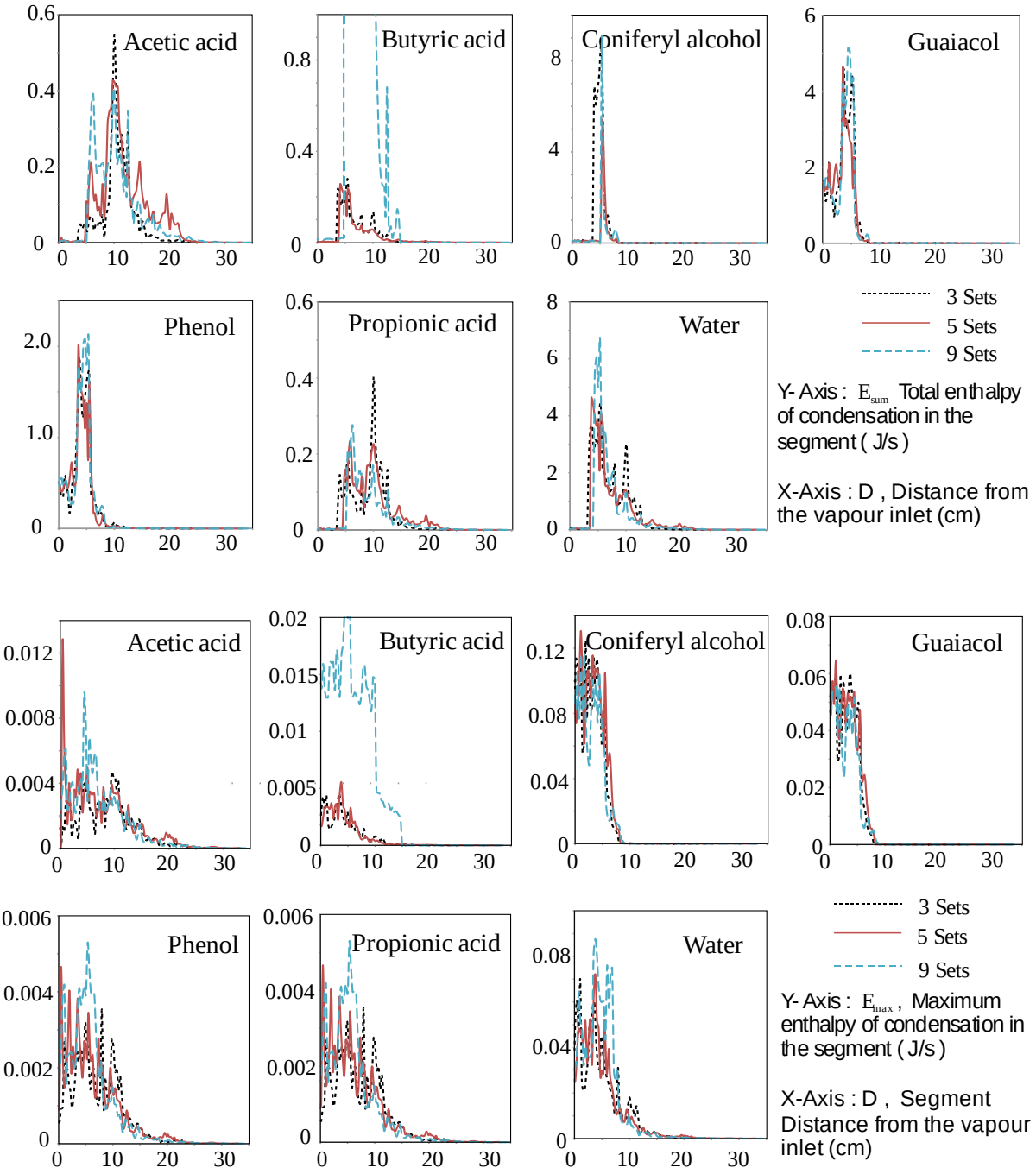

Figure 5.45– Total and maximum enthalpies of condensation per segment.

5.4.4 Conclusion

A species transport model was implemented within the immiscible Eulerian multiphase approach to model the pyrolysis vapour condensation in a disc and donut quenching column. It was found that the design of this equipment needs to be a trade-off between two fundamental factors; the hydrodynamic performance, which will ensure the continuous operation of the column and the maximum degree of vapour to liquid conversion. In this step, it was shown that the lower coolant temperatures and higher pressure build up in the column promote the condensation of the higher volatility compounds. However, the limiting factor will always be the desired pyrolysis vapours conversion and hydrodynamic stability of the column.

In step 3, it was shown that the lower volatility compounds were rapidly and totally condensed in all three different column configurations. However, significant differences in the final degree of conversion were observed for the higher volatility compounds. Partial condensation was observed for the acidic components except formic acid which was not condensed at any configuration. It was shown that the higher pressure build up in the column, due to the increased number of stages, can significantly aid the conversion of the compounds with higher volatility, such as butyric acid. The highly volatile compounds such as the aldehyde group as well as formic acid were not condensed at any column configuration, leading to the conclusion that secondary low temperature condensers will be required in the system.

It has to be noted that the presented numerical model can be used for the design and optimisation of most of heat exchangers used for the condensation of fast pyrolysis vapours. However, the fluid dynamic and heat transfer characteristics which will eventually affect the equilibrium properties of the selected compounds will be specific to the condenser under study. And hence the model needs to be attuned to suit the flow conditions of the particular condensers such as turbulence modelling methods. The results presented in this study are

specific to the proposed quenching column and cannot be extrapolated to other types of condensers.

Chapter 6 Conclusions

This chapter outlines the conclusions made throughout this work and describes its contributions to the science of research. Potential areas of future work also suggested at the end.

6.1 Attainment of objectives

The aim of the current work was to expand the capabilities of numerical modelling and build a strategy to simulate complex phase interactions such as mass, momentum, heat transport and phase transition phenomena among biomass pyrolysis vapours, liquid bio-oil and liquid coolant in direct contact heat exchangers. The key objectives were outlined as below.

To progress CFD modelling in the liquid collection system design and optimisation through

a) The development of a hydrodynamic model to examine the flooding phenomena.
b) The evaluation of design parameters and their effect on the performance of the quenching column.

To develop condensation model for the liquid collection system through

a) The development of a fractional condensation model for indirect contact condensers.
b) The validation of the results obtained from the model with experimental observations.

To deploy the condensation model for direct contact condensers through

a) The implementation of the fractional condensation model in a quenching column.

b) The evaluation of the effect of different number of stages on the final liquid bio-oil yields.

6.2 Overall conclusion

This report presented the development and application of computational modelling applied to liquid collection system used in pyrolysis technology. The simulation platform used was the commercial CFD code FLUENT and the condensation models were implemented in the form of user defined functions (UDF). The main concept behind the code was to visualise the flow behaviour inside the quenching column (liquid collection system) which can bring some significant insights during the design stage of such equipment in the future.

6.2.1 Hydrodynamics and design optimisation study

The first part of the simulations involves the hydrodynamics study of the quenching column which involves multiphase flow phenomena. Initially baseline conditions were simulated for two different flow conditions, one with 10% design gas flow rate and another with 50% design gas flow rate. In the 50% condition, flooding of the liquid coolant was observed at the upper most donut plate as it was also observed during the experiments. It was identified that the flow area near the donut plate was not sufficient for the specified amount of gas flow rates even though it was designed by considering the design correlations using standard design methods. Modified designs were developed by providing extra flow area to the gas phase. The effect of the design alterations on the liquid to gas heat transfer has also been investigated. Four new design variants, based on the Souders-Brown coefficients, were developed and simulated. It was shown that the gas flow is greatly affected by weirs on the donut discs (gas flow similarities between types 1 and 3), while the presence of weirs on the disc plates greatly affected the liquid flow distribution at each stage. From this step an optimum design called hybrid configuration for the quenching column has been identified.

6.2.2 Condensation model development

In the second part of the simulations, a condensation model was developed to account for the phase change and validated. A species transport model has been implemented for this and the Eulerian multiphase approach was used to model the fractional condensation of bio-oil. The generalised corresponding states method was used to estimate the saturation vapour pressure of the individual components. In this study, 11 discrete chemical compounds were selected to represent the pyrolysis vapours composition, together with Nitrogen which represents the carrier gas and the non-condensable fraction. The mixture of pyrolysis vapours was treated as an ideal gas mixture.

From the simulations, it was observed that only few components condensed completely in this stage of the condenser something that it is in good agreement with the experimental observation in the same equipment. According to Fivga's [47] experimental study, only 30% of the water vapour was condensed. This was well in agreement with the CFD model predictions about amount of water condensed. Guaiacol, Coniferyl Alcohol and Phenol components were completely condensed within the first half of the length of the condenser. As observed in the experimental results, the acids were the least condensed especially acetic acid. It was also observed that the marginal increase in the pressure at the lower temperature towards the outlet of the condenser resulted in a significant increase of the relative saturation of water and other acidic components. The reduced temperatures within the condensing region for most of the components fall in the range of 1 to 0.5, which is the recommended range for using the Pitzer correlation for estimating the enthalpy of condensation. The model can be utilised for the design and optimisation of condensers and/or heat exchangers used in bio-oil liquid collection systems. More over the understanding of the detailed condensation process enable engineers and researchers to design equipment to control the bio-oil quality and properties such as viscosity, composition water content and acid numbers to suit to the specific applications.

6.2.3 Condensation model deployment

As a final step towards the modelling of the complete quenching column, the optimum design obtained from the simulations carried out in step one was used with the condensation model developed in step two. It was found that the design of this equipment needs to be consider two fundamental factors; the hydrodynamic performance, which will ensure the continuous operation of the column and the maximum degree of vapour to liquid conversion. It was shown that the lower coolant temperatures and higher pressure build up in the column promote the condensation of the higher volatility compounds. However, the limiting factor will always be the desired pyrolysis vapours conversion and hydrodynamic stability of the column. A species transport model was implemented within the immiscible Eulerian multiphase approach to model the pyrolysis vapour condensation in a disc and donut quenching column.

In step 3, it was shown that the lower volatility compounds were rapidly and totally condensed in all three different column configurations. However, significant differences in the final degree of conversion were observed in the higher volatility compounds. Partial condensation was observed for the acidic components except formic acid which was not condensed at any configuration. It was shown that the higher the pressure build up in the column, due to the increased number of stages, can significantly aid the conversion of the compounds with higher volatility, such as butyric acid. The highly volatile compounds such as the aldehyde group as well as formic acid were not condensed at any column configuration, leading to the conclusion that secondary low temperature condensers will be required in the system.

The presented model can be used for the design and optimisation of any type of heat exchanger used for the condensation of fast pyrolysis vapours. However, the fluid dynamic and heat transfer characteristics which will eventually affect the equilibrium properties of the selected compounds will be specific to the condenser under study. The results presented in

this study are specific to the proposed quenching column and cannot be extrapolated to other types of condensers.

6.2.4 Future scope of the work

This thesis demonstrated the condensation modelling capability for the liquid collection systems used in pyrolysis technology. There are several areas that can be addressed in future while continuing this work or while extending it.

In the present model, only one type of vapour composition was used. However there is a wide range of compositions that are available in the literature. Sensitivity studies focused on composition dependent condenser performance can be evaluated in the future. More over this should be backed up by the direct experimental results which need to be constructed based on the suggested design methods.

In terms of the condensation model, the bio-oil is considered as single species in this work. This will however impose restriction on the species diffusivity due to concentration differences. Moreover, a more robust VLE mechanism needs to be accounted by computing the vapour and liquid fugacity separately.

The current study was focused on the development of the computational code for simulating the flow behaviour inside the liquid collection system (in this case the quenching column). In the future, the spray regime inside the quenching column can be studied which also falls under the category of direct contact heat exchangers. This involves Lagrangian and Eulerian multiphase equations coupled together with species transport equations. It is also highly recommended that the proposed quenching column be constructed for further experimental investigation and identification of the operational difficulties. Given a choice on which one is implemented first, the construction of the experiments with the modified design needs to be addressed on priority.

6.3 Contribution to the science

The work presented in this Thesis has made several contributions to the scientific research.

The key contributions are

- The possibility to investigate multiphase flow regimes especially in the liquid collection system.
- To successfully modify the multi-fluid VOF model to capture flooding effects, thereby reducing the grid requirements compared to traditional VOF methods.
- The investigation of the working principles of the heat exchangers those are different in the case of pyrolysis technology. The design key areas focus on rapid cooling with the minimum residence time. The models addressed these issues elegantly and showed the careful balance between the rapid cooling and avoidance of flooding due to pressure built-up.
- The development of the fractional condensation model in accordance with the needs of the researchers and engineers who are working in pyrolysis technology.
- The successful demonstration that species transport modelling along with multiphase models can capture the individual species condensation phenomena.
- The successful implementation of the condensation model on direct contact condensers.

Several sections of this work have been published and presented to the academic and industrial peers at various international forums. The list of publications and presentations are supplied in detail in the List of publications section.

List of publications

International Journal Publications:

1. V.S. Kiran Kumar Palla, K. Papadikis and Sai Gu , "Computational modelling of the condensation of fast pyrolysis vapours in a quenching column. Part A: Hydrodynamics, heat transfer and design optimisation", Fuel processing technology, 131 (2015), 59-68.
2. V.S. Kiran Kumar Palla, K. Papadikis and Sai Gu, "A numerical model for the fractional condensation of pyrolysis vapours", Biomass & Bioenergy, 74 (2015), 180-192.
3. V.S. Kiran Kumar Palla, K. Papadikis and Sai Gu, "Computational modelling of the condensation of fast pyrolysis vapours in a quenching column. Part B: Direct contact condensation, Fuel processing technology", Fuel processing technology, 144 (2016), 42-55.

International conference presentations:

1. A numerical model for the fractional condensation of pyrolysis vapours, Pyro2014, 20th International symposium on analytical & applied pyrolysis, 19-23 May 2014, Birmingham, United Kingdom.
2. Hydrodynamic modelling of a direct contact heat exchanger used for Bio-oil condensation, Ninth International Conference on Computational Fluid Dynamics in the Minerals and Process industries, 10-12 December 2012, Melbourne, Australia.
3. Key note presentation on "Hydrodynamic modelling of a direct contact heat exchanger used for Bio-oil condensation", International Conference on Biomass-Energy Technologies 2012, 22-24 October 2012, Nanjing, China.

References

[1] UN-FCCC/CP/2009/L.7, Copenhagen Accord, 18 December 2009.

[2] ANEFA. Forest biomass: opportunity and value. National association of forestry, agricultural and environment enterprises, 2011.

[3] S. Rafael, L. Tarelho, A. Monteiro, E. Sá, A.I. Miranda, C. Borrego, M. Lopes, Impact of forest biomass residues to the energy supply chain on regional air quality, Science of The Total Environment, Volume 505, 1 February 2015, Pages 640-648.

[4] A.V Bridgwater, G.V.C Peacocke, Fast pyrolysis processes for biomass, Renewable and Sustainable Energy Reviews, Volume 4, Issue 1, March 2000, Pages 1-73.

[5] A.V. Bridgwater, Review of fast pyrolysis of biomass and product upgrading, Biomass and Bioenergy, Volume 38, March 2012, Pages 68-94.

[6] J. Lehto, A. Oasmaa, Y. Solantausta, M. Kytö, D. Chiaramonti, Fuel oil quality and combustion of fast pyrolysis bio-oil, VTT Technology 87, April 2013.

[7] S. Czernik, A.V. Bridgwater, Overview of application of biomass fast pyrolysis oil, Energy and Fuels , Volume 18 (2) , 2004, Pages 590-598.

[8] Foster A. Agblevor, O. Mante, R. McClung, S.T. Oyama, Co-processing of standard gas oil and biocrude oil to hydrocarbon fuels, Biomass and Bioenergy, Volume 45, October 2012, Pages 130-137.

[9] J.P. Diebold, Preliminary Results in the Fast Pyrolysis of Biomass to Lower Olefins, Petroleum Chemistry division of ACS Symposium on Alternate Feed stocks for Petrochemicals, August 24-29, Las Vegas, NV,USA, 1980.

[10] A.G.W. Bradbury, Y. Sakai, F. Shafizadeh, A Kinetic Model for Pyrolysis of Cellulose, Journal of Applied Polymer Science, Volume 23 (11) , June 1979, Pages 3271-3280.

[11] R.J.M. Westerhof, N.J.M. Kuipers, S.R.A. Kersten, W.P.M. van Swaaij, Controlling the Water Content of Biomass Fast Pyrolysis Oil, Industrial and Engineering Chemistry Research, Volume 46 (26), November 2007, Pages 9238–9247.

[12] R. J. M. Westerhof, D. W. F. Brilman, M. Garcia-Perez, Z. Wang, S. R. G. Oudenhoven, W. P. M. van Swaaij , S. R. A. Kersten, Fractional condensation of biomass pyrolysis vapors, Energy & Fuels, Volume 25(4), March 2011, Pages 1817-1829.

[13] R. Yin, R. Liu, Y. Fei Mei, X. W. Sun, Characterization of bio-oil and bio-char obtained from sweet sorghum bagasse fast pyrolysis with fractional condensers, Fuel, Volume 112, October 2013, Pages 96-104.

[14] C. Gustavsson , L. Nilsson , Co-production of pyrolysis oil in district heating plants: Systems analysis of dual fluidized-bed pyrolysis with sequential vapor condensation , Energy & Fuels, Volume 27 (9), August 2013, Pages 5313-5319.

[15] V. Karlsson, L. Nilsson, Co-production of pyrolysis oil and district cooling in biomass-based CHP plants: Utilizing sequential vapour condensation heat as driving force in an absorption cooling machine, Applied Thermal Engineering, Volume 79, 25 March 2015, Pages 9-16.

[16] E. J. Henley, J. D. Seader, Equilibrium-Stage Separation Operations in Chemical Engineering; Wiley: New York, 1981.

[17] N. Robinson, Design, modelling and construction of a novel ablative fast pyrolysis reactor and product collection system, PhD thesis, Aston University, U.K, 2000.

[18] D. Meier, O. Faix, State of the art of applied fast pyrolysis of lignocellulosic materials – a review, Bioresource Technology, Volume 68 (1), April 1999, Pages 71-77.

[19] I.Ph. Boukis, P. Grammelis, S. Bezergianni, A.V. Bridgwater, CFB air-blown flash pyrolysis. Part I: Engineering design and cold model performance, Fuel, Volume 86 (10-11), July–August 2007, Pages 1372-1386.

[20] C.W. Gorton, R.J. Kovac, J.A. Knight, T.I. Nygaard, Modeling pyrolysis oil production in an entrained-flow reactor, Biomass, Volume 21(1), 1990, Pages 1-10.

[21] K. Maniatis, J. Baeyens, H. Peeters, G. Roggeman, The Egemin ash pyrolysis process: commissioning and initial results, Advances in thermochemical biomass conversion, Blackie (1994), 1257-1264.

[22] S. Scott Donald, Piskorz Jan, A. Bergougnou Maurice, Graham Robert, P. Overend Ralph, The role of temperature in the fast pyrolysis of cellulose and wood, Industrial and Engineering Chemistry Research, Volume 27(1), 1988, Pages 8 -15.

[23] Union Fenosa, Production, treatment and utilisation of bio-oils from pyrolysis, for energy and alternative fuels and chemicals, Final report of the AIR2-CT93-1086 EU project, February 1997.

[24] W.J. Bogley, W.R. Mixon, C. Dean, D.J. Lizdas Solid waste utilization-pyrolysis Oak Ridge National Laboratory, Oak Ridge (TN),1977.

[25] R. G. Graham, A characterisation of the fast pyrolysis of cellulose and wood biomass, PhD thesis, University of Western Ontario, 1993.

[26] J. P. Diebold, J. Scahill, Production of Primary Pyrolysis Oils in a Vortex Reactor, Pyrolysis Oils from Biomass, Chapter 4, ACS Symposium Series, Volume 376, 1988, Pages 31–40.

[27] G.V.C. Peacocke, Ablative pyrolysis of biomass. PhD thesis, Aston University, UK, October 1994.

[28] C. Roy, B. de Caumia, P. Plante, H. Menard, Proceedings of the conference on energy from biomass and wastes VII, Lake Buena Vista, FL, 24–28 January 1983. Inst. Gas Techn., Chicago (IL), Page 1147.

[29] J. P. Diebold, J. W.Scahill, S. Czernik, S. D. Phillips, C.J. Feik, Progress in the Production of Hot-Gas Filtered Biocrude Oil, Bio-Oil Production &Utilisation, CPL Press, 1996, Pages 66-81.

[30] A. V. Bridgwater, Principles and practice of biomass fast pyrolysis processes for liquids, Journal of Analytical and Applied Pyrolysis, Volume 51, Issues 1–2, July 1999, Pages 3-22.

[31] A. V. Bridgwater, G. V. C. Peacocke, Fast Pyrolysis Proceses for Biomass, enewable and Sustainable Energy Reviews, Volume 4, Issue 1, March 2000, Pages 1-73.

[32] A. Oasmaa, S. Czernik, Fuel Oil Quality of Biomass Pyrolysis Oils-State of the Art for the End Users, Energy & Fuels, Volume 13(4), 1999, Pages 914− 921.

[33] D. C. Elliott, Historical Developments in Hydroprocessing Biooils, Energy & Fuels, Volume 21(3), 2007, Pages 1792−1815.

[34] F. de Miguel Mercader, M. J. Groeneveld, S. R. A. Kersten, C. Geantet, G. Toussaint, N. W. J. Way, C. J. Schaverien, J. A. Hogendoorn, Hydrodeoxygenation of pyrolysis oil fractions: process understanding and quality assessment through co-processing in refinery units, Energy Environmental Science. Volume 4, 2011, Pages 985−997.

[35] D. Mohan, C. U. Pittman, P. H. Steele,Pyrolysis of Wood/ Biomass for Bio-oil: A Critical Review, Energy & Fuels , Volume 20 (3), 2006, Pages 848− 889.

[36] A. V. Bridgwater, K. Maniatis, The production of biofuels by the thermochemical processing of biomass, Molecular to global photosynthesis, London: IC Press, 2004, Pages 521–612.

[37] A. V. Bridgwater, The production of biofuels and renewable chemicals by fast pyrolysis of biomass, International Journal of Global Energy Issues, Volume 27, 2007, Pages 160–203.

[38] S. W. Scott, D. J. Nowakowski, A. V. Bridgwater, J. M. Jones, Assess the impact of alkali metals in bio mass on the physical and chemical properties of fast pyrolysis bio-oil , Proceedings of the Bioten conference on biomass bioenergy and biofuels ,Newbury , UK, CPL Press , 2010.

[39] G.V.C. Peacocke, E.S. Madrali, C.-Z. Li, A.J. Güell, F. Wu, R. Kandiyoti, A.V. Bridgwater, Effect of reactor configuration on the yields and structures of pine-wood derived pyrolysis liquids: A comparison between ablative and wire-mesh pyrolysis, Biomass and Bioenergy, Volume 7, Issue 1, 1994, Pages 155-167.

[40] K. Papadikis , S. Gu, A. V. Bridgwater, H. Gerhauser, Application of cfd to model fast pyrolysis of biomass, Fuel Processing Technology, Volume 90, Issue 4, April 2009, Pages 504-512.

[41] H. Gerhauser, A. V. Bridgwater, CFD modelling of biomass pyrolysis for better fluidised bed design, Proceedings of pyrolysis and gasification of biomass and waste, Strasbourg, France. Newbury, UK, CPL Scientific Press,2003.

[42] H. Gerhauser, S.C. Generalis, R. A. Hague, A. V. Bridgwater, CFD for the modelling of char entrainment in fluidised bed fast pyrolysis of biomass, Progress in thermochemical biomass conversion. Oxford, UK, Blackwell, 2001.

[43] K. Papadikis, S. Gu, A. V. Bridgwater, Computational modelling of the impact of particle size to the heat transfer coefficient between biomass particles and a fluidised bed, Fuel Processing Technology, Volume 91, Issue 1, January 2010, Pages 68-79.

[44] K. Papadikis, S. Gu, A. V. Bridgwater, CFD modelling of the fast pyrolysis of biomass in fluidised bed reactors: modelling the impact of biomass shrinkage, Chemical Engineering Journal, Volume 149, Issues 1–3, 1 July 2009, Pages 417-427.

[45] K. Papadikis, S. Gu, A. V. Bridgwater, CFD modelling of the fast pyrolysis of biomass in fluidised bed reactors. Part B heat, momentum and mass transport in bubbling fluidised beds, Chemical Engineering Science, Volume 64, Issue 5, March 2009, Pages 1036-1045.

[46] K. Papadikis, A. V. Bridgwater, S. Gu , CFD modelling of the fast pyrolysis of biomass in fluidised bed reactors, part A: Eulerian computation of momentum transport in bubbling fluidised beds, Chemical Engineering Science , Volume 63, Issue 16, August 2008, Pages 4218-4227.

[47] A. Fivga, Comparison of the effect of pre-treatment and catalysts on liquid quality from fast pyrolysis of biomass. Ph.D. Thesis, Bio-energy Research Group, Aston University, 2011.

[48] E. H. Salter, Catalytic pyrolysis of biomass for improved liquid fuel quality. Ph.D. Thesis, Bio-energy Research Group, Aston University, 2001.

[49] Nanhang Dong, CFD modelling of the thermal degradationof biomass in fluidised bed. Ph.D. Thesis, Faculty of Engineering and the Environment, University of Southampton, 2014.

[50] T. Chen, C. Wu, R. Liu,W. Fei, S. Liu, Effect of hot vapour filtration on the characterization of bio-oil from rice husks with fast pyrolysis in a fluidized-bed reactor, Bioresource Technology, Volume 102, Issue 10, May 2011, Pages 6178-6185.

[51] T. Chen, C. Deng, R. Liu, Effect of selective condensation on the characterization of bio-oil from pine sawdust fast pyrolysis using a fluidized-bed reactor, Energy and Fuels, Volume 24 (12), 2010, Pages 6616-6623.

[52] R. H. Liu, C. J. Shen, H. J. Wu, C. J. Deng, S. Y. Liu, Characterisation of bio-oil from fast pyrolysis of rice husk in a fluidised bed reactor , Journal of the Energy Institute, Volume 84 (2), 2011, Pages 73-79.

[53] A. A. Boateng, D. E. Daugaard, N. M. Goldberg, K. B. Hicks, Bench-scale fluidized-bed pyrolysis of switchgrass for bio-oil production, Industrial and Engineering Chemistry Research, Volume 46(7), 2007,Pages 1891–1897.

[54] A. A. Boateng, C. A. Mullen, N. Goldberg, K. B. Hicks, H. J. G. Jung, J. F. S. Lamb, Production of bio-oil from alfalfa stems by fluidized-bed fast pyrolysis , Industrial and Engineering Chemistry Research, Volume 46(7), 2008, Pages 4115-4122.

[55] A.S. Pollard, M.R. Rover, R.C. Brown, Characterization of bio-oil recovered as stage fractions with unique chemical and physical properties, Journal of Analytical and Applied Pyrolysis, Volume 93, January 2012, Pages 129-138.

[56] Marjorie R. Rover, Patrick A. Johnston, Lysle E. Whitmer, Ryan G. Smith, Robert C. Brown, The effect of pyrolysis temperature on recovery of bio-oil as distinctive stage fractions, Journal of Analytical and Applied Pyrolysis, Volume 105, January 2014, Pages 262-268.

[57] Donald S. Scott, Jan Piskorz, Maurice A. Bergougnou, Robert Graham, Ralph P. Overend, The role of temperature in the fast pyrolysis of cellulose and wood, Industrial and Engineering Chemistry Research, Volume 27 (1), 1988, Pages 8-15.

[58] Jacques Lédé, François Broust, Fatou-Toutie Ndiaye, Monique Ferrer, Properties of bio-oils produced by biomass fast pyrolysis in a cyclone reactor, Fuel, Volume 86, Issues 12–13, August 2007, Pages 1800-1810.

[59] N. Jendoubi, F. Broust, J.M. Commandre, G. Mauviel, M. Sardin, J. Lédé, Inorganics distribution in bio oils and char produced by biomass fast pyrolysis: The key role of aerosols, Journal of Analytical and Applied Pyrolysis, Volume 92, Issue 1, September 2011, Pages 59-67.

[60] N. Doassans-Carrère, J. H. Ferrasse, O. Boutin, G. Mauviel, J. Lédé, Comparative study of biomass fast pyrolysis and direct liquefaction for bio-oils production: Products yield and characterizations, Energy and Fuels, Volume 28 (8), 2014, Pages 5103-5111.

[61] F. Broust, Le cyclone: un reacteur multifonctionnel. Application´ à la pyrogazeification et à la pyroliquefaction de la biomasse. Ph.D.´thesis, Institut National Polytechnique de Lorraine, Nancy, France, 2003.

[62] J. Ledé, ´ The Cyclone: A Multifunctional Reactor for the Fast Pyrolysis of Biomass, Industrial and Engineering Chemistry Research,Volume 39(4), 2000, Pages 893−903.

[63] P. T. Williams, A. J. Brindle, Temperature selective condensation of tyre pyrolysis oils to maximise the recovery of single ring aromatic compounds , Fuel, Volume 82, Issue 9, June 2003, Pages 1023-1031.

[64] Hameed B. Mahood, Alasdair.N. Campbell, Rex.B. Thorpe, Adel.O. Sharif, Experimental measurements and theoretical prediction for the volumetric heat transfer coefficient of a three-phase direct contact condenser, International Communications in Heat and Mass Transfer, Volume 66, August 2015, Pages 180-188.

[65] R.J. M. Westerhof, N. J.M. Kuipers, S. R. A. Kersten, W. P. M. van Swaaij, Controlling the water content of biomass fast pyrolysis oil, Industrial & engineering chemistry research, Volume 46(26), 2007, Pages 9238–9247.

[66] R. J. M. Westerhof, D. W. F. Brilman, W. P. M. van Swaaij, S. R. A. Kersten, Effect of temperature in fluidized bed fast pyrolysis of biomass: Oil quality assessment in test units, Industrial & engineering chemistry research, Volume 49(3) , 2010, Pages 1160–1168.

[67] Roel J. M. Westerhof, D. Wim F. Brilman, Manuel Garcia-Perez, Zhouhong Wang, Stijn R. G. Oudenhoven, Wim P. M. van Swaaij, Sascha R. A. Kersten, Fractional Condensation of Biomass Pyrolysis Vapors, Energy & Fuels Volume 25(4), 2011, Pages 1817–1829.

[68] G. V.C. Peacocke, E. S. Madrali, C. Z. Li, A. J. Güell, F. Wu, R. Kandiyoti, A. V. Bridgwater, Effect of reactor configuration on the yields and structures of pine-wood derived pyrolysis liquids: A comparison between ablative and wire-mesh pyrolysis, Biomass and Bioenergy, Volume 7 (1-6), 1994, Pages 155-167.

[69] G. V. C. Peacocke, A. V. Bridgwater, Ablative plate pyrolysis of biomass for liquids , Biomass and Bioenergy, Volume 7 (1-6),1994, Pages 147-154.

[70] Nicolas M Robinson, Design, modelling and construction of a novel ablative fast pyrolysis reactor and product collection system , Ph.D. Thesis, Bio-energy Research Group, Aston University, 2000.

[71] Abba Sani Kalgo, The Development and Optimisation of a Fast Pyrolysis Process for Bio-oil Production, Ph.D. Thesis, Bio-energy Research Group, Aston University, 2011.

[72] C.E. Greenhalf, D.J. Nowakowski, A.B. Harms, J.O. Titiloye, A.V. Bridgwater, A comparative study of straw, perennial grasses and hardwoods in terms of fast pyrolysis products, Fuel, Volume 108, June 2013, Pages 216-230.

[73] M. Mos, S.W. Banks, D.J. Nowakowski, P.R.H. Robson, A.V. Bridgwater, I.S. Donnison, Impact of Miscanthus x giganteus senescence times on fast pyrolysis bio-oil quality, Bioresource Technology, Volume 129, February 2013, Pages 335-342.

[74] Scott Banks, Ash control methods to limit biomass inorganic content and its effect on fast pyrolysis bio-oil stability, Ph.D. Thesis, Aston University, 2014.

[75] J. R. Fair, Design of Direct-contact Gas Coolers, Petro/Chem Engineer, August 1961, Page 57.

[76] Fair J.R., Process Heat Transfer By Direct Fluid-Phase Contact, AIChE Symposium series, No. 118, Vol. 68, Pages 1-11.

[77] Ranga Nadig, Design studies for direct contact condensers with and without the presence of non-condensable gas, Ph.D. Thesis, The University of Utah, 1984.

[78] F. Kreith, D. Bharathan, Heat Transfer Research for Ocean Thermal Energy Conversion, Journal of Heat Transfer, Volume 110, 1988, Pages 5-22.

[79] J. A. Garcia, J. R. Fair, Distillation sieve trays without downcomers: Prediction of performance characteristics, Industrial and Engineering Chemistry Research, Volume 41 (6), 2002, Pages 1632-1640.

[80] R. H. Weiland, Hydraulic Stability of Dual flow Trays. In AIChE Spring National Meeting. New Frontiers in High Capacity Tray Technology, Houston, TX, 2001, Page 12.

[81] Z. P. Xu, A. Afacan, K. T. Chuang, Efficiency of dualflow trays in distillation, The Canadian Journal of Chemical Engineering, Volume 72(4), 1994, Pages 607-613.

[82] J. R. Fair, How to Predict Sieve Tray Entrainment and Flooding. Petro/Chem. Eng. 1961,Pages 33-45.

[83] J. A. Garcia, J. R. Fair, A Fundamental Model for the Prediction of Distillation Sieve Tray Efficiency. 1. Database Development. Industrial and Engineering Chemistry Research, Volume 39(6), 2000, Pages 1809 - 1817.

[84] F. I. Zuiderweg, Sieve trays: A view on the State of the Art., Chemical Engineering Science , Volume 37(10), 1982, Pages 1441-1464

[85] M. Souders, G. Brown, Design of fractionating columns. i. Entrainment and capacity, Journal of Industrial & Engineering Chemistry, Volume 2, 1934 , Pages 98-103.

[86] V. Kolar, The Structure of Gas-Liquid Mixtures on Sieve Trays´ of Separation Columns. Chemical Engineering Science.Volume 24, 1969, Page 1285.

[87] F. D. Mayer, L. A. Feris,N. R. Marcilio, V. Baldo, R. Hoffmann, Review of hydraulics correlations for sieve trays without downcomers , Industrial and Engineering Chemistry Research, Volume 53 (20), 2014, Pages 8323-8331.

[88] http://www.aspentech.com/hysys/

[89] A. Tumbalam Gooty, D. Li, C. Briens, F. Berruti, Fractional condensation of bio-oil vapors produced from birch bark pyrolysis, eparation and Purification Technology, Volume 124, 18 March 2014, Pages 81-88.

[90] A. Tumbalam Gooty, D. Li, F. Berruti, C. Briens, Kraft-lignin pyrolysis and fractional condensation of its bio-oil vapors, (Journal of Analytical and Applied Pyrolysis, Volume 106, March 2014, Pages 33-40 .

[91] E. J. Henley, J. D. Seader, Equilibrium-Stage Separation Operations in Chemical Engineering; Wiley: New York, 1981.

[92] K. Papadikis, A. V. Bridgwater, S. Gu. CFD modelling of the fast pyrolysis of biomass in fluidised bed reactors, Part A: Eulerian computation of momentum transport in bubbling fluidised, Chemical Engineering Science, Volume 63, Issue 16, August 2008, Pages 4218-4227.

[93] K. Papadikis, S. Gu, A. V. Bridgwate, CFD modelling of the fast pyrolysis of biomass in fluidised bed reactors. Part B. Heat, momentum and mass transport in bubbling fluidised, Chemical Engineering Science, Volume 64, Issue 5, March 2009, Pages 1036-1045.

[94] K. Papadikis, S. Gu, A. V. Bridgwater, CFD modelling of the fast pyrolysis of biomass in fluidised bed reactors: Modelling the impact of biomass shrinkage, Chemical Engineering Journal, Volume 149, Issues 1–3, 1 July 2009, Pages 417-427.

[95] K. Papadikis, S. Gu, A. V. Bridgwater, Geometrical optimization of a fast pyrolysis bubbling fluidized bed reactor using comutational fluid dynamics, Energy and Fuels, Volume 24 (10), 2010, Pages 5634-5651.

[96] Xi Yu, Mohamed Hassan, Raffaella Ocone, Yassir Makkawi, A CFD study of biomass pyrolysis in a downer reactor equipped with a novel gas–solid separator-II thermochemical performance and products, Fuel Processing Technology, Volume 133, May 2015, Pages 51-63.

[97] Pelle Mellin, Efthymios Kantarelis, Weihong Yang, Computational fluid dynamics modeling of biomass fast pyrolysis in a fluidized bed reactor, using a comprehensive chemistry scheme, Fuel, Volume 117, Part A, 30 January 2014, Pages 704-715.

[98] Soroush Aramideh, Qingang Xiong, Song-Charng Kong, Robert C. Brown, Numerical simulation of biomass fast pyrolysis in an auger reactor, Fuel, Volume 156, 15 September 2015, Pages 234-242.

[99] Zhan Shu, Junwu Wang, Quan Zhou, Chuigang Fan, Songgeng Li, Evaluation of multifluid model for heat transfer behavior of binary gas–solid flow in a downer reactor, Powder Technology, Volume 281, September 2015, Pages 34-48

[100] Mehdi Azadi, Mohsen Azadi, Ali Mohebbi, A CFD study of the effect of cyclone size on its performance parameters, Journal of Hazardous Materials, Volume 182, Issues 1–3, 15 October 2010, Pages 835-841.

[101] Arman Raoufi, Mehrzad Shams, Homayoon Kanani, CFD analysis of flow field in square cyclones, Powder Technology, Volume 191, Issue 3, 24 April 2009, Pages 349-357.

[102] G. Skodras, S.P. Kaldis, D. Sofialidis, O. Faltsi, P. Grammelis, G.P. Sakellaropoulos, Particulate removal via electrostatic precipitators — CFD simulation, Fuel Processing Technology, Volume 87, Issue 7, July 2006, Pages 623-631.

[103] B.S. Choi, C.A.J. Fletcher, Turbulent particle dispersion in an electrostatic precipitator, Applied Mathematical Modelling, Volume 22, Issue 12, December 1998, Pages 1009-1021.

[104] A.H. Van Sinderen, E.F. Wijn, R.W.J. Zanting, Entrainment and Maximum Vapour Flow Rate of Trays, Chemical Engineering Research and Design, Volume 81, Issue 1, January 2003, Pages 94-107.

[105] E.F. Wijn, Weir flow and liquid height on sieve and valve trays, Chemical Engineering Journal, Volume 73, Issue 3, June 1999, Pages 191-204.

[106] Wenxing Zhang, R.B.H Tan, A model for bubble formation and weeping at a submerged orifice with liquid cross-flow, Chemical Engineering Science, Volume 58, Issue 2, January 2003, Pages 287-295.

[107] G. Gesit, K. Nandakumar, K. T. Chuang, CFD Modeling of Flow Patterns and Hydraulics of Commercial-Scale Sieve Trays, A.I.Ch.E. J.,Volume 49 (4) ,April 2003, Pages 910-924.

[108] S. Hirschberg, E.F. Wijn, M. Wehrli, Simulating the Two Phase Flow on Column Trays, Chemical Engineering Research and Design, Volume 83, Issue 12, December 2005, Pages 1410-1424.

[109] R. Rahimi, M.R. Rahimi, F. Shahraki, M. Zivdar Efficiencies of sieve tray distillation columns by CFD simulation, Chemichal engineering and technology, Volume 29 (3). March 2006, Pages 326–335.

[110] Ali Zarei, Seyyed Hossein Hosseini, Rahbar Rahimi, CFD study of weeping rate in the rectangular sieve trays, Journal of the Taiwan Institute of Chemical Engineers, Volume 44, Issue 1, January 2013, Pages 27-33.

[111] Ali Zarei, Seyyed Hossein Hosseini, Rahbar Rahimi, CFD and experimental studies of liquid weeping in the circular sieve tray columns, Chemical Engineering Research and Design, Volume 91, Issue 12, December 2013, Pages 2333-2345.

[112] Asghar Alizadehdakhel, Masoud Rahimi, Ammar Abdulaziz Alsairafi, CFD and experimental studies on the effect of valve weight on performance of a valve tray column, Computers & Chemical Engineering, Volume 34, Issue 1, 11 January 2010, Pages 1-8.

[113] Randheer L. Yadav, Ashwin W. Patwardhan, CFD modeling of sieve and pulsed-sieve plate extraction columns, Chemical Engineering Research and Design, Volume 87, Issue 1, January 2009, Pages 25-35.

[114] D.K. Shen, S. Gu, The mechanism for thermal decomposition of cellulose and its main products, Bioresource Technology, Volume 100, Issue 24, December 2009, Pages 6496-6504.

[115] Kai Sipilä, Eeva Kuoppala, Leena Fagernäs, Anja Oasmaa, Characterization of biomass-based flash pyrolysis oils, Biomass and Bioenergy, Volume 14, Issue 2, 23 March 1998, Pages 103-113.

[116] Yong S. Choi, Patrick A. Johnston, Robert C. Brown, Brent H. Shanks, Kyong-Hwan Lee, Detailed characterization of red oak-derived pyrolysis oil: Integrated use of GC, HPLC, IC, GPC and Karl-Fischer, Journal of Analytical and Applied Pyrolysis, Volume 110, November 2014, Pages 147-154.

[117] B. Scholze, D. Meier, Characterization of the water-insoluble fraction from pyrolysis oil (pyrolytic lignin). Part I. PY–GC/MS, FTIR, and functional groups, Journal of Analytical and Applied Pyrolysis, Volume 60, Issue 1, June 2001, Pages 41-54.

[118] W.L.H. Hallett, N.A. Clark, A model for the evaporation of biomass pyrolysis oil droplets, Fuel, Volume 85, Issue 4, March 2006, Pages 532-544.

[119] R.L. Cotterman, J.M. Prausnitz, Flash calculations for continuous or semi continuous mixtures using an equation of state, Industrial and Engineering Chemistry Process Design and Development, Volume 24(2), 1985, Pages 434–443.

[120] M.T. Rätzsch, H. Kehlen, Continuous thermodynamics of complex mixtures, Fluid Phase Equilibria, Volume 14, 1983, Pages 225-234.

[121] W.L.H. Hallett, N.V. Legault, Modelling biodiesel droplet evaporation using continuous thermodynamics, Fuel, Volume 90, Issue 3, March 2011, Pages 1221-1228.

[122] Youngchul Ra, Rolf D. Reitz, A vaporization model for discrete multi-component fuel sprays, International Journal of Multiphase Flow, Volume 35, Issue 2, February 2009, Pages 101-117.

[123] James Brett, Andrew Ooi, Julio Soria, The effect of internal diffusion on an evaporating bio-oil droplet – The chemistry free case, Biomass and Bioenergy, Volume 34, Issue 8, August 2010, Pages 1134-1140.

[124] K. Papadikis, S. Gu, A. V. Bridgwater, Eulerian model for the condensation of pyrolysis vapors in a water condenser, Energy and Fuels, Volume 25 (4), 2011, Pages 1859-1868.

[125] O. Baker, Simultaneous flow of oil and gas, Oil and Gas Journal, Volume 53, 1954, Pages 185‑195.

[126] Sandra C.K. De Schepper, Geraldine J. Heynderickx, Guy B. Marin, CFD modeling of all gas–liquid and vapor–liquid flow regimes predicted by the Baker chart, Chemical Engineering Journal, Volume 138, Issues 1–3, 1 May 2008, Pages 349-357.

[127] C.W. Hirt, B.D. Nichols, Volume of fluid (VOF) method for the dynamics of free boundaries, Journal of Computational Physics, Volume 39, Issue 1, January 1981, Pages 201-225.

[128] L. Schiller, A.Z. Naumann,Ver Deut Ing, 1933, 77: 318.

[129] E.E. Michaelides, Particles, bubbles & drops. Thier motion, heat transfer and mass transfer. 2006: World Scientific Publishing Co. Pte. Ltd.

[130] J.U. Brackbill, D.B. Kothe, C. Zemach, A continuum method for modeling surface tension, Journal of Computational Physics, Volume 100, Issue 2, June 1992, Pages 335-354.

[131] W. Ranz, W. Marshall. Evaporation from drops, Part II, Chem Eng Prog 1952; 48: 173–180.

[132] Reynolds Osborne, On the Dynamical Theory of Incompressible Viscous Fluids and the Determination of the Criterion,Philosophical Transactions of the Royal Society of London, Volume 186, 1895, Pages 123-164.

[133] L. Prandtl, (1925). "Z. angew". Math. Mech. 5 (1): 136–139.

[134] T. Ba, A. Chaala, M. Garcìa-Pérez, C. Roy ,Colloidal properties of bio-oils obtained by vacuum pyrolysis of softwood bark. Storage stability, Energy & Fuels, Volume 18 (3), 2004, Pages 188–201.

[135] Hooshang Pakdel, Hong-Gen Zhang, Christian Roy, Production and characterization of carboxylic acids from wood, part II: High molecular weight fatty and resin acids, Bioresource Technology, Volume 47, Issue 1, 1994, Pages 45-53.

[136] J.P. Diebold , A review of the chemical and physical mechanisms of the storage stability of fast pyrolysis bio-oils, A.V. Bridgwater (Ed.), et al., Fast pyrolysis of biomass: a handbook, vol. 2CPL Press, Newbury, UK (2002), p. 243.

[137] C. Branca, P. Giudicianni, C. Di Blasi, GC/MS characterization of liquids generated from low-temperature pyrolysis of wood, Industrial Engineering and Chemistry Research, Volume 42 (14), 2003, Pages 3190–3202.

[138] M. Garcia-Perez, A. Chaala, H. Pakdel, D. Kretschmer, C. Roy, Characterization of bio-oils in chemical families, Biomass and Bioenergy, Volume 31, Issue 4, April 2007, Pages 222-242.

[139] A. S. Lawal, Aconsistent rule for selecting roots in cubic equations of state, Industrial & Engineering Chemistry Research, Volume 26 (4), 1987, Pages 857-859.

[140] Akanni S. Lawal, Ernst T. van der Laan, A partial molar fugacity coefficient useful for changing mixing rules of cubic equations of state, Fluid Phase Equilibria, Volume 95, 1994, Pages 109-121.

[141] B. E. Poling, J. M. Prausnitz, and J. P. O'Connell, "Properties of Gases and Liquids", 5th ed., McGraw-Hill, New York, 2001.

[142] Silberberg, Martin A. (2006). Chemistry (4th ed.). New York: McGraw-Hill. pp. 431–434.

[143] C. Antoine, "Tensions des vapeurs; nouvelle relation entre les tensions et les températures" [Vapor Pressure: a new relationship between pressure and temperature], Comptes Rendus des Séances de l'Académie des Sciences (in French), Volume 107, 1888, Pages 681–684, 778–780, 836–837.

[144] W. Wagner, New vapour pressure measurements for argon and nitrogen and an new method for establishing rational vapour pressure equations, Cryogenics, Volume 13 (8), 1973, Pages 470–482.

[145] Kh. Mejbri, A. Bellagi, Corresponding states correlation for the saturated vapor pressure of pure fluids, Thermochimica Acta, Volume 436, Issues 1–2, 1 October 2005, Pages 140-149.

[146] D. E. Dean, L. I. Stiel, The viscosity of non-polar gas mixtures at moderate and high pressures. AIChE J. , Volume 11(3), 1965, Pages 526–532.

[147] T-H. Chung, M. Ajlan, L.L. Lee, K.E. Starling, Generalized multiparameter correlation for nonpolar and polar fluid transport properties, Industrial & Engineering Chemistry Research, Volume 27(4), 1988, Pages 671-679.

[148] R.C. Reid, J.M. Prauznitz, T.K. Sherwood, The properties of gases and liquids. McGraw-Hill, 1977.

[149] D.R. Stull, E.F. Jr. Westrum, G.C. Sinke, The chemical thermodynamics of organic compounds, John Wiley & Sons, Inc., 1969.

[150] T. L. Nielsen, Molecular Structure Based Property Prediction, 15-point Project Department of Chemical Engineering, Technical University of Denmark., Lyngby, DK-2800, 1998.

[151] L. Constantinou, R. Gani, New group contribution method for estimating properties of pure compounds, AIChE J., Volume 40, a994, Pages 1697–1710.

[152] K.S. Pitzer, D.Z. Lippmann, R.F. Jr. Curl, C.M. Huggins, D.E. Petersen, The Volumetric and Thermodynamic Properties of Fluids. II. Compressibility Factor, Vapor Pressure and Entropy of Vaporization, Journal of the American Chemical Society, Volume 77(13), 1955, Pages 3433-3440.

[153] A. Oasmaa, C. Peacocke, A guide to physical property characterisation of biomass-derived fast pyrolysis liquids, VTT Publications, VTT technical research centre of Finland, ESPOO, 2001.

[154] A. Oasmaa, B. Van De Beld, P. Saari, D.C. Elliot, Y. Solantausta, Norms, Standards, and Legislation for Fast Pyrolysis Bio-oils from Lignocellulosic Biomass, Energy & Fuels, Volume 29(4), 2015, Pages 2471-2484.

[155] A. Oasmaa, C. Peacocke, S. Gust, D. Meier, R. McLellan, Norms and Standards for Pyrolysis Liquids. End-User Requirements and Specifications, Energy & Fuels, Volume 19(5), 2005, Pages 2155-2163.

[156] L. Raynal, A. Royon-Lebeaud, A multi-scale approach for CFD calculations of gas–liquid flow within large size column equipped with structured packing, Chemical Engineering Science, Volume 62, Issue 24, December 2007, Pages 7196-7204.

[157] J. Tamim, W.L.H. Hallett, A continuous thermodynamics model for multicomponent droplet vaporization, Chemical Engineering Science, Volume 50, Issue 18, September 1995, Pages 2933-2942.

[158] Lei Zhang, Song-Charng Kong, High-pressure vaporization modeling of multi-component petroleum–biofuel mixtures under engine conditions, Combustion and Flame, Volume 158, Issue 9, September 2011, Pages 1705-1717.

[159] Lei Zhang, Song-Charng Kong, Multicomponent vaporization modeling of bio-oil and its mixtures with other fuels, Fuel, Volume 95, May 2012, Pages 471-480.

Appendix A Multiphase UDF

A.1 Mass transfer calculation

```
#define R_atm 82.05746   /* cm3.atm/ Kmol */
#define R_cal 1.9858775  /* cal/molK */
#define R 8.314472       /* J/molK*/

#define acetic_acid      0    /*   C2H4O2          */
#define butanal          1    /*   C4H8O     */
#define butyric_acid     2    /*   C4H8O2          */
#define coniferyl_alcohol 3   /*   C10H12O3  */
#define formic_acid      4    /*   C2H2O2          */
#define guaiacol         5    /*   C7H7O2          */
#define pentanal         6    /*   C5H10O          */
#define phenol           7    /*   C6H6O     */
#define propanal         8    /*   C3H6O     */
#define propionic_acid   9    /*   C3H6O2          */
#define water vapour     10   /*   H2O             */
#define Nitrogen         11   /*   N2              */

#define gamma_1 -5.53357241
#define gamma_2 11.0210515
#define gamma_3 -0.51243147
```

```
#define gamma_4 -10.6722729
#define gamma_5 29.4364927
#define gamma_6 -0.44101891
#define n_species 12        /* number of species defined in vapour phase */

#define primary 0
#define secondary 1

double Mw_i(int i);             /* Molecular weights of the vapor phase species (g/mol) */
double Tc_i(int i);             /* Critical temperature (K) */
double Pc_i(int i);             /* Critical pressure (atm) */
double Af_i(int i);             /* Acentric factor */
double Vc_i(int i);             /* Critical volume (cm3/gmol) */
double Zc_i(int i);             /* Critical compressibility factor*/

static int counts=0;
static real relaxation=1;
static int last_ts = -1;
static real RFact=1.0;

DEFINE_ON_DEMAND (set_variables)
{
        counts = 0;
        RFact = 0.1;
}

DEFINE_INIT (set_memory,mixture_domain)
```

```
{
        cell_t c;
        Thread *mixture_thread;
        real xc[ND_ND];
        int i;
        thread_loop_c(mixture_thread,mixture_domain)
        {
                begin_c_loop_all(c,mixture_thread)
                {
                        /*intialise the memory locations here*/
                        for (i=0; i<=25;i++ )
                        {
                                C_UDMI(c,mixture_thread,i)=0.0;
                        }
                }
                end_c_loop_all(c,mixture_thread)
        }
}

DEFINE_EXECUTE_AT_END(execute_at_end)
{
        int i;
        int zone_ID=2;
        Domain *mixture_domain=Get_Domain(1);
        Thread *mixture_thread = Lookup_Thread(mixture_domain,zone_ID);
        cell_t c;
        thread_loop_c(mixture_thread,mixture_domain)
```

```
        {
                begin_c_loop_all(c,mixture_thread)
                {
                        for (i=0; i<=12;i++ )
                        {
                                C_UDMI(c,mixture_thread,i+13)=C_UDMI(c,mixture_thread,i);
                        }
                }
                end_c_loop_all(c,mixture_thread)
        }
}

DEFINE_ADJUST(Initial_calc,mixture_domain)
{
        real vapourFugacity;
        real liquidFugacity, reducedVapourFugacity, reducedLiquidFugacity;
        real lnReducedLiquidFugacity,ReducedTemperature;
        real tau, f0, f1;
        real relativeSaturation, liquidMassSource,M_source_total;
        real operatingPressure, totalPressure, vapourPressure;
        real vapourEnergySource, deltaH,condensation_enthalpy,sensible_enthalpy;
        real Mixture_mol_tot;
        real Molf_i[14],M_source[14],speciesEnergySource[14];
        int zone_ID=2; /* zone ID of fluid region (user input)*/
        int index;
        cell_t c;
        Thread *mixture_thread = Lookup_Thread(mixture_domain,zone_ID);
```

```
Domain *primary_domain=DOMAIN_SUB_DOMAIN(mixture_domain,primary);
Domain *secondary_domain=DOMAIN_SUB_DOMAIN(mixture_domain,secondary);
Thread **phase_thread;
phase_thread= THREAD_SUB_THREADS(mixture_thread);
condensation_enthalpy=0;
M_source_total=0;
begin_c_loop(c,mixture_thread)
{
        operatingPressure = RP_Get_Real ("operating-pressure");
        totalPressure = operatingPressure + C_P(c,mixture_thread);
        vapourPressure=totalPressure;
        condensation_enthalpy=0;
        M_source_total=0;
        for (index=0,Mixture_mol_tot=0; index <n_species; index++)
        {
        Mixture_mol_tot = Mixture_mol_tot + (C_YI(c,phase_thread[primary],index)/Mw_i(index));
        }
        /* here only '(n_species-1)'used since the nitrogen mass transfer is neglected*/
        for (index=0; index <(n_species-1); index++)
        {
        Molf_i[index]=(C_YI(c,phase_thread[primary],index)/Mw_i(index))/MAX(Mixture_mol_tot,
SMALL);
                vapourFugacity = Molf_i[index]*vapourPressure;
                reducedVapourFugacity = vapourFugacity/Pc_i(index);
                tau = Tc_i(index)/C_T(c,phase_thread[primary]);
                f0 = gamma_1*(tau - exp(1-tau)) + gamma_2*(pow(tau,gamma_3) - exp(1-tau));
                f1 = gamma_4*(tau - exp(1-tau)) + gamma_5*(pow(tau,gamma_6) - exp(1-tau));
                lnReducedLiquidFugacity = f0 + Af_i(index)*f1;
```

```
                    reducedLiquidFugacity = exp(lnReducedLiquidFugacity);
                    liquidFugacity = reducedLiquidFugacity*Pc_i(index)*totalPressure;
                    relativeSaturation = vapourFugacity/liquidFugacity;
                    if (relativeSaturation <= 1.0)
                            M_source[index] = 0;
                    else if (relativeSaturation>1.0 && relativeSaturation<2.0)
                            M_source[index] = (relativeSaturation-
1)*C_VOF(c,phase_thread[primary])*C_R(c,phase_thread[primary])*C_YI(c,phase_thread[primary],index);
                    else
                            M_source[index] =
(C_VOF(c,phase_thread[primary])*C_R(c,phase_thread[primary])*C_YI(c,phase_thread[primary],index));

                    M_source[index]=M_source[index]*1.0/CURRENT_TIMESTEP; /*relaxation*/

                    M_source_total=M_source_total+M_source[index]; /* liquid mass source */
                    ReducedTemperature = C_T(c,phase_thread[primary])/Tc_i(index);
                    if (ReducedTemperature<=0.4)
                    {
                            deltaH = 0.0;
                    }
                    else
                            deltaH = (7.08*pow((1-ReducedTemperature ),0.354) +
10.95*Af_i(index)*pow((1-ReducedTemperature ),0.456))*R_cal*Tc_i(index)*(4.184/(0.001*Mw_i(index)));
/* ( J/Kg) */
                    speciesEnergySource[index] = M_source[index]*deltaH; /* (J/m3-s) */
                    condensation_enthalpy=condensation_enthalpy+speciesEnergySource[index];/*
(J/m3-s) */
            }
            C_UDMI(c,mixture_thread,0) = C_UDMI(c,mixture_thread,13)+RFact*(M_source[0]-
C_UDMI(c,mixture_thread,13));
```

```
C_UDMI(c,mixture_thread,1) = C_UDMI(c,mixture_thread,14)+RFact*(M_source[1]-
C_UDMI(c,mixture_thread,14));

C_UDMI(c,mixture_thread,2) = C_UDMI(c,mixture_thread,15)+RFact*(M_source[2]-
C_UDMI(c,mixture_thread,15));

C_UDMI(c,mixture_thread,3) = C_UDMI(c,mixture_thread,16)+RFact*(M_source[3]-
C_UDMI(c,mixture_thread,16));

C_UDMI(c,mixture_thread,4) = C_UDMI(c,mixture_thread,17)+RFact*(M_source[4]-
C_UDMI(c,mixture_thread,17));

C_UDMI(c,mixture_thread,5) = C_UDMI(c,mixture_thread,18)+RFact*(M_source[5]-
C_UDMI(c,mixture_thread,18));

C_UDMI(c,mixture_thread,6) = C_UDMI(c,mixture_thread,19)+RFact*(M_source[6]-
C_UDMI(c,mixture_thread,19));

C_UDMI(c,mixture_thread,7) = C_UDMI(c,mixture_thread,20)+RFact*(M_source[7]-
C_UDMI(c,mixture_thread,20));

C_UDMI(c,mixture_thread,8) = C_UDMI(c,mixture_thread,21)+RFact*(M_source[8]-
C_UDMI(c,mixture_thread,21));

C_UDMI(c,mixture_thread,9) = C_UDMI(c,mixture_thread,22)+RFact*(M_source[9]-
C_UDMI(c,mixture_thread,22));

C_UDMI(c,mixture_thread,10) = C_UDMI(c,mixture_thread,23)+RFact*(M_source[10]-
C_UDMI(c,mixture_thread,23));

C_UDMI(c,mixture_thread,11) = C_UDMI(c,mixture_thread,24)+RFact*(M_source_total-
C_UDMI(c,mixture_thread,24));

if (M_source_total<SMALL)

        C_UDMI(c,mixture_thread,12)=0.0;

else

{

        if (C_T(c,phase_thread[secondary])<273.0 &&
C_T(c,phase_thread[secondary])>700.0 )

        {

                C_UDMI(c,mixture_thread,12)=0.0;

        }

        else

                C_UDMI(c,mixture_thread,12)= C_UDMI(c,mixture_thread,25)+
RFact*(condensation_enthalpy-C_UDMI(c,mixture_thread,25)); /* latent heat of condensation */
```

```
                }
        }
        end_c_loop(c,mixture_thread)
}
```

A.2 Mixture property calculation

```
DEFINE_PROPERTY(mixture_Viscosity,c,vapour_thread)
{
        real mean_Mw, mixture_Tc, mixture_Pc;
        real mixture_Af,mixture_Z,mixture_Vc, mixtureViscositySI,mixtureThermalConductivitySI;
        real mixtureKsi,mixture_TR,Mixture_mol_tot;
        real mixtureThermalConductivity;
        real mixtureViscosity=0.0;
        real Molf_i[14];
        int index;
        Thread **phase_thread;
        Thread *mixture_thread;
        mixture_thread= THREAD_SUPER_THREAD(vapour_thread);
        phase_thread= THREAD_SUB_THREADS(mixture_thread);

        /*Initialisation section*/
        Mixture_mol_tot=0;
        mean_Mw                 = 0;
        mixture_Tc      = 0;
        mixture_Pc      = 0;
        mixture_Af      = 0;
        mixture_Z       = 0;
```

```
        mixture_Vc      = 0;

        for (index=0; index <n_species; index++)

                {

                        Mixture_mol_tot = Mixture_mol_tot +
(C_YI(c,phase_thread[primary],index)/Mw_i(index));

                }


        for (index=0; index <n_species; index++)

                {


        Molf_i[index]=(C_YI(c,phase_thread[primary],index)/Mw_i(index))/MAX(Mixture_mol_tot,SMALL)
;  /* converting mass fraction to molfraction with assumption of ideal gas*/

                        mean_Mw = mean_Mw + Molf_i[index]*Mw_i(index);  /* g/mol */

                        mixture_Tc = mixture_Tc  + Molf_i[index]*Tc_i(index); /* K */

                        mixture_Af = mixture_Af + Molf_i[index]*Af_i(index); /* dimensionless */

                        mixture_Z = mixture_Z + Molf_i[index]*Zc_i(index); /* dimensionless */

                        mixture_Vc= mixture_Vc+ Molf_i[index]*Vc_i(index); /* cm3/gmol */

                }

        mixture_Pc = R_atm*mixture_Tc*mixture_Z/mixture_Vc;
                                        /* atm */

        mixture_TR = C_T(c,phase_thread[primary])/mixture_Tc;

        mixtureKsi = pow(mixture_Tc,0.16667)/(pow(mixture_Pc,0.6667)*pow(mean_Mw,0.5));

        if (mixture_TR <= 1.5)

                {

                        mixtureViscosity = 3.40*pow(mixture_TR,0.8889)/mixtureKsi;
                                /*microPoise*/

                }

        else

                {
```

```
                        mixtureViscosity = 16.68*pow((0.1338*mixture_TR - 0.0932),0.5556)/mixtureKsi;
        /*microPoise*/

                }

        mixtureViscositySI = mixtureViscosity*0.0000001;            /*kg/ms*/

        mixtureThermalConductivity =
(mixtureViscosity*0.000001/mean_Mw)*(C_CP(c,phase_thread[primary])*(0.001*mean_Mw/4.184)-R_cal +
4.47); /*cal/cm s K*/

        mixtureThermalConductivitySI = mixtureThermalConductivity*4.184/0.01;      /*W/mK*/

        C_UDMI(c,mixture_thread,26)=mixtureViscositySI;

        C_UDMI(c,mixture_thread,27)=mixtureThermalConductivitySI;

        return mixtureViscositySI;

}


DEFINE_PROPERTY(mixture_Thermal_Conductivity,c,mixture_thread)

{

        return C_UDMI(c,mixture_thread,27);

}
```

A.3 Macros for mass transfer

```
DEFINE_MASS_TRANSFER(C2H4O2,c,mixture_thread,from_phase_index,from_species_index,to_phase_ind
ex,to_species_index)

{

                return C_UDMI(c,mixture_thread,0);

}

DEFINE_MASS_TRANSFER(C4H8O,c,mixture_thread,from_phase_index,from_species_index,to_phase_inde
x,to_species_index)

{

                return C_UDMI(c,mixture_thread,1);

}
```

```
DEFINE_MASS_TRANSFER(C4H8O2,c,mixture_thread,from_phase_index,from_species_index,to_phase_ind
ex,to_species_index)

{

        return C_UDMI(c,mixture_thread,2);

}

DEFINE_MASS_TRANSFER(C10H12O3,c,mixture_thread,from_phase_index,from_species_index,to_phase_i
ndex,to_species_index)

{

        return C_UDMI(c,mixture_thread,3);

}

DEFINE_MASS_TRANSFER(C2H2O2,c,mixture_thread,from_phase_index,from_species_index,to_phase_ind
ex,to_species_index)

{

        return C_UDMI(c,mixture_thread,4);

}

DEFINE_MASS_TRANSFER(C7H7O2,c,mixture_thread,from_phase_index,from_species_index,to_phase_ind
ex,to_species_index)

{

        return C_UDMI(c,mixture_thread,5);

}

DEFINE_MASS_TRANSFER(C5H10O,c,mixture_thread,from_phase_index,from_species_index,to_phase_ind
ex,to_species_index)

{

        return C_UDMI(c,mixture_thread,6);

}

DEFINE_MASS_TRANSFER(C6H6O,c,mixture_thread,from_phase_index,from_species_index,to_phase_inde
x,to_species_index)

{

        return C_UDMI(c,mixture_thread,7);

}
```

```
DEFINE_MASS_TRANSFER(C3H6O,c,mixture_thread,from_phase_index,from_species_index,to_phase_inde
x,to_species_index)

{

                return C_UDMI(c,mixture_thread,8);

}

DEFINE_MASS_TRANSFER(C3H6O2,c,mixture_thread,from_phase_index,from_species_index,to_phase_ind
ex,to_species_index)

{

                return C_UDMI(c,mixture_thread,9);

}

DEFINE_MASS_TRANSFER(watervapour,c,mixture_thread,from_phase_index,from_species_index,to_phase_
index,to_species_index)

{

                return C_UDMI(c,mixture_thread,10);

}

DEFINE_SOURCE(bio_oil_liquid_energy_source,c,pt,dS,eqn)

{

        Thread *mixture_thread=THREAD_SUPER_THREAD(pt);

        dS[eqn]= 0.;

        return (-(C_UDMI(c,mixture_thread,12)));

}

/* Molecular weights of the vapor phase species (g/mol) */
```

A.4 Critical property functions

```
double Mw_i(int i)

{

 double mi[20];

 mi[0]    = 60.05;                    /*acetic acid*/
```

```
 mi[1]    = 72.11;                /*butanal*/
 mi[2]    = 88.11;                /*butyric acid*/
 mi[3]    = 180.2;                /*coniferyl alcohol*/
 mi[4]    = 46.02;                /*formic acid*/
 mi[5]    = 124.14;               /*guaiacol*/
 mi[6]    = 86.13;                /*pentanal*/
 mi[7]    = 94.11;                /*phenol*/
 mi[8]    = 58.08;                /*propanal*/
 mi[9]    = 74.08;                /*propionic acid*/
 mi[10]  = 18.01528;              /*water*/
 mi[11]  = 28.0134;               /*Nitrogen*/
 return mi[i];
}
/* Critical temperature (K) */
double Tc_i(int i)
{
 double Tc[20];
 Tc[0]    = 594.0;                /*acetic acid*/
 Tc[1]    = 524.0;                /*butanal*/
 Tc[2]    = 628.0;                /*butyric acid*/
 Tc[3]    = 569.9;                /*coniferyl alcohol*/
 Tc[4]    = 580.0;                /*formic acid*/
 Tc[5]    = 696.8;                /*guaiacol*/
 Tc[6]    = 554.0;                /*pentanal*/
 Tc[7]    = 694.2;                /*phenol*/
 Tc[8]    = 496.0;                /*propanal*/
 Tc[9]    = 612.0;                /*propionic acid*/
```

```
 Tc[10]  = 647.3;                    /*water*/
 Tc[11]  = 126.19;                   /*Nitrogen*/
  return Tc[i];
}
/* Critical pressure (atm) */
double Pc_i(int i)
{
 double Pc[20];
 Pc[0]    = 57.1;                    /*acetic acid*/
 Pc[1]     = 40.0;                   /*butanal*/
 Pc[2]    = 52.0;                    /*butyric acid*/
 Pc[3]    = 33.6;                    /*coniferyl alcohol*/
 Pc[4]    = 57.34;                   /*formic acid*/
 Pc[5]    = 46.613;                  /*guaiacol*/
 Pc[6]    = 35.0;                    /*pentanal*/
 Pc[7]    = 60.5;                    /*phenol*/
 Pc[8]    = 47.0;                    /*propanal*/
 Pc[9]    = 53.0;                    /*propionic acid*/
 Pc[10]  = 217.6;                    /*water*/
 Pc[11]  = 33.534;                   /*Nitrogen*/
  return Pc[i];
}
/* Acentric factor */
double Af_i(int i)
{
 double Af[20];
 Af[0]    = 0.454;            /*acetic acid*/
```

```
 Af[1]    = 0.352;          /*butanal*/
 Af[2]    = 0.67;           /*butyric acid*/
 Af[3]    = 1.155;          /*coniferyl alcohol*/
 Af[4]    = 0.368;          /*formic acid*/
 Af[5]    = 0.563;          /*guaiacol*/
 Af[6]    = 0.4;            /*pentanal*/
 Af[7]    = 0.44;           /*phenol*/
 Af[8]    = 0.313;          /*propanal*/
 Af[9]    = 0.536;          /*propionic acid*/
 Af[10]   = 0.344;          /*water*/
 Af[11]   = 0.040;          /*Nitrogen*/
  return Af[i];
}

/* Critical volume (cm3/gmol) */
double Vc_i(int i)
{
 double Vc[20];
 Vc[0]    = 171.0;                 /*acetic acid*/
 Vc[1]    = 278.0;                 /*butanal*/
 Vc[2]    = 292.0;                 /*butyric acid*/
 Vc[3]    = 482.0;                 /*coniferyl alcohol*/
 Vc[4]    = 120.0;                 /*formic acid*/
 Vc[5]    = 338.0;                 /*guaiacol*/
 Vc[6]    = 333.0;                 /*pentanal*/
 Vc[7]    = 229.0;                 /*phenol*/
 Vc[8]    = 223.0;                 /*propanal*/
```

```
 Vc[9]    = 230.0;                    /*propionic acid*/
 Vc[10]  = 56.0;                      /*water*/
 Vc[11]  = 90.1;                      /*Nitrogen*/
  return Vc[i];
}

/* Critical compressibility factor*/
double Zc_i(int i)
{
 double Zc[20];
 Zc[0]    = 0.2;              /*acetic acid*/
 Zc[1]    = 0.26;             /*butanal*/
 Zc[2]    = 0.295;            /*butyric acid*/
 Zc[3]    = 0.346;            /*coniferyl alcohol*/
 Zc[4]    = 0.1445;           /*formic acid*/
 Zc[5]    = 0.275;            /*guaiacol*/
 Zc[6]    = 0.26;             /*pentanal*/
 Zc[7]    = 0.24;             /*phenol*/
 Zc[8]    = 0.26;             /*propanal*/
 Zc[9]    = 0.242;            /*propionic acid*/
 Zc[10]  = 0.229;             /*water*/
 Zc[11]  = 0.292;             /*Nitrogen*/
  return Zc[i];
}
```

Appendix B Group contribution

In many instances, engineers and researchers often need mixture and pure component properties in order to design efficient equipment. Many property models are intended for the whole set of compositions at the pure component level. Pure component property constants like critical temperature pressures often used as the basis for corresponding state correlations to estimate properties like saturation pressures and viscosity.

This section shows how the pure component property constants can be estimated in the absence of experimental data. There are different estimation methods available in the literature namely group, atomic or bond contribution methods. The basis for all these methods is that the intermolecular forces that determine the critical constants of the property depend mostly on bonds between atoms of the molecules. In the case of group contribution method, bonds within and among small group of atoms are considered.

Vapour – liquid critical temperatures are of greatest interests like critical temperature, pressures, and volumes. They are used to estimate many thermodynamic transport properties. Finding them experimentally is difficult task especially for larger components present in pyrolysis vapours and bio-oils , can chemically degrade at their very high critical temperatures.

Earliest group contribution method developed to estimate critical properties was by Lydersen. With more availability of the experimental values efficient statistical techniques have been deployed to get different group contributions with optimized parameters. Out of which, methods of Joback, Constantinou and Gani , Wilson and Jasperson, and Marrero and Pardillo

are the famous group contribution methods listed by poling et al. In this section method used by Marrero and pardillo was described in detail for estimating critical properties.

B.1 Method of Marrero and Pardillo

Marrero-Marejo´n and Pardillo-Fontdevila described group interaction contribution technique which is a bond contribution method for estimating Tc, Pc, and Vc. They give equations that use values from pairs of atoms alone, such as >C< & —N< , or with hydrogen attached, such as CH3— & —NH2.

$$T_c = T_b/[0.5851 - 0.9286(\sum_k N_k\, tcbk) - (\sum_k N_k\, tcbk)^2]. \quad \text{B-1}$$

$$P_c = [0.1285 - 0.0059N_{atoms} - \sum_k N_k\, pcbk]^{-2}. \quad \text{B-2}$$

$$V_c = 25.1 + \sum_k N_k\, vcbk. \quad \text{B-3}$$

Table- B-1 Group contributions (sample).

Pair #	Atom/Group Pairs	tcbk	pcbk	vcbk	tbbk
1	CH3 — & CH3—	-0.0213	-0.0618	123.2	113.12
2	CH3 — & —CH2—	-0.0227	-0.0430	88.6	194.25
3	CH3 — & —CH—	-0.0223	-0.0376	78.4	194.27
4	CH3 — & —C	-0.0189	-0.0354	69.8	186.41
5	CH3 — &CH—	0.8526	0.0654	81.5	137.18

A) Acetic acid (C2H4O2):

Number of atoms (N_{atoms}) : 8

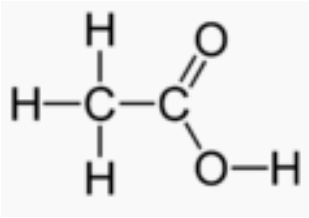

Fig. B.1 Skeletal representation of Acetic acid.

Table- B-2 Group contributions for Acetic acid.

Pair #	Atom/Group Pairs	tcbk	pcbk	vcbk	tbbk	Nk
19	CH3— & —COOH	-0.0890	-0.0499	145.9	1228.84	1

Estimated Values:

1. Boiling point temperature :390.9503 K (391.2 ± 0.6 from NIST)
2. Critical Temperature :592.5066 K (593. ± 3 from NIST)
3. Critical Pressure :58.09414 bar (57.81 bar from NIST)

B) Pentanal (C5H10O):

Number of atoms (N_{atoms}) : 16

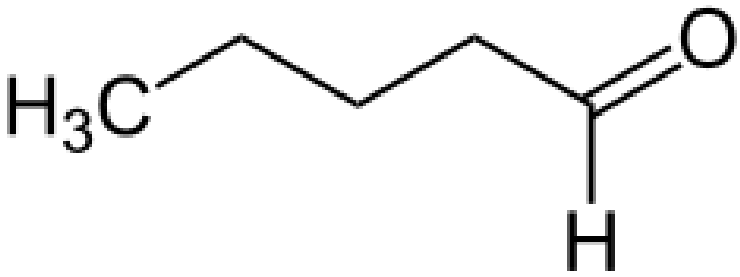

Fig. B.2 Skeletal representation of Pentanal.

Table- B-3 Group contributions for Pentanal.

Pair #	Atom/Group Pairs	tcbk	pcbk	vcbk	tbbk	Nk
2	CH3 — & —CH2—	-0.0227	-0.043	88.6	194.25	1
29	—CH2— & —CH2 —	-0.0206	-0.0272	56.6	244.88	2
45	—CH2— & —CHO	-0.0267	-0.021	106.1	648.7	1

Estimated Values:

1. Boiling point temperature :376.2588 K (376. ± 2.)
2. Critical Temperature :569.207 K (568.3)
3. Critical Pressure :42.99919 bar (39.18)

C) Phenol(C6H6O):

Number of atoms (N_{atoms}) : 13

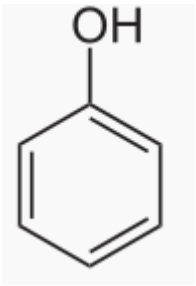

Fig. B.3 Skeletal representation of Phenol.

Table- B-4 Group contributions for Phenol

Pair #	Atom/Group Pairs	tcbk	pcbk	vcbk	tbbk	Nk
149	=C< [r] & —OH	0.0931	-0.0388	8.5	456.25	1
134	=CH— [r] &=C<[r]	0.219	-0.1324	29.8	237.22	1
130	—CH[=] [r] & —CH[=] [r]	-0.2246	0.1542	36.5	112	2

133	=CH— [r] &=CH— [r]	0.2089	-0.1822	39.3	285.07	2
131	—CH[=] [r] & >C[=] [r]	-0.3586	0.149	34.4	291.15	1

Estimated Values:

1. Boiling point temperature :439.6407 K (455.0 ± 0.6)
2. Critical Temperature :674.9482 K (694.3)
3. Critical Pressure :59.1716 bar (59.30)

Appendix C Fugacity calculation

C.1 Transformed equation of state

The general equation of state, which was given by Lawal et al., is shown in equation (4-1).

$$P = \frac{RT}{v - b} - \frac{a(T)}{v^2 + \alpha b v - \beta b^2}$$

The real gas equation can be expressed in terms of Z as shown in equation C-1.

$$Z = \frac{Pv}{RT} \qquad \text{C-1}$$

By multiplying both sides of equation (4-1) with $\frac{v}{RT}$ will give equation C-2.

$$P\frac{v}{RT} = \frac{v}{RT}\left(\frac{RT}{v - b} - \frac{a(T)}{v^2 + \alpha b v - \beta b^2}\right) \qquad \text{C-2}$$

Re arranging the equation C-2 with Z form for , equation C-3 can be obtained.

$$Z = \frac{\frac{ZRT}{P}}{\frac{ZRT}{P} - b} - \frac{\frac{a(T)}{RT}\frac{ZRT}{P}}{\left(\frac{ZRT}{P}\right)^2 + \alpha b\frac{ZRT}{P} - \beta b^2} \qquad \text{C-3}$$

By multiplying denominator and numerator of the with $\frac{P}{RT}$ the equation C-3 becomes equation C-4.

$$Z = \frac{Z}{Z - \frac{bP}{RT}} - \frac{\frac{a(T)P}{(RT)^2}Z}{Z^2 + \alpha\frac{bP}{RT}Z - \beta\left(\frac{bP}{RT}\right)^2} \quad \text{C-4}$$

Equation C-4 can be expressed in more compact form as shown in equation C-5.

$$Z = \frac{Z}{Z - B} - \frac{AZ}{Z^2 + \alpha BZ - \beta B^2} \quad \text{C-5}$$

Where, the terms A and B can be expressed as shown in equations

$$A = \frac{a(T)P}{(RT)^2} \quad \text{C-6}$$

$$B = \frac{bP}{RT} \quad \text{C-7}$$

By dividing each side of the equation C-5 with Z and multiplying with $(Z - B)(Z^2 + \alpha BZ - \beta B^2)$ yields equation C-8.

$$(Z - B)(Z^2 + \alpha BZ - \beta B^2) = Z^2 + \alpha BZ - \beta B^2 - AZ - AB \quad \text{C-8}$$

In simplified cubic form, the equation of state can be written as shown in equation C-9.

$$Z^3 + \mathrm{K}_1 Z^2 + \mathrm{K}_2 Z + \mathrm{K}_3 = 0 \quad \text{C-9}$$

Where, the coefficients are expressed as shown in the equations C-10 to C-12.

$$\mathrm{K}_1 = [1 + (1 - \alpha)B] \quad \text{C-10}$$

$$\mathrm{K}_2 = [A - \alpha B - (\alpha + \beta)B^2] \quad \text{C-11}$$

$$\mathrm{K}_3 = [AB - \beta(B^3 - B^2)] \quad \text{C-12}$$

C.2 Calculating roots for EOS

Equation C-9 contains three roots and they can be computed in different ways.

In the first step, parameters Q and R calculated as follows,

$$Q = \frac{{\mathrm{K}_1}^2 - 3\mathrm{K}_2}{9} \quad \text{C-13}$$

$$S = \frac{2{\mathrm{K}_1}^3 - 9\mathrm{K}_1\mathrm{K}_2 + 27\mathrm{K}_3}{54} \quad \text{C-14}$$

By considering $D = S^2 - Q^3$ be the discriminant, following cases are considered,

a) If D <0, the polynomial equation have three real roots shown in the equations C-15 to C-17.

$$\mathrm{Z}_1 = -\left(2\sqrt{Q}\,cos\frac{\theta}{3}\right) - \frac{\mathrm{K}_1}{3} \quad \text{C-15}$$

$$\mathrm{Z}_2 == -\left(2\sqrt{Q}\,cos\frac{\theta + 2\pi}{3}\right) - \frac{\mathrm{K}_1}{3} \quad \text{C-16}$$

$$\mathrm{Z}_3 == -\left(2\sqrt{Q}\,cos\frac{\theta - 2\pi}{3}\right) - \frac{\mathrm{K}_1}{3} \quad \text{C-17}$$

Here, the θ needs to be calculated in radians as shown in equation C-18.

$$\theta = arccos\left(\frac{S}{\sqrt{Q^3}}\right) \quad \text{C-18}$$

b) If D > 0, the polynomial equation have one single root shown in the equation C-19.

$$Z_1 = \sqrt[3]{-S+\sqrt{D}} + \sqrt[3]{-S-\sqrt{D}} - \frac{K_1}{3} \quad \text{C-19}$$

C.3 Fugacity for pure component

The fugacity equation for General EOS can be shown in equation

$$\ln\frac{f}{P} = \int_{p^*}^{p}\left(\frac{v}{RT}-\frac{1}{P}\right)dP \quad \text{C-20}$$

By doing the separation of the integration, equation C-20 can be written as

$$\ln\frac{f}{P} = \int_{p^*}^{p}\frac{v}{RT}dP - \int_{p^*}^{p}\frac{dP}{P} \quad \text{C-21}$$

By doing integration by parts on the first part of the integral in equation C-21,

$$\ln\frac{f}{P} = \frac{1}{RT}\left[vP|_{P^*}^{P} - \int_{v^*}^{v}Pdv\right] - \ln\frac{P}{P^*} \quad \text{C-22}$$

$$\ln\frac{f}{P} = \frac{vP}{RT} - \frac{v^*P^*}{RT} - \frac{1}{RT}\int_{v^*}^{v}Pdv - \ln\frac{P}{P^*} \quad \text{C-23}$$

At $P^* = 0$ condition, Z is equal to 0. Therefore the equation C-23 becomes

$$\ln\frac{f}{P} = Z - 1 - \frac{1}{RT}\int_{v^*}^{v} P dv - \ln\frac{P}{P^*} \quad \text{C-24}$$

By substituting P using equation 4.1, equation C-24 expressed as

$$\ln\frac{f}{P} = Z - 1 - \frac{1}{RT}\int_{v^*}^{v}\left(\frac{RT}{v-b} - \frac{a(T)}{v^2 + \alpha b v - \beta b^2}\right) dv - \ln\frac{P}{P^*} \quad \text{C-25}$$

$$\ln\frac{f}{P} = Z - 1 - \frac{1}{RT}\int_{v^*}^{v}\frac{RT}{v-b}dv + \frac{1}{RT}\int_{v^*}^{v}\left(\frac{a(T)}{v^2 + \alpha b v - \beta b^2}\right) dv - \ln\frac{P}{P^*} \quad \text{C-26}$$

$$\ln\frac{f}{P} = Z - 1 - \ln(v-b)\,|_{v^*}^{v} + \frac{1}{RT}\int_{v^*}^{v}\left(\frac{a(T)}{v^2 + \alpha b v - \beta b^2}\right) dv - \ln\frac{P}{P^*} \quad \text{C-27}$$

$$\ln\frac{f}{P} = Z - 1 - \ln\left(\frac{v-b}{v^*-b}\right) - \ln\frac{P}{P^*} + \frac{a(T)}{RT}\int_{v^*}^{v}\left(\frac{1}{v^2 + \alpha b v - \beta b^2}\right) dv \quad \text{C-28}$$

$$\ln\frac{f}{P} = Z - 1 - \ln\left(\frac{v-b}{v^*-b}\right) - \ln\frac{P}{P^*} + \frac{a(T)}{RT}\int_{v^*}^{v}\left(\frac{1}{(v + M\frac{b}{2})(v + N\frac{b}{2})}\right) dv \quad \text{C-29}$$

Where M and N are defined as

$$M = (\alpha + (\alpha^2 + 4\beta)^{0.5}) \quad \text{C-30}$$

$$N = (\alpha - (\alpha^2 + 4\beta)^{0.5}) \quad \text{C-31}$$

By simplifying the equation C-29 further,

$$\ln\frac{f}{P} = Z - 1 - \ln\left(\frac{v-b}{v^*-b}\right) - \ln\frac{P}{P^*} + \frac{2a(T)/RT}{(M-N)b}\left[\int_{v^*}^{v}\left(\frac{1}{(v+M\frac{b}{2})}\right)dv - \int_{v^*}^{v}\left(\frac{1}{(v+N\frac{b}{2})}\right)dv\right] \quad \text{C-32}$$

$$\ln\frac{f}{P} = Z - 1 - \ln\left(\frac{(v-b)/RT}{(v^*-b)/RT}\right) - \ln\frac{P}{P^*} + \frac{2a(T)/RT}{(M-N)b}\left[\int_{v^*}^{v}\left(\frac{1}{(v+M)}\right)dv - \int_{v^*}^{v}\left(\frac{1}{(v+N)}\right)dv\right] \quad \text{C-33}$$

Assuming v^* is lot bigger than b, we get

$$\ln\frac{f}{P} = Z - 1 - \ln\left(\frac{(v-b)/RT}{v^*/RT} * \frac{P}{P^*}\right) + \frac{2a(T)/RT}{(M-N)b}\ln\left(\frac{v+M\frac{b}{2}}{v+N\frac{b}{2}}\right)|_{v^*}^{v} \quad \text{C-34}$$

$$\ln\frac{f}{P} = Z - 1 - \ln\left(\frac{\frac{Pv}{RT} - \frac{bP}{RT}}{\frac{v^*P^*}{RT}}\right) + \frac{2a(T)/RT}{(M-N)b}\ln\left(\frac{v+M\frac{b}{2}}{v+N\frac{b}{2}}\right) \quad \text{C-35}$$

$$\ln\frac{f}{P} = Z - 1 - \ln\left(\frac{\frac{Pv}{RT} - \frac{bP}{RT}}{\frac{v^*P^*}{RT}}\right) + \frac{2a(T)/RT}{M-N}\ \frac{\frac{P}{RT}}{\frac{P}{RT}}\ln\left(\frac{\left(v + M\frac{b}{2}\right)\frac{P}{RT}}{\left(v + N\frac{b}{2}\right)\frac{P}{RT}}\right) \quad \text{C-36}$$

By using real gas equation, the fugacity relation can be expressed in terms of compressibility factor as shown in the equation C-37.

$$\ln\frac{f}{P} = Z - 1 - \ln(Z-1) + \frac{2A}{B(M-N)}\ \ln\left(\frac{(Z+M)B}{(Z+N)B}\right) \quad \text{C-37}$$